UNIVERSITÀ DEGLI STUDI DI MESSINA

TESI DI DOTTORATO DI RICERCA IN BIOLOGIA APPLICATA E MEDICINA SPERIMENTALE XXXIII CICLO

SSD BIO/19

Alzheimer's Disease: IgGs against β-amyloid conformational epitopes exposed by engineered phages as novel biomarkers for state/stage diagnosis

Candidato:
Dott.ssa Maria Giovanna Rizzo

Relatore:
Chiar.mo Prof. Salvatore P. P. Guglielmino

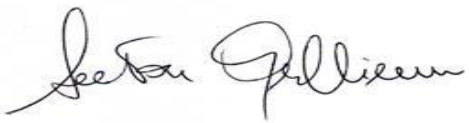

Coordinatore:
Chiar.ma Prof.ssa Nunziacarla Spanò

2017/2020

INDEX

BACKGROUND

CHAPTER 1

Alzheimer's Disease: definition, epidemiology, pathophysiology and diagnosis

Alzheimer's disease (AD) is the most common neurodegenerative disease, accounting for approximately two thirds of all cases of dementia and affecting up to 20% of individuals older than 80 years [1]. It results in a progressive and irreversible decline in memory and a deterioration of various other cognitive abilities. The disease is characterized by the destruction of nerve cells and neural connections in the cerebral cortex of the brain and by a significant loss of brain mass (Fig.1).

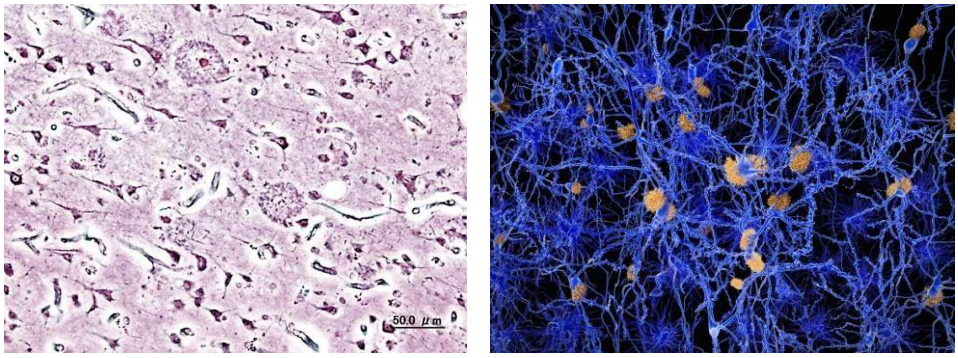

Fig. 1 *(a) Histopathologic image of neuritic plaques in the cerebral cortex in a patient with Alzheimer disease; (b) A neuron network affected by amyloid plaques.*

An estimated 40 million people, mostly older than 60 years, have dementia worldwide, and this fi gure is projected to double every 20 years, until at least 2050. Projected increases in the prevalence of dementia are proportionally much higher for developing countries with young populations than for western Europe and the USA, which already have a much older population (Dementia statistics, Alzheimer's Disease International).

Multiple processes have been implicated in AD including: abnormal β-amyloid (Aβ) production [2–8], tau hyperphosphorylation and neurofibrillary tangles (NFTs) [9, 10], synaptic pathology [11–13], oxidative stress [14–16], inflammation [5, 17–20], protein processing or misfolding [21, 22], calcium dyshomeostasis [16, 21–27], aberrant reentry of neurons into the cell cycle [28, 29], cholesterol synthesis [30, 31],

hormones [24, 32] or growth factors [18, 33]. However, the factors that promote these processes still remain unclear.

Macroscopic and microscopic markers are known and may help the understanding of the disease pathogenesis and in the development of possible strategies [34, 35]. At the macroscopic level (Fig. 2) there is the atrophy of the hippocampus and cerebral cortex, which in AD appears more sharply [36, 37]. Microscopically it is possible to observe the formation of amyloid plaques, or senile plaques, which are amorphous structures of Aβ, and accumulation of hyperphosphorylated Tau protein which implies the formation of neurofibrillary tangles, and extensive neuronal loss [34, 35, 38-41].

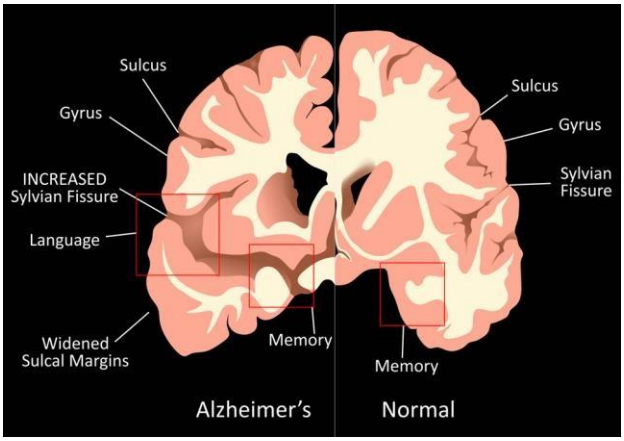

Fig. 2 *Macroscopic changes. Atrophy of the hippocampus and cerebral cortex*

Although the course of the disease is different for each individual patient, AD has a number of common symptoms that can be classified into three main phases:

Mild: phase characterized by a slight loss of memory on sporadic episodes of daily life (on-going memory) and of prospective memory; states of confusion can also occur.

Intermediate: In this phase the subject has greater difficulty in remembering recent events, begins to lose retrograde memory and manifests the first forms of aggression and / or passivity.

Advanced: This phase is characterized by speech difficulties, severe cognitive deficits and violent, anxious and paranoid attitudes. There are also motor alterations which are followed by the loss of autonomy.

As a rule, the disease is often anticipated by the so-called mild cognitive impairment (MCI), a slight decline in the performance of various cognitive functions related to memory, orientation and verbal skills.

The major neuropathological characteristics of Alzheimer's appear to be correlated with the formation of neurofibrillary plaques and tangles. The plaques appear to develop first in brain areas associated with cognition and as disease progresses in cortical areas. Senile plaques consist of insoluble deposits of amyloid β-peptide (Aβ), a fragment of the amyloid precursor protein (APP). The Aβ peptide is generated by two consecutive cleavage events. There appear to be two types of Aβ: a longer species, Aβ42, and a shorter species, Aβ40. Aβ42 appears toxic to the neuron causing inflammation or increasing the production of free radicals. Accumulation of neurofibrillary tangles in neurons is a second distinguishing feature of AD. Neurofibrillary tangles are mostly formed from chemically altered (abnormally folded and phosphorylated) tau proteins, a protein involved in the formation of microtubules. The formation of nodes is related to the severity of the disease; the more advanced the stage of the disease, the more tau becomes entangled in the brain.

Diagnosis

AD was identified for the first time in 1901 by Dr. Alois Alzheimer, a German psychiatrist who identified the symptoms of this neurodegeneration in a patient. In 1984, the Association of Alzheimer's Patients established the NINCDS-ADRDA (National Institute of Neurological and Communicative Disorders and Stroke and Alzheimer's Disease and Related Disorders Association) diagnostic criterion, later updated in 2007, which requires that the presence of cognitive deficits and a suspected one dementia syndrome must be confirmed by neuropsychological tests. To date, neuropsychological and cognitive assessments, allow tests to characterize the state of the disease. In particular, are examined: memory, language, perceptual ability, attention, constructive ability, orientation, problem solving and functional skills. Moreover, the application of advanced biomedical imaging systems such as computed tomography (CT), magnetic resonance imaging (MRI), single photon emission tomography (SPECT), positron emission tomography (PET), were used for differential diagnosis of dementia, through Lewi bodies generalized in the cortex and identification of markers of β-amyloid plaques deposited in neuronal tissue. Also

laboratory blood tests can be used in support for diagnosis of AD as: complete blood count, serum urea, creatinine, thyroxine (T4), Thyroid Stimulating Hormone (TSH), albumin, liver enzymes (SGOT, SGPT, gamma GT), vitamin B12, calcium, serologic tests for syphilis, complete HIV serology. In particular, cerebrospinal fluid exams are used to analyze the changes in two biomarkers: reduced Aβ 42 which is a component of neuritic plaques and increased levels of Tau protein (total and phosphorylated) that is related to neuronal decay [42].

For global cognitive function, the main clinical examination established by NINCDS-ADRDA is the Mini-Mental State Examination (MMSE). The MMSE is one of the most used tests in the world. The test consists of 30 questions, which refer to seven different cognitive areas: orientation in time, orientation in space, recording of words, attention and calculation, recall, language, constructive practice.

The total score is between a minimum of 0 and a maximum of 30 points. A score equal to or less than 18 indicates a severe impairment of cognitive abilities; a score between 18 and 24 indicates moderate to mild impairment, a score of 25 is considered borderline, and a score of 26 to 30 indicates cognitive normality. The indications are however indicative, since there are calibration factors linked to the age and schooling of the subject.

However, a confirmed diagnosis of AD can only be obtained through post-mortem identification of neurofibrillary tangles and/or abnormal plaque deposits in the brain (Fig.3) known to be associated with AD [43].

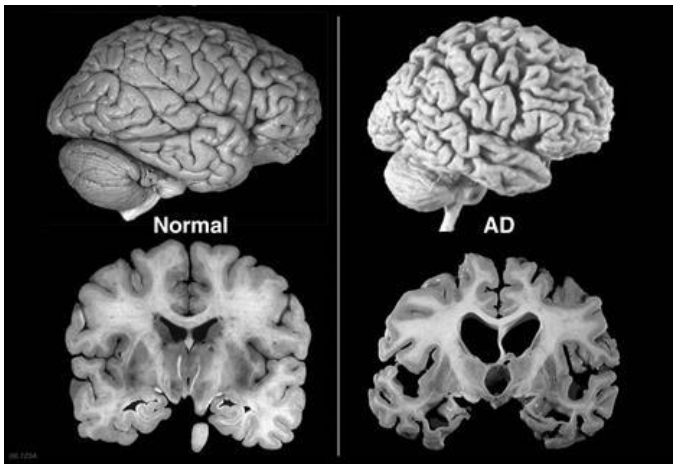

Fig. 3 *Brain atrophy in advanced Alzheimer's Disease*

As the number of people developing AD is expected to increase sharply in the next decades, there is an urgent need to develop diagnostic tests applicable to living people. The confirmatory diagnosis of AD in early stages could facilitate early therapeutic intervention and treatment of the disease. Compared to biomarkers that require brain imaging and collection of the cerebrospinal fluid (CSF), the blood-based biomarkers are particularly desirable because they are less expensive, relatively non-invasive, and easily accessible [44, 45]. Through the search of such blood-derived biomarkers, (e.g. antibodies-autoantibodies) have emerged as potentially effective bio-markers for AD.

CHAPTER 2

β-amyloid in Alzheimer's Disease: amyloid polymorphism and structural basis

Pathogenic Aβ peptides are produced by a proteolytic cleavage of amyloid precursor protein (APP) by enzyme complexes β- and γ-secretases. APP cleavage occurs via two distinct pathways (Fig.4).

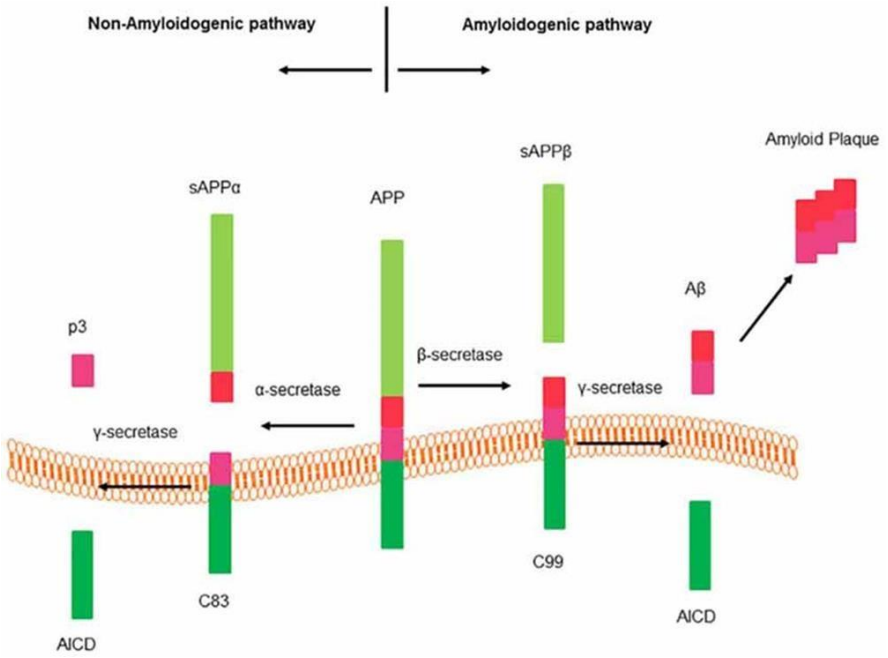

Fig. 4 *Pathways to produce β-amyloid peptide*

The non-amyloidogenic pathway that involves cleavage of APP by α-secretase and generate two fragments: an 83 amino acid C-terminal fragment (C83) that remains in the membrane and an N-terminal ectodomain (sAPPα) released into the extracellular medium. The cleavage of APP by α-secretase occurs within the Aβ domain and consequently prohibits Aβ peptide production. C83 membrane fragment subsequently cleaved by γ-secretase produce a short fragment called P3 peptide and an APP intracellular domain (AICD).

The amyloidogenic pathway leads to neurotoxic Aβ generation. β-secretase (BACE1) produce a large N-terminal ectodomain (sAPPβ) into the extracellular medium. A 99-amino acid C terminal fragment (C99) remains in the membrane [46, 47]. The exposed C99 N-terminus corresponds to the first amino acid of Aβ. Sequential cleavage of this fragment by γ-secretase (between residues 38 and 43) releases the

Aβ peptide. Most of the Aβ peptides are 40 residues in length (Aβ 1–40), with a minor percentage containing 42 residues (Aβ 1–42). Aβ 1–42 is considered the more neurotoxic form because the extra two amino acids provide a greater tendency to misfold and subsequently aggregate [48]. Infact, higher plasma levels of Aβ 1–42 have been correlated with Alzheimer's disease [49].

Conformational variation of β-amyloid

The role of Aβ in AD and the lack of correlation between Aβ in the brain and the cognitive ability of patients it is not known. Infact, some patients with Aβ deposits show no symptoms of AD [50,51].

The heterogeneity to Alzheimer's disease may lie in structural variations of Aβ, which can form polymorphic Aβ oligomers in a process known as segmental polymorphism. The segments that form beta sheets vary between different fibril structures [52–54].

Therefore, forms of structurally distinct Aβ might be deposited in places and state different in the brains of patients with Alzheimer's disease. However, it remains unclear which types of deposit are more closely linked with the cognitive symptoms of the disease [55].

Amyloid Polymorphism and structural basis

Recent studies highlight the medical importance of amyloid self-propagation in neurodegenerative diseases [56 – 68]. Polymorphism is another important property of amyloid fibrils. For Aβ peptide associated with AD, fibrils formed by a single peptide or protein can be polymorphic, and exhibit multiple distinct forms as shown in transmission electron microscopy (TEM) images (Fig.5). Although, amyloid polymorphs could be different bundled arrangements of the same basic amyloid ''protofilament'' structure, ssNMR measurements show that amyloid polymorphs contain distinct molecular structures, and that each molecular structure can propagate itself [69-73].

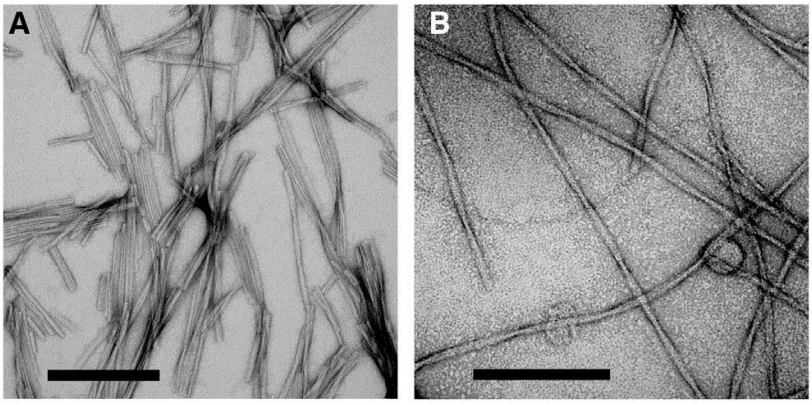

Fig.5. *Polymorphism of Amyloid Fibrils and Aggregation Intermediates, (A) striated ribbon morphologies. (B) twisted morphologies in TEM images.*

Aggregation intermediates can be neurotoxic types in neurodegenerative diseases. The toxicity of fibrils in cell cultures depends on their state of self-association and/or their lengths [73;74]. The relationship between inherent cytotoxicity and molecular structure (e.g., cross-β versus non-cross-β structure, parallel β sheet versus antiparallel β sheet structure) is not yet clear. In animal models, indication exists that oligomeric aggregates have antagonistic effects on neuronal function and memory [75-78]. In the case of AD, immunohistochemical studies show that definite oligomeric species exist in human brain tissue [79, 80]. In AD, both fibrillar and non-fibrillar aggregates contribute to neurodegeneration by different mechanisms.

Experiments by Petkova et al. showed that Aβ40 fibril morphologies can be controlled reproducibly by subtle variations in growth conditions in vitro [73]. Specifically, Aβ40 fibrils grown at 24°C and pH7.4 with moderate agitation of the Aβ40 solution during the growth period have a predominant ‘‘striated ribbon’’ morphology (Fig. 5A), whereas fibrils grown under the same conditions except without agitation have a predominant ‘‘twisted’’ morphology (Fig. 5B). These results demonstrate that distinct fibril morphologies correspond to distinct molecular structures. In general, molecular structures within amyloid fibrils formed in vitro are not determined individually by the amino acid sequences of amyloid-forming peptides and protein. Instead, they are determined by the precise details of growth conditions.

Full molecular structural models for striated ribbon and twisted Aβ40 fibrils, shown in Fig. 6A and 6B, were developed from combinations of structural constraints from ssNMR and electron microscopy [81, 82]. The principal difference between the two

polymorphs is their symmetry, with the striated ribbon protofilament containing two cross-b subunits, related by 2-fold rotational symmetry on the fibril growth axis, and the twisted fibril containing three cross-b units, related by approximate 3-fold rotational symmetry. In addition, the detailed conformations of the bend segments differ in the two polymorphs. The bend segment within 2-fold symmetric striated ribbon protofilaments is bridged by an electrostatic interaction between oppositely charged side chains of Asp23 and Lys28. This interaction is absent in 3-fold symmetric twisted fibrils.

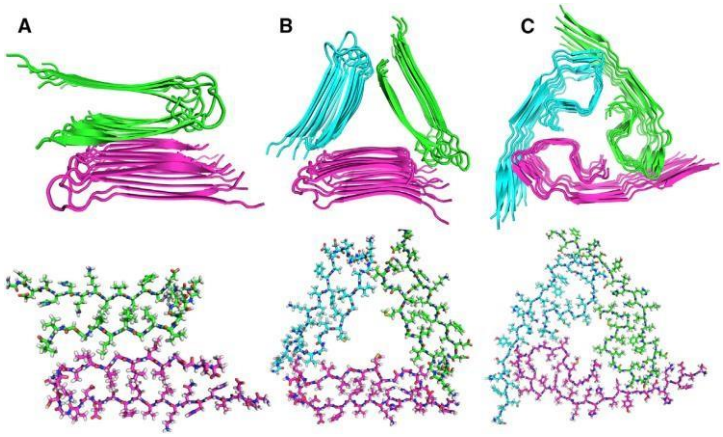

Fig. 6 *(A) Fibrils grown in vitro: striated ribbon morphology (B) twisted morphology (C) Fibrils derived from brain tissue of a patient with AD. Data from ssNMR and Electron Microscopy.*

The ratio of Aβ40 to Aβ42 is around 5:1 in cerebrospinal fluid of normal individuals [83], the insoluble Aβ in AD brain tissue is frequently predominantly Aβ42 [84].

Aβ42 fibrils prepared in vitro have similar morphologies to Ab40 fibrils, contain parallel b sheets that interact through similar hydrophobic contacts, and may also exist as both 2-fold symmetric and 3-fold symmetric polymorphs [85-89]. Fig. 7 represent the generic motifs for protofibrillar and non-fibrillar intermediates in amyloid formation.

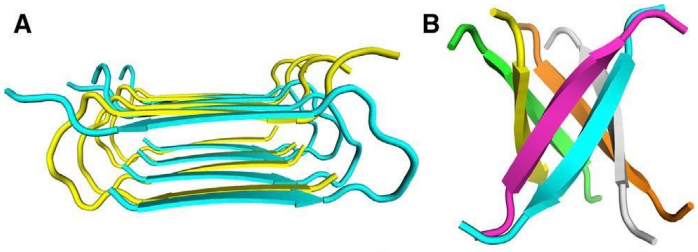

Fig. 7 *Molecular Structural Models for Two Types of Aggregation Intermediates (A) Protofibrils formed antiparallel cross-β structure identified by ssNMR (B) Cylindrin oligomer the 3-fold symmetry axis of the cylindrin lies vertically in the phage.*

CHAPTER 3

Antibodies and Neurobiological Relevance

Several studies indicates that the immune system is involved in the progression of AD, and that particular antibodies may have the potential to serve as diagnostic/prognostic biomarkers for AD. Some may contribute to the pathogenesis of AD, and others may play a protective role, thus facilitating the development of effective immunotherapies for AD.

Autoantibodies against Aβ

Although the pathogenesis of AD is not fully understood, it is widely accepted that accumulation of Aβ in the brain, especially the more amyloidogenic Aβ42, due to overproduction or impaired clearance initiates the pathogenic cascade, ultimately leading to neurodegeneration and dementia [90]. The potential of using Aβ as a blood-based biomarker for AD has been investigated extensively but it technical challenges and the results are inconsistent [91-92]. Earlier studies indicated that AD patients had significantly lower levels of unbound serum Aβ-autoantibodies than healthy age-matched individuals [93-97]. Other studies showed that both AD and control subjects had low and variable concentrations of Aβ-autoantibodies and that neither the presence nor the levels of Aβ-autoantibodies were correlated with the status of AD [98-100]. In circulation, Aβ-autoantibodies may exist either as unbound form or as antigen-antibody complexes, which could affect the capture efficiency for Aβ-autoantibody and the accuracy of assays as well as the sample preparations could also affect the assay resultsand may explain the wide-range of discrepancy in different studies [101]. Using an other approach, Mruthinti et al. observed that the levels of Aβ-autoantibodies were significantly higher in AD patients than in controls [102]. Gruden et al. showed that the levels of autoantibodies reacting with oligomers of a short but neurotoxic fragment of Aβ, Aβ(25-35), were significantly higher in AD patients than in the control group who had undetectable autoantibodies to the Aβ fragment. Further analysis showed that there was a biphasic relationship between autoantibodies to aggregated Aβ(25-35) and the stage of dementia, with the level of

the autoantibodies rising during the mild to moderate phase and then descending within the moderate to severe stage [103].

Using acidic dissociation approach to measure both the bound and unbound antibodies, Gustaw-Rothenberg et al. also observed that the levels of total serum Aβ autoantibodies were significantly higher in AD patients than the aged-matched control subjects [101-104]. However, there are concerns about this acidic dissociation approach as it has been shown that exposure of sera to low pH resulted in partial denaturation of antibodies and caused an artifactual increase in apparent anti-Aβ antibody titers [105]. To further clarify the biomarker value of the bound Aβ-autoantibodies, Maftei et al. developed a new strategy to specifically determine the antigen-bound Aβ-autoantibodies (intact Aβ-IgG immune complexes) in the serum and CSF from AD patients and control subjects [106]. They found that both serum and CSF levels of Aβ-IgG immune complexes were significantly higher in AD patients compared to control subjects. Moreover, the levels of Aβ-autoantibody immune complexes were negatively correlated with the cognitive status across the groups, declining cognitive test performance accompanied by the increasing levels of Aβ- autoantibody complexes [106]. These findings most likely indicate that there is a decrease in clearance of Aβ-IgG immune complexes in AD rather than an increase in the level of free autoantibodies to Aβ. Indeed, consistent with many previous studies, a recent study showed that the levels of unbound autoantibodies to Aβ were significantly reduced in the serum of patients with AD compared to those of healthy controls, especially in individuals over 65 years of age [107].

These studies demonstrate that Aβ-autoantibodies show promise as an effective blood biomarker for AD. However, due to different methodologies, varied sample sizes and disease stages, and the existence of bound and unbound forms, the measurements of Aβ-autoantibodies were highly variable and the conclusions were sometimes inconsistent.

A uniform procedure needs to be applied so that results can be compared across studies with subjects from different populations. The additional value of using the level of Aβ-autoantibodies for diagnosing AD, predicting/tracking disease progression, and monitoring treatment efficacy in a panel of blood- derived biomarkers warrants further investigation.

Conformation dependent monoclonal antibodies

Information of a more qualitative nature about structures of aggregation intermediates has also been obtained from experiments with conformation-dependent antibodies that preferentially recognize definite classes of structures [79-90]. These antibodies have been used to identify the presence of both nonfibrillar and fibrillar oligomers [108-110] in AD brain tissue.

Asa Hatami et. al. [111] have investigated the humoral immune response to Aβ42 fibrils and produced 23 OC-type monoclonal antibodies recognizing distinct epitopes differentially associated with polymorphic structural variants: parallel, in-register β-sheets, antiparallel β-sheets, β-solenoids, β-barrels, and β-cylindrins. These groups share many common properties, some amyloid sequences form polymorphic variants. These mOC antibodies defined at least 18 different immunological profiles represented in amyloid-β (Aβ) aggregates, mainly recognizing amyloid aggregates versus monomers, indicating that they recognized conformational epitopes.

The antibodies that recognized linear Aβ segments reacted with fibrils formed from unrelated amyloid sequences, indicating that reactivity with linear parts of Aβ does not was sequence-specific. The antibodies display altered patterns of immunoreactivity in Alzheimer disease and transgenic mouse brain and recognized spatially and temporally unique amyloid deposits. These results indicated that immune response to Aβ42 fibrils was correlated by the structural polymorphisms in fibrillar amyloid. These polymorphisms may contributed to differences in toxicity and at the effects of pathological processes.

Rakez Kayed et al., [112] immunized rabbits with a morphologically homogeneous population of Aβ42 fibrils and showed that immune serum (OC) recognizes fibrils, but not random coil monomer or prefibrillar oligomers, indicating fibrils display a distinct conformation dependent epitope absent in prefibrillar oligomers. The fibril epitope is also displayed by fibrils of other types of amyloids, indicating that the epitope is a generic feature of the polypeptide backbone. This proved that the fibril specific antibodies were conformation dependent, sequence-independent.

Rakez Kayed et al., [113] have produced several monoclonal antibodies that recognize prefibrillar oligomers and do not recognize amyloid fibrils, monomer or natively folded proteins. Immunological analysis of different prefibrillar Aβ

oligomer preparations showed that structural polymorphisms exist in Aβ prefibrillar oligomers that can be distinguished on the basis of their reactivity with monoclonal antibodies.

The need for conformation-specific antibodies

The biomedical importance of Aβ structural variation, conformation-specific, will play a central role in the future of Alzheimer's research.

Research in humans has shown the clinical relevance of Aβ structural variation. Tissue taken from two Alzheimer's disease patients with distinct clinical histories revealed that each patient had a predominant Aβ fibril structure [115].

Furthermore, the complexity of Aβ structure is correlated with the immune system, the antibodies produced in response to Aβ fibrils are diverse, reflecting their structural variation [114,116]. Considering all the studies, it is becoming increasingly clear that a single antibody will not be enough to study or target all the possible pathological aggregates of Aβ contributing to Alzheimer's disease. This makes conformation-specific Aβ antibodies an essential tool for the future of Alzheimer's disease research [117-120].

CHAPTER 4

Phage display technology

Phage display allows the exposition of several peptides on the surface a filamentous phage M13, which leads to the selection of peptides and proteins, including antibodies, with high affinity and specificity to target. The technology involves the introduction of exogenous peptide sequences into a site in the genome of the phage capsid proteins. The encoded peptides are expressed on the phage surface as a fusion product with one of the phage coat proteins. Random insertion of peptides into the amino-terminal portion of the pVIII major coat protein allows the formation of large molecular libraries, one billion of different exposed peptides, which can be used to discovery "new biomarkers", epitope mapping and sequence selection that can mimic the characteristics of many biological molecules.

M13 Bacteriophage

Several bacteriophage can be utilized for phage display, as the T4, lambda, the filamentous M13 bacteriophage [121]. The M13 phage only infect *Escherichia coli* strains that express the F pilus as the adsorption of the phage to the bacterium needs binding of a phage coat protein to the tip of the F pilus [122]. The phage contains a genome of single-stranded DNA (ssDNA) with a length of 6407 bp [123] that consists of nine genes encoding 11 different proteins. Five of these proteins are coat proteins, and the remaining six proteins are involved in replication and assembly of the phage. The M13 phage has a length of 900 nm and a width of 6.5 nm [124]. The most abundant of the coat proteins is the capsid protein G8P, which forms an envelope of approximately 2700 protein units (Fig.8).

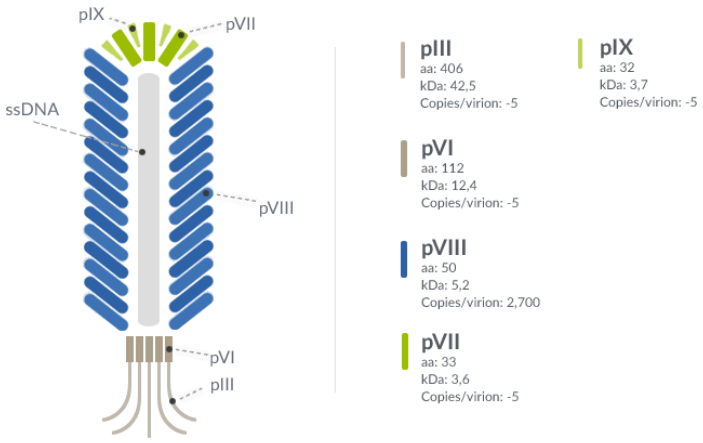

Fig. 8 *Schematic representation of M13 Bacteriophage*

The first step of the M13 infection consists in the the adsorption process, binding of the N2 domain of the G3P coat protein to the F pilus on the surface of *E. coli* [125–127] (Fig. 9). Contact between the G3P-N2 domain and the F pilus mediates the allocation of the G3P-N1 domain and allows it to bind TolA, co-receptor on the surface of the bacterium. Three Tol proteins in E. coli are essential for depolymerization of the phage coat and translocation of the ssDNA into the bacterium. Upon infection, the single stranded (+) chromosome of M13 is converted into the double stranded replicative forme RF. Replication of the M13 chromosome uses the replicative form and carried out by rolling circle replication. The 3′ end that is generated from the nick will then be elongated by DNA polymerase using the (−) strand as a template. G5P binds the ssDNA, dimerizes in a back-to-back conformation leading to the conversion from the circular appearance of the ssDNA to a more rodshaped appearance. The ssDNA bound by the G5P protein determine to phage assembly.

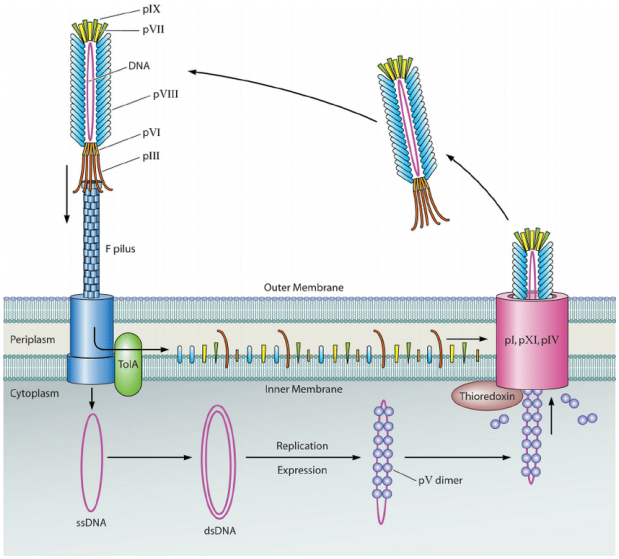

Fig. 9 *Life cycle of Phage M13*

Assembly of the M13 phage particles consists in an complex of pre-initiation formed by G1P, G11P, and G4P that interacting in the periplasmic domains. A multimeric complex of G1P and G10P form a channel [128]. During the elongation step, the G5P bound to the phage genome is replaced with G8P for translocation of the DNA through the membrane-spanning channel. The translocation continues until the phage genome has become completely coated with G8P, at which point G3P and G6P will collaborate in the release of the phage from the bacterium. During pre-termination, membrane-embedded G3Ps complexed with G6Ps are incorporated at the terminal end of the phage particle. Termination involved the realease of the phage, brought about by a conformation in the G3P-G6P compelx [129-131].

Phage display technology step

The key advantage of phage display is the possibility to identify target-binding proteins from a library of zillions of different random peptides without the need to screen each molecule individually. Phage display cycle can be describes in three steps: library creation, biopanning and selected clone analysis.

Library Creation: to construct an phage display library, a phagemid vector pc89 is used for the visualization of peptides on the main coating protein pVIII of the filamentous bacteriophage, in which the expression of the fusion of the peptides on the pVIII is subjected under the control of an unducible promoter. A library is generated by inserting randomly synthesized oligonucleotides “degenerate” near the

N terminus of the pVIII protein. A library contain zillions of DNA clones harboring sequences of interest.

A typical random peptide library has about a $10^{14} – 10^{19}$ different phage clones.

Biopanning: a typical phage library is used for screening through an Biopanning affinity-based. This process involves a repeated series of selection, elution and amplification cycles to isolate phages that expose peptides on the capsid able to interact with a specific target protein (antibody, receptor, enzyme, etc. [132].

Biopanning is characterized by the following stages (Fig.10):

- **Location of the target**: the target on which to carry out the selection can be of different nature and size, in fact it can be represented by protein molecules, peptides, antibody, nucleic acids, carbohydrates, or whole cells of prokaryotic and eukaryotic origin. The immobilization of the target can be carried out in various ways: on a solid support through the biotin-streptavidin interaction, or by passive adhesion on magnetic beads or micro plates. In the case of insoluble materials, biopanning can be performed in a suspension.

- **Interaction with the phage library**: The phage display random peptide library is added to the target present that allows its stability. It is important to start the first cycle with a large and diverse library to have more possibilities to isolate the peptides of interest.

- **Removal of the unbound phage**: at the end of the first cycle of biopanning, between the phage library and the target of interest, phage clones that have not bound will be eliminated, through consequential washes.

- **Elution of the phages binding the target**: following washing to eliminate the unbound phages, the phages that are instead linked to the target of interest will be recovered, through a process called "specific elution" which is generally carried out with solution acids in order to disassemble the bond established between the specific clones, binding the target, and the target itself.

- **Amplification of the related phages**: promotes the multiplication of the selected phages, and therefore the growing number of phage clones that bind to the target at each cycle.

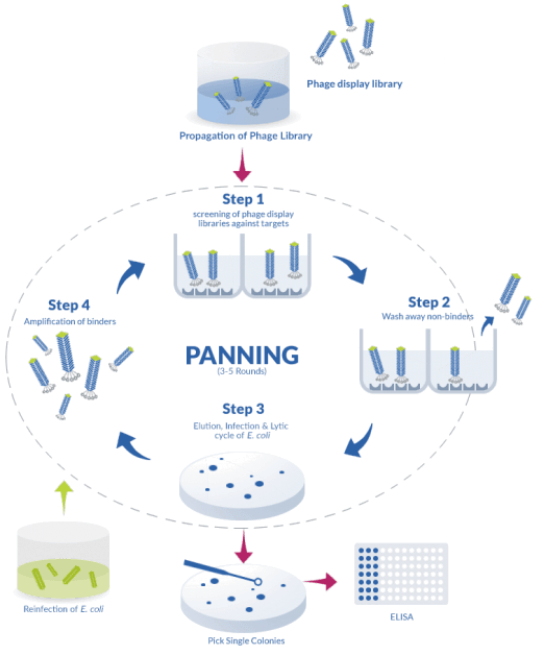

Fig. 10 *Biopanning step*

Screening procedure consists of several rounds of biopanning (generally 2 or 3 rounds) to be carried out before being able to characterize the phage clones and obtained the amino acid sequence of the peptide.

To make a good selection it is necessary to consider two parameters in particular:

-**stringency**: condition in which the most specific peptides are favored during the selection over the less suitable ones.

-**yield**: fraction of viral particles that remains at the end of the selection.

Finally, a step of extraction and subsequent analysis, by Sanger sequencing, of DNA is carried to identify the aminoacid sequences of the foreign peptides displayed by the selected phage clones.

Selected clone analysis

Typically, standard selective tests are the so-called phage enzyme-linked immunosorbent assay (phage-ELISA), immune-screening and/or western blot, these can evaluate the affinity and specificity of individual clones or entire eluate populations after biopanning. Those save the cost of synthesis of peptides which may have been enriched due to artifacts in the screening process described above. Successively, to assure a reasonable significance, 50–100 phage clones should be sequenced and frequency of each amino acid and the distribution in the peptide fragments evaluated. All the data lead to identify the peptides ability and the

contribution in the bound with targets of their amino acids The find peptides can be "epitope", that is the part of a ligand with which the receptor makes specific contact, when show ability against the target. These epitopes will be "continuous," if the sequence motif in the selected peptides matches with the primary amino acid sequence of the natural ligand, or "discontinuous" when carry of critical binding residues that are distant in the primary sequence but close in the folded native conformation. Geysen and colleagues introduced for the first time the term "mimotope" to refer at small peptides that specifically bind a receptor's binding site without matching the natural epitope in the amino acid sequence, considering just cases of these "conformation-dependent" epitopes or where the natural ligand is non proteinaceous [133].

Phage Applications

The phage display technology born for identification novel interacting protein-proteins. In this prospective, phage libraries is used to predicted the potential binding residues that involved in different conditions such as between: bacterial membrane transport proteins; intracellular interactions of distinct protein domains (molecular mapping) [134; 135]; to map epitope involved in specific interaction receptor/antibody or receptor/intrabody [136]. In enzymology, phage display is used to develop modulators positive or negative of both the active and allosteric sites of the enzyme or for structure and function of receptors.

Recently, phage display is applied in the identification of protein and/or amino acid involved in the interaction with inorganic materials [137]. Therefore, phage has been applied in a several fields such as biosensing [138], cellular imaging [139], vaccine development [140] and drug and genedelivery [141].

Moreover, recent advances describe the use of phage display in the discovery of novel bioactive molecules to produce proteins and peptides able to minimize the use of antibodies, antibiotic and cancer drug.

Final Remarks

Applications of phage display technology are being actively explored with the aim of finding and producing numerous and diverse biomarket peptides that may prove useful for basic and clinical research. The use of antibody detection with new phage

diplay procedures would allow them to be exploited in diagnostic practices, targeted therapies improving the basic conditions of numerous diseases. In this context, phage screening can be widely used as a new alternative for treatment and diagnosis in humans.

AIM OF THE THESIS

Alzheimer's Disease (AD) is a chronic and progressive neurodegenerative disease and is characterized by the presence of neurotoxic Aβ plaques in the brain. These plaques are formed by monomeric Aβ spontaneously assembling into soluble oligomers, which cluster together to form insoluble fibrils. The solubility of Aβ, and the quantity of Aβ in different pools, may be more closely related to disease state. The composition of these pools of Aβ reflects different populations of amyloid deposits, and has definite correlates with the clinical status of the patient [142].

It is the most common cause of dementia of the elderly population in developed countries: at present it is estimated that about 5% of the population will be affected over the age of 65 and about 20% of over-85 or older, although in many cases can also occur an early onset around the age of 50.

Currently, the diagnosis of Alzheimer's Disease is based on the analysis of clinical history, neurological examinations and neuropsychological tests.

According to the NINCDS/ADRDA criteria (National Institute of Neurological and Communication Disorders/Alzheimer's Disease and Associated Disease Association), the absence of other symptomatic disorders and a progressive worsening of memory loss are necessary for the correct diagnosis.

To assess changes in a patient's cognitive abilities, neuropsychological tests, such as the Mini-Mental State Examination (MMSE), are widely used. In addition, single photon emission tomography (SPECT) and positron emission tomography (PET) can be very useful in association with mental status assessments. However, a confirmed diagnosis of AD can only be obtained through post-mortem identification of neurofibrillary tangles and/or abnormal plaque deposits in the brain. The confirmatory diagnosis of AD in early stages could facilitate early therapeutic intervention and treatment of the disease.

Many studies have been focused on biomarkers discovery in a non-invasive way in different body fluids, such as cerebrospinal fluid (CSF), saliva, urine and blood. Serum levels of antibodies specifically binding Aβ (Aβ-autoantibodies) in AD and in non-AD control subjects are extensively investigated as potential blood biomarkers applied to AD diagnosis [143-144-145-146].

These results appeared inconsistent due to several factors affecting the detection of specific IgGs against Aβ42, including nonspecific bindings [147], low avidity and

level in serum [148], incorrect diagnosis [149], the circulation of Aβ-autoantibodies both in free and antigen-bound form [150-152], and, not least, the structural conformation of Aβ42 [153].

It has been hypothesized that the inhomogeneity of data about the specificity of the antibodies revealed with the different methods of analysis may depend on the fact that different and distinct variants or multimers of Aβ, involved in AD, can be recognized as conformational antigens, generating antibody populations that remain largely unknown, as well as their specific function. The structural plasticity of amyloid is partially based on its polymorphism, the ability to form aggregates of different structures [154-156]. The different deposition of Aβ-42 in size, shape and structure different from the native form, could generate discontinuous and conformational epitopes.

Consequently, during the immune response, antibodies could be directed not only against the primary structure of the protein, but also against its misfolding.

Many of the antisera and monoclonal antibodies produced against oligomeric and fibrillar forms of Aβ-42 are directed against conformation specific epitopes that are specifically associated with the aggregated state and are absent in normal proteins [157-160]. Conformation-dependent antibodies have been reported to recognize a generic epitope that is specific to many types of amyloid fibrils and not soluble monomer regardless of their sequences [161,162].

It has been investigated [114] the humoral immune response against Aβ-42 fibrils and it has been reported that 23 different OC-type monoclonal (mOC) antibodies, recognizing distinct epitopes differentially associated with polymorphic structural variants, were produced. These mOC antibodies define at least 18 different immunological profiles represented in aggregates of Aβ. All of the antibodies strongly prefer amyloid aggregates over monomer, indicating that they recognize conformational epitopes. It is possible to hypothesize that different aggregational states are also present in patients with AD and that these evoke a conformation-dependent antibody response.

However, it is not possible to precisely define the aggregation state of the protein and its misfolding. About that, various possible conformational misfondings of proteins similar to Aβ already present have been searched, eg. in bacterial proteins.

Thus, in our work [163] a set of proteins having conformational motifs homologous to Aβ-42 through bioinformatics tools have been screened. Among microbial proteins, the epitopic region of *Yersinia pestis* F1 capsular antigen (Caf 1) showed the most significant structural homology with the fibrillar form of Aβ. In order to search for IgG autoantibodies in AD sera against a potential "generic conformational antigen" of Aβ-42 in *vivo* and to evaluate the possibility to use them as state/stage biomarkers of AD, monoclonal antibodies directed against Caf 1 were used in alternate biopanning cycles, the so-called "double binding" phage display selection. Thanks to the phage display technology it is possible to select "conformational mimotopes" that can be recognized by conformation-dependent antibodies. It uses engineered M13 filamentous bacteriophage, in which the major coat protein pVIII (2700 copies) displays a foreign peptide specific for a target.

The reactivity of the phage clones isolated were evaluated in ELISA assay against monoclonal Ab that recognized Caf1 of *Y. pestis* and IgGs of AD-patients. From the selected clones, one clone, named 12III1, detected a significant level of IgG for discrimination between AD and non-AD subjects. Furthermore, this phage clone was able to interfere with Aβ-42 fibrillation *in vitro* and to promote its disaggregation in SH-SY5Y cells.

The data obtained suggested that the peptides displayed, although selected also by the monoclonal antibody specific for Caf1, probably mimicked several conformational epitopes recognized by circulating IgG from patients with AD. Thus, in order to investigate the immune response for a state/stage diagnosis of AD, different phage clones resulting from the same double binding selection were investigated. The ability to interact with amyloid plaques in AD mouse brain sections with high significance, confirmed that the peptides were amyloid mimotopes recognized by conformation-dependent antibodies.

Thus, to detect conformational antibodies present in the different stages and states of the disease, the peptides were used in a new combinatorial diagnostic micro-array besed on Phage mediated Immuno PCR CDC Biochip, able to discriminate AD from healthy sera.

The data would pave the way for the use of these Aβ-42 conformational mimotopes to determine the status and stage of AD. This could be very useful for a personalized

pharmacological treatment, avoiding the progression of the disease. Since these peptides were able to interact with amyloid plaques in brain sections, they could also be used as detection probes for imaging. Furthemore, their ability to interact and disaggregate Aβ-42 fibrils could lead to their use in therapeutic practices.

Workflow of thesis:

I. **Conformation dependent antibodies research**

II. **Double binding phage display selection**

III. **Phage ability to interact with Aβ42 *in vitro* test**

IV. **E*x-vivo* immunostaining analysis**

V. **Phage diplay mediated Immuno PCR for Alzheimer's diagnosis**

VI. **Microarray system in CDC-Biochip**

E.S. - EXPERIMENTAL SECTION

I. Conformation dependent antibodies

AD is associated with misfolding and aggregation states of Aβ-42. Significant structural polymorphism among fibrillar amyloid aggregates are thought to be responsible for the brain degeneration observed in AD patients [164-167].

On the other hand, conformation dependent antibodies have been reported to recognize a generic epitope common to amyloid fibrils regardless of their amino acid sequences, as they also bind other disease related amyloid fibrils and amyloid like aggregates derived from other proteins of unrelated sequence. These antibodies do not bind the native amyloid protein precursors, nor other kinds of protein aggregates, indicating that fibrils display a distinct conformation dependent and sequence independent epitope that is absent in prefibrillar oligomers. In addition, similar amyloid oligomer conformations were found in several bacterial proteins resulting immune positive to conformation dependent antibodies.

At this purpose, conformational mimotopes in unrelated amyloidogenic proteins able to recognize IgG autoantibodies in AD sera against a potential "generic conformational antigen" of Aβ-42 were searched. Among microbial proteins, suitable "surrogates of Aβ 42" were screened by bioinformatics tools.

E.S. I.1 Conformational similarities research by tool bioinformatics

"Conformational similarities" between different forms of Aβ-42 and other amyloid-like proteins have been screened using bioinformatics tools.

Template proteins were searched among proteins with similar conformation or self-assembly, using UniProtKB tool (https://www.uniprot.org/). For the structural similarity, structures having a β strand, basic component of amyloid have been searched. Then it has been started: i) field: UniProtKB AC Term: beta strand. ii) field: structure; 3D structure available. iii) field: NOT Homo sapiens (Human) [9606]. iv)field: binary interaction. v) field: NOT function Function CC, enzyme classification, activity regulation, catalytic activity. The use of UniProtKB tool has allowed the identification of 47 proteins.

From selected proteins, F1 capsule antigen (UNIPROT ID: P26948) was considered to the following steps in 3D alignment recognition to verify the match with Aβ amyloid structures.

First of all, amino acid sequences of Aβ-42 and F1 antigen were aligned using Clustal X2.167 (Gonnet 250 Protein Weight Matrix, Gap opening 10, Gap extend 0.1) tool to identify similar regions based on physico-chemical properties of side chain amino acids.

Then, alignment of 3D protein structure was performed to verify the conformational match of F1 protein with Aβ amyloid structures. The PDB IDs associated to 3D structure of the F1 capsule antigen (1p5u, 1z9s, 3dos, 3dpb, 3dsn) were obtained from Uniprot KB, through the ENTRY code P26948 and excluding those which were not in the mature conformation.

EMBL-EBI tool was used in PDB&fold section (http://www.ebi.ac.uk/msd-srv/ssm/), setting SSM submission form to obtain the alignment with all the structures. The 3D alignment with Aβ amyloid in fibril form (PDB ID 2nao) was carried out using Sequence & Structure Alignment tool available in https://www.rcsb.org/pages/analyze_features#Sequence, with algorithm JFATCAT rigid.

R.S. Results Section

Bioinformatics analyses

Using UniProtKB 47 proteins were identified.

Among them, the Caf1 of *Yersinia pestis* F1 antigen (UNIPROT ID:P26948) was chosen as target of analysis in 3D alignment to verify the conformational match with Aβ amyloid structures.

Caf1 is a beta-structural protein that in the polymeric form has very high conformational stability. The 2.2 Å resolution crystal structure of the ternary Caf1M:Caf1:Caf1N complex revealed that Caf1 is an incomplete β-sandwich immunoglobulin-like fold. The final stable fold is the result of replacement of the chaperone parallel β-strand by the "spare" anti-parallel β-strand from the N terminus of the subsequent subunit, thus linking them to form a chain. Similarly, it is known that the 3D structure of the Aβ-42 protofilament is formed by two stacked, intermolecular, parallel, in-register β-sheets that perpetuate along the fibril axis [168]. A recent study by cryo–electron microscopy to 4-Å resolution, complemented by solid-state nuclear magnetic resonance experiments, showed the β strands are staggered with relation to one another in a zipper-like manner [169]. On the other hand, it is well known that Aβ exists in several polymorphs with varying width and helical pitch, different cross-section profiles and different interactions between the monomers.

Linear alignment between the F1 protein and Aβ-42 was initially conducted. On Caf1 the regions mainly involved in alignment (Fig. 11) fall within two B (84-101; 121-144) and one T (102-116) cell epitopes, the immunodominant and highly immunogenic sequences of F1 protein, which is recognized by a high amount of antibodies raised against the native F1 antigen [170,171].

The other regions involved in the alignment were on Aβ(1–16), epitopic for immunoglobulins and involved in the formation of proto-filaments [172,173], and the region Aβ (21–37), recognized by "fibril-inhibiting" Aβ-autoantibodies [174,175]. Moreover, it is known that Aβ (4–10) is epitopic for "plaque-specific" antibodies inhibiting both Aβ fibrillogenesis and cytotoxicity [176,177].

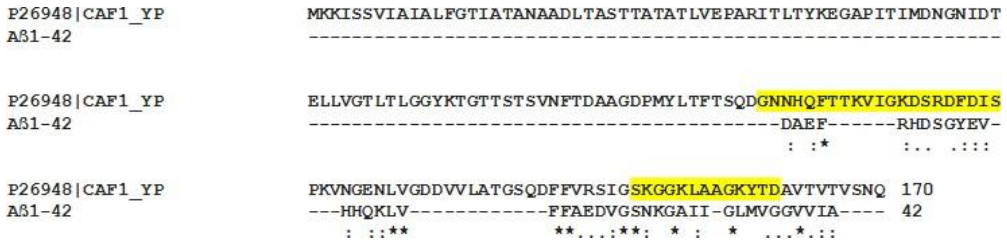

Fig.11 *Sequence alignment between Aß42 and Caf1 by Clustal X2.1*

In particular, the sequence overlap between the C-terminal of β amyloid and the immunodominant region of Caf1 observed in linear alignment (50% similarity, 29% identity) concerned the GxxxG, GxxxxG and GxxxxA repeating motifs [178] (Fig. 11), which conferred the particular conformation to the proteins and are recently demonstrated as primarily responsible for both Aβ self-assembly and neurotoxicity [179].

Conformational similarity analyses were then conducted, based on identifying residues occupying an equivalent geometric shape in space.

3D structure similarity analyses confirmed that conformational alignment fell within the same immunodominant region as evoked by the primary sequence alignment.

In addition, RCSB Sequence & Structure Alignment tool was used in order to perform the 3D alignment of fibrillar amyloid (PDB ID 2nao) with the single specific chains of F1 antigen (identified by PDB identification numbers 1p5u, 1z9s, 3dos, 3dpb, 3dsn) (Fig. 12). The Aβ-42 regions involved in 3D alignment are the following: 18-VFFAEDVGSNKGAIIGLM-35 (with 1p5u.C, 3dsn.C), 9-GYEVHHQKLVFFAE-22 (with 1z9s.C, 3dpb.C) and 1-DAEF--------RHDSGYEVHHQKLVFFAE-22 (with 3dos.C). Intriguingly, on Caf1, in all the PDB analyzed, conformational alignment with Aβ-42 fibril falls within the immunodominant region (from 121-F to 143-T).

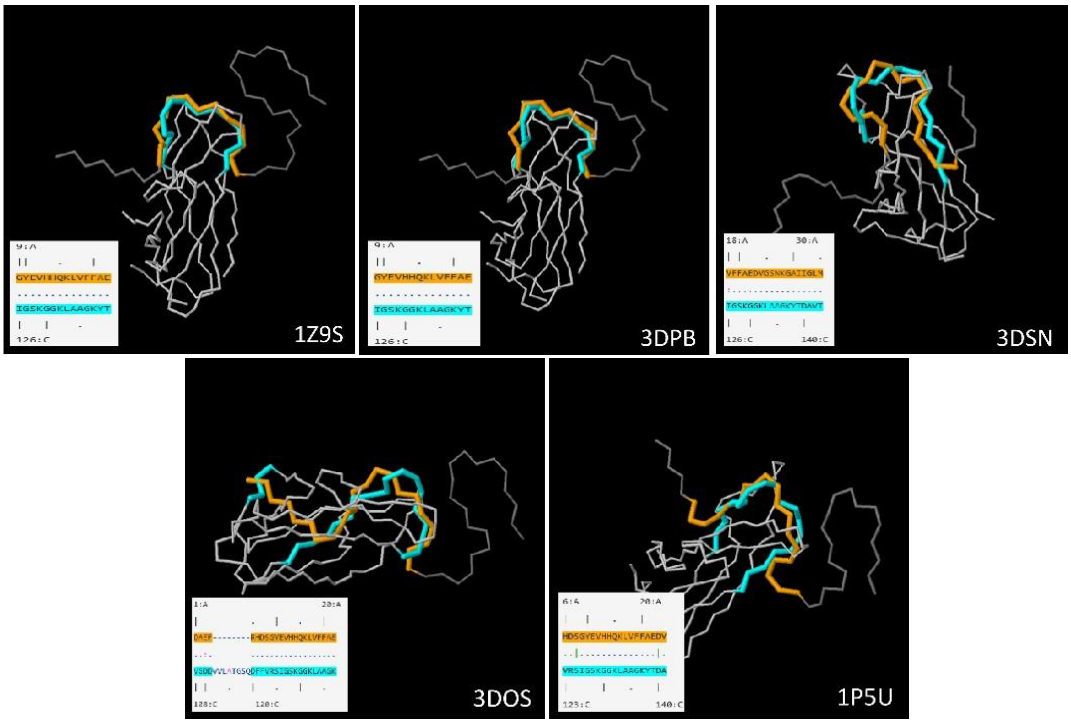

Fig. 12 *Alignment of Amyloid fibrils (PDB ID 2nao) with F1 capsule antigen using "Sequence and Structure Alignment" (https://www.rcsb.org/pages/analyze_features#Sequence)- algorithm JFATCAT rigid*

The conformational homology found between the different forms assumed by Caf1 and Aβ-42 fibrils confirmed the non-probability that these were randomly similar. Based on the bioinformatic analysis, F1 was considered as a protein with an amyloid oligomeric conformation such as the Aβ-42 protein. Moreover, a monoclonal antibody - mAb-YPF19 - of *Y. pestis* recognized the common trait of interest between the immunodominant regions of Caf1 and Aβ-42.

II. "Double binding" phage display selection

It is known that antibody ligands with structures partly or completely similar to the native antigen can be isolated by phage display library screening. In this section, peptide libraries have been successfully screened for "**conformational mimotopes**" that bind to target-specific antibodies.

pVIII M13 phage display libraries were then screened against anti-Caf1 monoclonal antibody, and against IgGs of AD-patients, in alternate biopanning cycles of a so-called "**double binding**" selection. In the first round, the phage library was screened against the monoclonal Ab that recognized Caf1 to select specific mimotopes of the Caf1 and any "conformational antigens". Then eluted phages were used in the second round against a pool of sera from patients' AD, in order to select only "common" conformational mimotopes. A third round was carried out, with the eluted phages from the second selection round, against the mAbYPF19 again, and finally a fourth against IgG-AD, in order to select phage pools having more affinity for the latter. [*International patent application has been advanced No. PCT/IB2017/057422 Nov 27, 2017: Distretto Tecnologico Sicilia Micro e Nano Sistemi S.C.A.R.L. "Conformational mimotopes for detecting specific antibodies" (IT/28.11.16/ITA102016000012020]*.

E.S. II.1 Phage M13 libraries

Phage M13 libraries were used, kindly donated by Prof. Franco Felici, expressing random peptides, exposed on the pVIII protein, based on the phagemid vector pC89 on which random oligonucleotide sequences were inserted in the region 5' of the VIII gene present in the vector, under the control of the LacZ promoter. The digestion with the restriction enzymes EcoRI and BamHI linearized the vector and allowed the insertion of the oligonucleotides with random sequences which, flanked by the same restriction sites, allow the recircularization of the vector through ligase reaction. For the selection, four types of peptide libraries were used, expressing twelve amino acids in the pVIII amino terminus region: pVIII-12aa and pVIII-12aa-cys, and nine amino acids in the pVIII amino terminus region: pVIII-9aa and pVIII-9aa-cys, wherein the latter have a cysteine-cysteine constriction expressed in the peptide, so

as to stabilize the structure thereof. The amplitude of each library is comprised between 10 and 100 million independent clones.

II.2 "Double binding" phage display selection

The epitopic region of *Yersinia pestis* F1 capsular antigen (Caf 1) showed the most significant structural homology with the fibrillar form of Aβ. This portion was recognized by a monoclonal antibody mAb-YPF19, that recognized only this specific portion of *Y.pestis* and not other species such as *Y. enterocolitica* and *Y. pseudotubercolosis*. Then, a "**double binding**" biopanning screening of pVIII M13 phage display libraries was applied, using a monoclonal antibody against Caf 1 and a pool of AD sera, to identify a "common conformational" peptide to be used as target for serum circulating IgGs of AD patients.

Libraries were screened against antibodies immobilized on paramagnetic beads. Phages binding the targets were eluted and amplified in the bacterial host and reused in the next phage display biopanning cycle, as described in the following:

Table 1. *Double binding selection*

I ROUND (against mAb-YPF19)	Libraries were screened against mAb-YPF19 to Select "**specific mimotopes**" and any "**conformational antigens**" of Caf1
II ROUND (against IgGs-AD sera)	The eluted phages (restricted Caf1 library) were used against IgGs of AD sera to select only "**common conformational mimotopes**"
III ROUND (against mAb-YPF19)	The eluted phages were used again against mAb-YPF19 to improve the recognition of "**common conformational mimotopes**"
IV ROUND (against IgGs-AD sera)	The eluted phages were used again against IgGs from AD sera, in order to select phage clone pools having the **most affinity for AD IgGs**

As a source of antibodies directed against possible conformational epitopes of human polymorphic beta-amyloid 1-42 (Aβ42 a pool of 5 human sera from patients with AD (IgGAD) (mean age of 77.4 years, mean value of MMSE = 15.2) has been used. On the other hand, the monoclonal antibody YPF19 (AbDSerotec® A Bio-Rad Company, IgG1-9820-5007) anti-*Yersinia pestis* F1 (reacting to *Y. pestis* F1 capsular antigen, Uniprot code P26948) was used to screen for putative conformational

mimotopes homologous to Caf1 of *Yersinia pestis* which results to be of interest in the conformational structure similarity with Aβ-42 as evoked by bioinformatics analysis.

For the immobilization of the antibodies, Dynabeads® Protein G (Thermo Fisher scientific) superparamagnetic beads of 2.8 μm were used. Buffers and reagents were purchased at Sigma Aldrich. 50 μl of Dynabeads® Protein G were washed 3 times with citrate-phosphate buffer under stirring for 10', separated with a magnetic device for 1-2', then incubated with respective sera pools containing IgG-AD diluted 1:10 and 5 μg of mAbYPF19, for 60' at room temperature (RT) under mild stirring.

Dynabeads, functionalized with IgG-AD (DYN-IgG-AD) or mAbYPF19 (DYN-mAbYPF19), were separated with a magnetic device for 2', washed 4 times with Conjugation Buffer (20 mM sodium phosphate, 0.15 M NaCl, pH 7-9), separated with a magnetic device for 2' and resuspended in 250 μl of 5 mM BS3 (bis (sulfosuccinimidyl) suberate) at RT for 30'. Cross-linking reaction was blocked by adding 12.5 μl of Quenching Buffer, from 25 mM to 60 mM Tris, incubated at room temperature for 15' with inclination/rotation. DYN-IgG-AD and DYN-mAbYPF19 were washed 3 times with 200 μl PBST and finally resuspended in 1 ml of storage solution (PBS + 1% BSA + 0.01% Tween 20 pH 7.4). Before using for phage display selection, beads were blocked for 1 h at room temperature with PBS pH 7.4-5% not fat milk-0.05% Tween 20.

II.3 Biopanning

100 μl of each library (1×10^{12} viral particles) were added to 50 μl of Dynabeads® Protein G and resuspended in 190 μl of TBS-Tween 0.1%. After 30' incubation, separate with a magnetic device for 1-2'; the supernatant is recovered and used to carry out again the two preceding steps twice before the use of the library for the selection.

In the first round of selection, 500μl of DYN-mAb YPF19 were incubated with 100 μl of each of the four phage libraries with a titer of 10^{12} for 3-4 h at room temperature under mild stirring. The beads were washed 3 times in PBS-0.05% Tween 20 and separated with a magnetic device for 1-2' to eliminate supernatants containing unbound phages. Selected phage clones were eluted from antibodies with 500 μl of eluting buffer, 0.2 M of glycine-HCl (pH 2.2) + 0.1% BSA, neutralized

immediately with 1 M Tris–HCl pH 9.6. The enriched phage pools were amplified by infecting TG1 *E. coli*, purified twice by PEG precipitation, titrated and used as the input for further panning. Biopanning affinity selection was repeated in the second round against DYNIgG- AD, then in the third round against DYN-mAb YPF19 again, and finally a fourth selection round was carried out as the second one.

II.4 Phage amplification

In order to exploit the phage clones in the experimental plan, these were amplified and then quantized in phage titration (TU/mL). Tenfold serial dilutions of M13 or engineered phage clones were dispensed in 90 µL of *E. coli* TG1 cultures. Then, incubated at 37 ℃ for 15 min in static condition and for 20 min in shaking (250 rpm) conditions. 100 µL of each engineered phage clones/*E. coli* TG1 suspension were dispensed into Luria-Bertani medium containing ampicillin (50 µg/mL) agar plates. All plates were incubated at 37 ℃ overnight. Plates that had between 30–300 colonies were considered, and the phage concentration was determined as Transducing Unit per milliliter (TU/mL), according the following equation (1):

$$\mathrm{TU} = \frac{(\text{number of colonies})}{\text{volume (0.1 ml)} \times \text{dilution factor}} \qquad \text{(Equation 1)}$$

II.5 M13 phage production

The protocol used is according to Kay et al. (1996), with some modification for our conditions. Briefly, a culture of *E. coli* strain TG1 (Kan-, Amp-, lacZ-) at OD_{600} = 0.7 was infected with M13K07 (Kan+), then incubated at 37 ℃ in static condition for 15 min, followed by shaking (250 rpm) for 20 min. The cells were collected by centrifugation, at 8000 x *g* for 15 min, transferred in 500 mL of Luria–Bertani (LB, Oxoid) medium containing kanamycin (100 µg/mL). Phages were produced by growing the culture overnight (o.n.) with shaking at 37 ℃. The infected culture was centrifuged at 8000 × *g* for 20 min at 25 ℃. The supernatant was mixed with 25% (v/v) of PEG/NaCl solution, containing 200 g PEG-8000 (polyethylene glycol; Sigma) and 150 g NaCl per liter, cooled in ice for 4 h and precipitated by centrifugation, at 15000 × *g*, for 45 min at 4 ℃. The pellet was resuspended in 10% (v/v) of TRIS buffered saline (TBS, 7.88 g/L of Tris hydrochloride and 8.77 g/L of NaCl in deionized water), mixed again with 25% (v/v) of PEG/NaCl, cooled in ice

for 4h, and the solution was centrifuged as above. The pellet, containing phage particles, was suspended in 10% (v/v) of TBS, filtered through 0.22 μm- pore size membrane (Millipore), and stored at 4 °C.

II.6 Engineered phage clone production

Protocol used is according to Kay et al. (1996), with some modification for our conditions. *E. coli* strain TG1 (Kan-, Amp-, lacZ-) broth culture (OD_{600}= 0.7) was infected with engineered phage clone (Amp+), then incubated at 37 °C in static condition for 15 min, followed by shaking (250 rpm) for 20 min. After incubation, suitable aliquots of culture were plated onto agarized Luria–Bertani (agar 20 g/L) plates containing ampicillin (50 μg/mL) and incubated at 37 °C in static condition. One colony of *E. coli* strain TG1, containing phage clones, was inoculated into 10 mL of LB medium containing ampicillin (50 μg/mL) and incubated at 37 °C with shaking (250 rpm) until reaching OD_{600}= 0.2. Then, the culture was added with isopropylthio-β-galactoside (IPTG, 40 μg/mL) and helper phage M13K07 (Kan+) (10^9 TU/mL), incubated at 37 °C in static condition for 30 min, and gently shaken for 30 min. The cells were harvested by centrifugation at 8000 x*g*, transferred to 500 mL of LB medium containing ampicillin (50 μg/mL) and kanamycin (10 μg/mL), and incubated overnight with shaking at 37 °C. The infected culture was centrifuged 8000 × *g* for 20 min at 25 °C, the supernatant was then mixed with 25% (v/v) of PEG/NaCl solution, cooled in ice for 4h, and precipitated by centrifugation at 15000 × *g* for 45 min at 4 °C. The pellet was resuspended in 10% (v/v) of TBS, mixed again with 25% (v/v) of PEG/NaCl, cooled in ice for 4 h, and the solution was centrifuged as above. The pellet, containing phage particles, was suspended in 10% (v/v) of TBS, filtered through 0.22 μm-pore size membrane, and stored at 4 °C.

II.7 Reactivity of phage clones isolated

The reactivity of phage clones isolated were evaluated in ELISA assay with YPf19 and IgG-AD.

10^{12} TU/ml phage preparations were dispensed in duplicate (100 μl/well) into a 96-well microtiter plate (Multisorp, Nunc, Roskilde, Denmark). Plates were left overnight at 4°C, blocked for 2 h at room temperature with blocking buffer (PBS - Tween 20 0.05% - 6% Not Fat milk), and washed in PBS-0.05% Tween 20. 100 μl of

mAb YPF19 diluted 1:100 in dilution buffer (PBS - Tween 20 0.1% - 1% Not Fat milk) or 100 µl of AD sera pool diluted 1:50 in dilution buffer were added in duplicate into wells and incubated 1 h at 37°C under stirring. The plates were washed 10 times as described above and exposed to (HRP)-conjugated anti-human IgG (IgG Fc AP113P) diluted 1:15000 in dilution buffer, or anti-mouse diluted 1:50000, for 1 h at 37°C under stirring. The plates were washed 5 times as described above and developed with TMB substrate, incubating in the dark for 30'-45' at room temperature, and stopped with 100 µl of 1N HCl. Optical absorbance was recorded at 450 nm (Labsystem Multiskan Bichromatic). TBS was used as a negative control (antigen non-coated wells) for the evaluation of the background noise reaction caused by hydrophobic binding of immunoglobulin components in sample specimens to solid surfaces. Wild-type vector pC89 (containing no insert) was used as an internal control for evaluation of nonspecific binding through M13 coat proteins interaction [163].

II.8 Sequence analysis of selected phage clones

The selected clones which simultaneously show greater reactivity against the two antibody categories, IgG present in the serum of AD subjects and mAbYPF19 (specific monoclonal antibody for the identified protein F1 capsular antigen having a high conformational similarity degree for fibrillar Aβ42), were amplified and sequenced to determine the amino acid sequences of the displayed peptides.

The sequencing primers M13-40Rev (5'-GTTTTCCCAGTCACGAC-3') and E24Fw (5'- GCTACCCTCGTTCCGATGCTGTC-3') were obtained from Proligo, Sigma (Milan, Italy). A sample (1µl) of the suspended colony was added to the PCR reaction tube, containing 49 µl of PCR mixture. The mix was then denatured in a thermal cycler for 10' at 95°C, and then 0.25 µl of my TAQ were added. Each sample was subjected to the following PCR cycles: 4' at 94°C; 25 cycles of: 30" 94°C/ 30" 52°C/ 30" 72°C; 7' 72°C. PCR products were analyzed by agarose gel electrophoresis (1%, w/v agarose, Sigma, Milan, Italy), and 35 µl were purified with the extraction Kit Nucleo Spin® (Macherey-Nagel), and sequenced by DNA sequencing service of BMR Genomics (Padova, Italy) using the primer M13-40Rev. The DNA sequences were translated into amino acids by using the "translate" program on the proteomics server of Swiss Institute of Bioinformatics Expert Protein

Analysis System (ExPASy http://www.expasy.ch/). Sequence alignments were performed by using the CLUSTAL X sequence alignment program (available at http://www.ebi.ac.uk/clustalw/). GeneDoc (http://www.psc.edu/biomed/genedoc/) was used as a tool for visualizing, editing, and analyzing multiple sequence alignments of the peptides. Each cluster of similar peptides was then aligned as a group with the amino acid sequence of F1 antigen and Aβ42 to identify regions with amino acid composition similar to that of the peptides.

II.9 Peptide analysis: functional motif and % epitopicity

The individual peptides exposed by the phage have been screened for a study of the functional motif and their degree of epitopicity. The functional significance of the motifs has been highlighted as the repeated presence of the typical traits present in many neurofibrillary isoforms described in AD, as well as in terms of amino acid residues involved in the formation of sheet structures in amyloids.

The degree of epitopicity was assessed using the bioinformatic tool LBtope: Prediction of Linear B-cell Epitopes, a web server LBtope for predicting and designing B-cell epitopes (https://webs.iiitd.edu.in/raghava/lbtope/mutant.php). In particular, Prediction of Epitopes in Mutated Peptides has been used. This module generate all possible mutants of a peptide. It also predicts B-cell epitope in these peptide mutants. This subroutine is important for identification of minimum mutation in a peptide in order to make it strong B-cell epitope.

Furthermore, to correlate the degree of epitopicity of the individual peptides with the regions of the Aβ, the amino acid sequences in FASTA format were aligned through ClustalW multiple sequence alignment program. It has been provided an integrated environment for performing multiple sequence and profile alignments and analyzing the results. The sequence alignment has been displayed in a window on the screen. A versatile coloring scheme has been incorporated allowing to highlight conserved features in the alignment.

R.S. Results Section

"Double-binding" phage-display selection

Antibodies-associated phages isolated in each biopanning cycle were separately amplified in *E. coli* strain TG1 and used for subsequent rounds of selection. The yield of phage eluted from each round of selection is shown in table 2(a-b).

Table 2. Yields of "double-binding" selection of M13 pVIII-9aa and pVIII-9aa-cys (a), pVIII-12aa, pVIII-12aa-cys (b) phage display libraries.

	9aa-cys			9aa		
	IN[a]	**OUT[b]**	**YIELD[c]**	**IN[a]**	**OUT[b]**	**YIELD[c]**
I ROUND	$2.5x10^{11}$	$3.3x10^{6}$	$1.32x10^{-5}$	$7x10^{12}$	$5x10^{7}$	$7.14x10^{-6}$
II ROUND	$1.65x10^{13}$	$2.45x10^{7}$	$1.48x10^{-6}$	$1.85x10^{13}$	$3.25x10^{7}$	$1.76x10^{-6}$
III ROUND	$3.25x10^{12}$	$1x10^{8}$	$3.08x10^{-5}$	$5.75x10^{12}$	$5x10^{7}$	$8.7x10^{-6}$
IV ROUND	$2x10^{12}$	$2.75x10^{9}$	$1.38x10^{-3}$	$6.5x10^{12}$	$2x10^{8}$	$3.08x10^{-5}$
	12aa-cys			**12aa**		
	IN[a]	**OUT[b]**	**YIELD[c]**	**IN[a]**	**OUT[b]**	**YIELD[c]**
I ROUND	$3.5x10^{12}$	$3.3x10^{7}$	$9.43x10^{-6}$	$1.5x10^{12}$	$1.3x10^{7}$	$8.67x10^{-6}$
II ROUND	$1.45x10^{13}$	$4.2x10^{9}$	$2.9x10^{-4}$	$1.7x10^{13}$	$2.65x10^{9}$	$1.56x10^{-4}$
III ROUND	$3.6x10^{12}$	$3.65x10^{8}$	$1.01x10^{-4}$	$5.32x10^{12}$	$8.25x10^{8}$	$1.55x10^{-4}$
IV ROUND	$8.75x10^{12}$	$2.75x10^{9}$	$3.14x10^{-4}$	$1.8x10^{12}$	$1.5x10^{9}$	$8.33x10^{-4}$

[a] Input quantity of engineered bacteriophages at the start of the biopanning process
[b] Quantity of phage recovered at the end of each selection round
[c] Input to output ratio to indicate the number of bacteriophages remained bound to the selection target

Phage clones selected from the eluted phage population of each library were tested in indirect ELISA assays using both mAb YPF19 and AD sera. The phage clones 12aa-cys and 12-aa resulted the most reactive. From the 9aa and 9cys-aa library, no reactive clones were selected after double binding. Probably, the shorter peptide did not allow for conformational stability, as observed with 12aa peptides. On the other hand, pC89 wildtype vector showed a very low reactivity against both mAb YPF19 and human sera (Fig. 13), suggesting that the displayed peptides, likely mimicking conformational epitopes, are recognized by circulating IgGs from AD patients but also by the monoclonal antibody specific for Caf1.

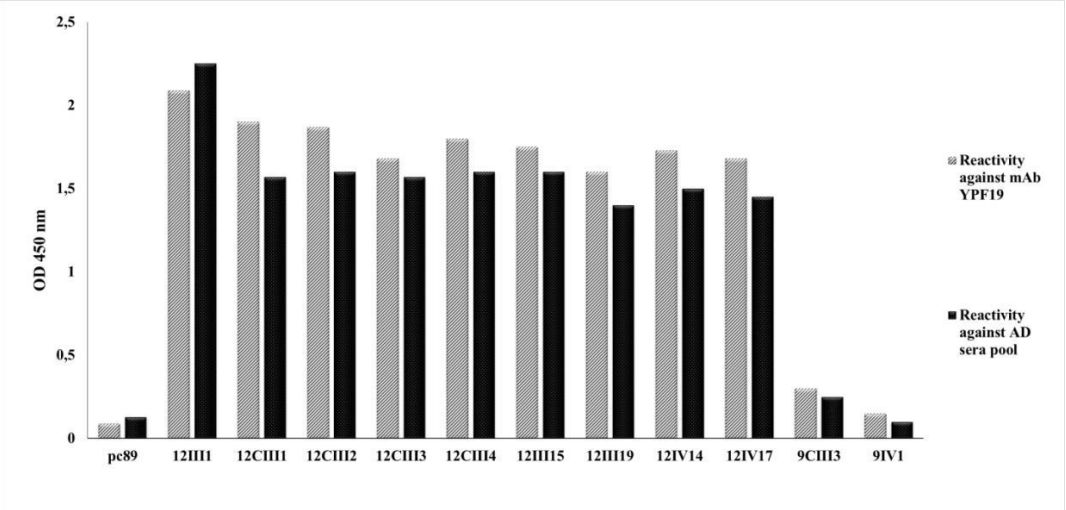

Fig. 13 *ELISA reactivity of phage clones isolated by "double binding" selection against mAb YPF19 and pool of AD sera*

Peptide analysis of selected phage clones

After sequencing the selected phage clones, the nucleotide sequences were converted in aminoacids sequence. In order to find typical traits present in neurofibrillar isoforms described in AD, as well as amino acids involved in the formation of sheet structures in amyloids, a screening on the peptide was performed. The sequences of the phage clones obtained by double binding selection, are shown in table 3.

Table 3. *The peptides of the phage clones sequenced*

Phage clones	Phage peptide (motif)
12III1	RWPPHFEWHFDD
12CIII1/12CIII2	GGGCIEGPCLEG
12CIII3	WVGCHGEWCGVW
12CIII4	HRGCIEGPCLDA
12III15/12III19	WEYDRYRGWHIG
12IV14/12IV17	GGHWEWHADYNL
9CIII3	YRPSAGWIE
9IV1	YNTIPSRRV

Interestingly, the peptides showed peculiar functional motifs, e.g. in clone 12III1 e 12IV14 presented the epitope EFRH, which acts as a regulatory site controlling both the formation and disaggregation process of the Aβ fibrils [180]. In clone 12CIII1, 12CIII3, 12CIII4 the GxxxG, GxxxxG and GxxxxA repeating motifs were present [178]. The aminoacid motif GxxxG within the APP transmembrane sequence has a regulatory impact on the Aβ species produced. In a neuronal cells system, mutations

of residues of the GxxxG motif reduce the formation of Aβ-42 [181]. In clone 12III15 were present both. In 9IV1, a functional motif correlated at Aβ was not present.

Thus, the 12III1, 12CIII1, 12III15 and 9IV1 clone sequences, on the Aβ-42 sequence on the Caf1 sequence, were aligned as model (Fig. 14).

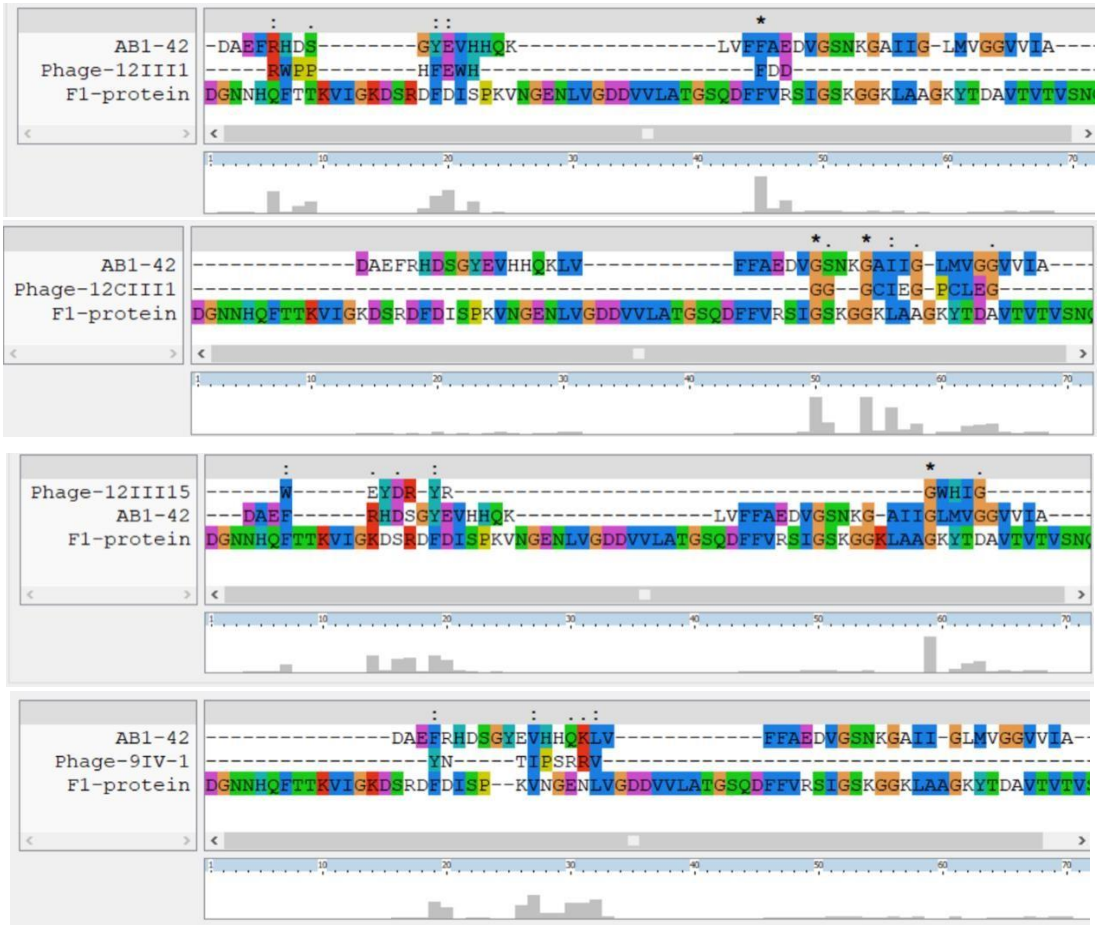

Fig. 14 *Sequence alignment (A)12III1(B)12CIII1(C)12III15 (D)9IV1 pepide-Aβ42-Caf1 by Clustal X2.1*

Although the clones 12III1, 12CIII1 and 12II15 aligned partially on the epitopic region 1-DAEFRHDSGYEVHHQK-16 in the Aβ-42 and in immunodominant region 126-IGSKGGKLAAGKYTDAVT-143 of the F1 protein, no clone had a specific native sequence identity. Consequently, the antibody recognition (by double binding selection) was referable to the conformational epitope, regardless of its linear structure.

III. Phage ability to interact with Aβ42 in vitro *test*

Fibrillation of Aβ implies self-aggregation of monomers. In order to confirm an amyloid mimotopic conformation of the peptide expressed by the clones derived from the selection of double binding, clone 12III1 was tested in interaction with the peptide Aβ-42 and on Aβ preassembled in SHSY-5Y cells. Then, the ability of the clone "amyloid mimotope" on disassembly of Aβ fibrils was assessed through the *in vitro* viability assay.

E.S. III.1 Inhibition test by 12III1 and pc89 on Aβ cytotoxicity

Aβ1-42 was purchased from Tocris Bioscience and was dissolved 1 mg/ml in sterile water. Human neuroblastoma SH-SY5Y cells were obtained from American Type Culture Collection (ATCC CLR-2266) and were grown to monolayer in a culture medium containing Dulbecco's Minimal Essential Medium (DMEM) and Ham's F12, modified with 2 mM L-glutamine, 1.0 mM sodium pyruvate, supplemented with fetal bovine serum (FBS) to 10%, streptomycin 50 mg/ml. SH-SY5Y cells were maintained at 37 °C and 5% CO_2.

For cell viability tests, $3x10^4$ cells were plated in 96-well plates (Corning Cell Culture) in a volume of 150 µl and differentiated with RA (100 nM) for 24h. In order to test the inhibition of Aβ-amyloid aggregation, different titers (10^6, 10^8 and 10^{10} TU/ml) of 12III1 phage clone or pC89 wild-type phage were added simultaneously to Aβ1-42 peptide 1 µg/ml, and cell viability was assayed after 24h incubation. For evaluation of cytotoxicity inhibition by phages on preassembled Aβ amyloid, differentiated SH-SY5Y cells were stimulated with Aβ1-42 peptide 1 µg/ml for 3, 6 or 12 hours and then, at each time, incubated with the different titers of 12III1/pC89 phage for other 24h.

Three sequential rounds of precipitation in 4% (w/v) PEG 8000, 500 mM NaCl supplemented with 2%(v/v) Triton X-100 were carried out to purify phage clones and remove LPS contamination, according Branston et al.75 Cell viability was evaluated by using the mitochondria-dependent dye 3-(4,5-dimethylthiazol-2-yl)-2,5-diphenyltetrazolium bromide (MTT) colorimetric assay as previously described,

expressed as % viability versus control cells grown in normal culture medium (Ctr). Cultures pre-treated with increasing concentrations of the test compound were incubated at 37 °C with MTT (0.2 mg/ml) for 1 h. Medium was removed and the cells lysed with dimethyl sulfoxide (100 µl). The extent of reduction of MTT to formazan was quantified by measurement of optical density at 550 nm with a microplate reader.

R.S. Results Section

Enhancement of 12III1 phage inhibition of Aβ-42 cytotoxicity in vitro

In order to evaluate the effect of 12III1 exposed peptide on disassembling Aβ fibrils compared to M13 phage (pC89), its ability to interact with Aβ-42 has been tested *in vitro*.

At first, 12III1 and pC89 phage clones have been used as inhibitors of Aβ-amyloid aggregation in SHSY-5Y cell viability *in vitro* test. Aβ-42 showed a cytotoxicity of about 60%; both 12III1 and pC89 wild type phages showed significant inhibition of Aβ-42-induced cytotoxicity when added to cell cultures simultaneously to Aβ-42. However, pC89 wild-type phage exhibited a lower inhibition of Aβ-42-induced cytotoxicity than 12III1 phage at all the assayed titers (Fig.15).

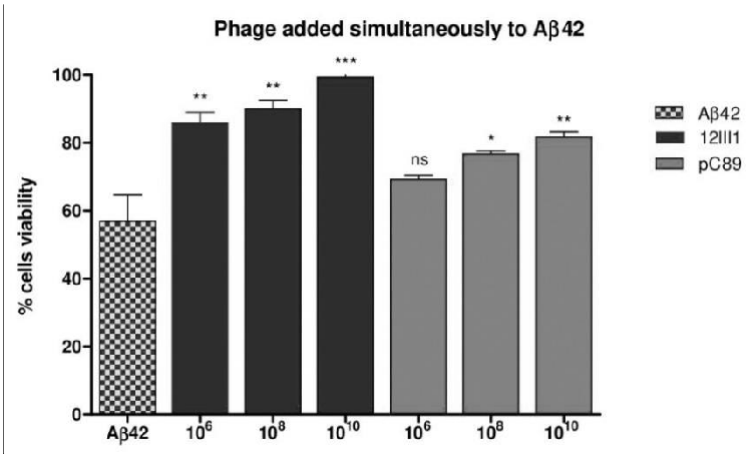

Fig. 15 *Inhibition of Aβ42-induced cytotoxicity at increasing concentrations of 12III1 recombinant phage clone and pC89 wild-type phage, as evaluated in SHSY-5Y cell viability in vitro test*

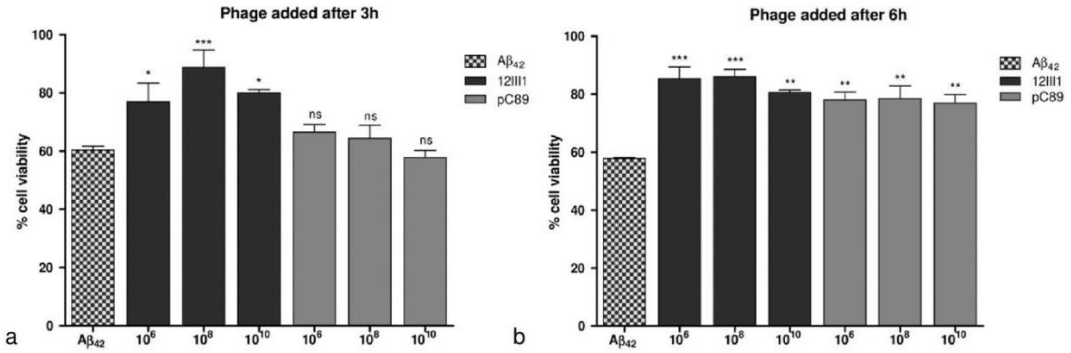

Fig. 16 *Reduction of Aβ-amyloid cytotoxicity in SHSY-5Y cell viability in vitro test after addition of pC89 wild-type phage and 12III1 recombinant phage clone, at 3h (a) and 6h (b) following Aβ-stimulation*

Moreover, when phages were added after 3h and 6h following Aβ stimulation, 12III1 phage restored cell viability (% comparable to control cells with no Aβ and no

phage), pC89 wild-type phage showed no activity at any tested titer after 3h whereas increased cell survival after 6h, but in any case, in a lower extent than 12III1 (Fig. 16). Data suggest that 12III1 displayed peptide increases affinity to Aβ fibrils, promoting disassembling of toxic preformed Aβ amyloid aggregates.

It is known that pIII M13 phage coat protein mediates a generic binding to the amyloid fold, through middle and C-terminal residues of the Aβ subunit, by β strand interactions. Moreover, it has been shown that highly purified preparations of M13 could mediate binding to and disruption of various misfolded protein assemblies, including Aβ [182, 183].

12III1 clone exposed peptide, inserted "in-frame" in the major pVIII coat protein, increased cell survival to a much greater extent than the wild-type phage (with no insert), even restoring cell viability (Fig. 15). In addition, this specific phage clone was able to prevent Aβ-42 amyloid fibrillation as well as to promote disaggregation of preformed fibrils (Fig. 16).

These data confirmed that the recombinant peptide displayed on pVIII coat protein was a conformational mimotope of Aβ, able to interact with Aβ fibrils and enhance both inhibition and disaggregation of Aβ-42 fibrillation.

IV. Ex-vivo *immunostaining analysis*

The combination of imaging markers for Aβ-42 and cerebral metabolism is opening exciting new opportunities for the *in vivo* research of AD. Since the peptides showed conformational similarities with the fibrillar aggregates of the Aβ-42, it has been possible to suppose their link for the visualization of plaques in the brain for a direct diagnosis. At this purpose, the mimotopes-phage selected were tested as probes of interaction in brain sections of AD mice by immunostaining analysis.

E.S. IV.1 Animals

The animals used were the double transgenic mice B6.Cg-Tg(APPswe,PSEN1dE9)85Dbo/J from the Jackson Laboratory (Bar Harbor, USA).
These transgenic mice express a chimeric mouse/human amyloid precursor protein (Mo/HuAPP695swe) and a mutant human presenilin 1 (PS1-dE9) both directed to CNS neurons. Both mutations are associated with early-onset (usually 6–7 months) of AD. By 9 months of age, histological examination of brain tissue reveals numerous amyloid deposits within the hippocampus and cortex.

IV.2 Immunohistochemistry

Brain tissue was fixed in 10% (w/v) buffered formaldehyde and 7 μm sections were prepared from paraffin-embedded tissues. After deparaffinization, endogenous peroxidase was quenched with 0.3% H_2O_2 in 60% methanol for 20 min. The sections were permeabilized with 0.1% Triton X-100 in phosphate-buffered saline (PBS; pH 7.4) for 20 min. Nonspecific adsorption was minimized by incubating the section in 2% normal goat serum in PBS for 20 min. Endogenous biotin- or avidin-binding sites were blocked by sequential incubation for 15 min with avidin and biotin. The sections were then incubated overnight with phage clones (12III1-12CIII1-12III15 and 9CIII3) at 10^{12} pfu/ml, and HRP anti-M13 monoclonal conjugate antibody (GE Healthcare 1:5000 in PBS, v/v), or control solutions. Controls included buffer alone or nonspecific-purified rabbit IgG. Immunohistochemistry photographs were assessed by densitometry by using Optilab Graftek software on a Macintosh personal computer.

IV.3 Densitometric analyses

For graphic display of densitometric analyses, the % of positive staining (brown staining) was measured by computer-assisted color image analysis (Leica QWin V3, UK). The percentage area of immunoreactivity (determined by the number of positive pixels) was expressed as % of total tissue area (red staining) within five random fields at x40 magnification. In particular, firstly the colors of the images that have been stained to the molecule of interest were defined. Once these colors were defined, they were automatically detected in all samples. This is a semi-quantitative analysis that measures areas and not intensities.

R.S. Results Section

12III1, 12CIII1 and 12III15 phage clones bonded Aβ plaques in double KO mice. A strong staining reaction with the brain tissue of Alzheimer double KO mice tissue were particularly localized in the cortex close to the hippocampus. In contrast, no staining was observed in control brain from WT mice (Figures 17-18-19 A-B). The clone 9CIII3 failed to stain any of the tissues insertions of brain (Fig 20 A-B).

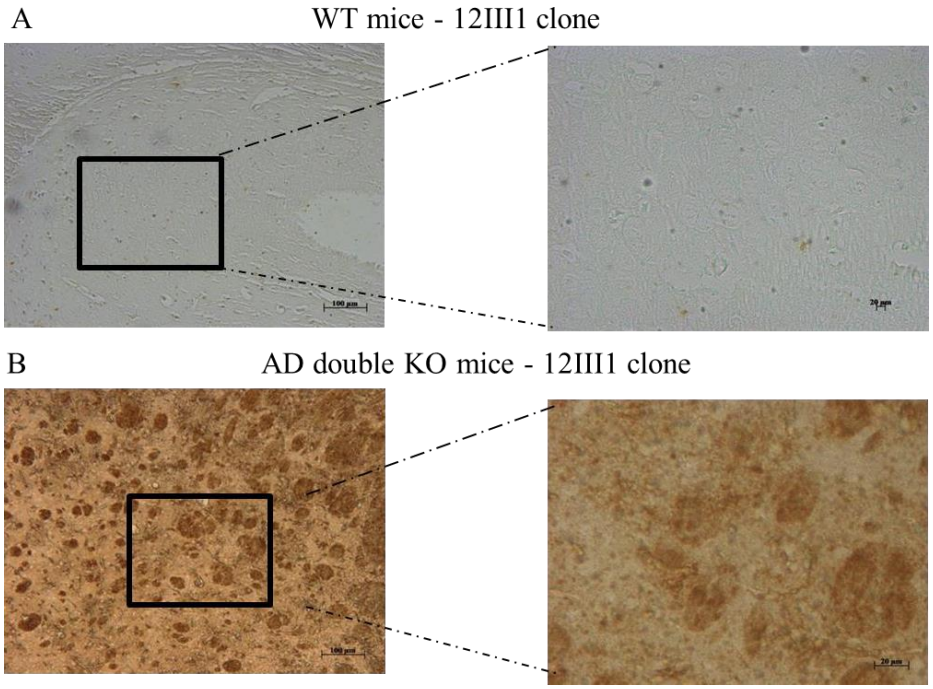

Fig. 17 *Immunohistochemical analysis of phage clone 12III1. Panel A represents the control group (WT mice, negative staining) at magnification 10X (100 µm) and 40X (20 µm). Panel B shows the positive binding staining for clone 12III1 in the cortex of AD double KO mice at 10X and 40X.*

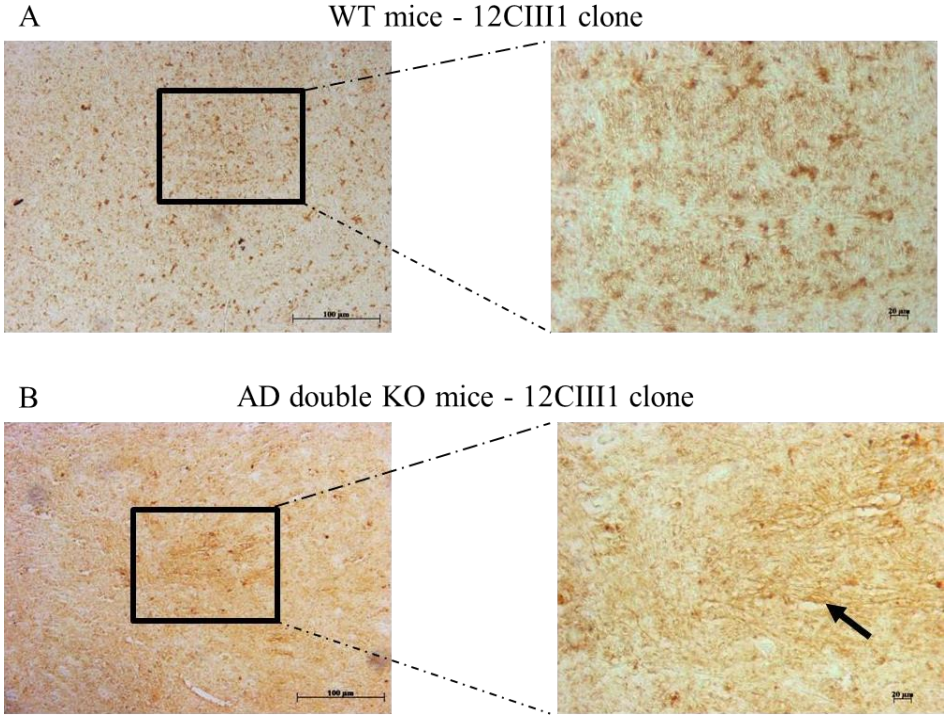

Fig. 18 I*mmunohistochemical analysis of phage clone 12CIII1. Panel A represents the control group (WT mice, negative staining) at magnification 10X (100 µm) and 40X (20 µm). Panel B shows the positive binding staining for clone 12CIII1 in the cortex of AD double KO mice at 10x and 40x.*

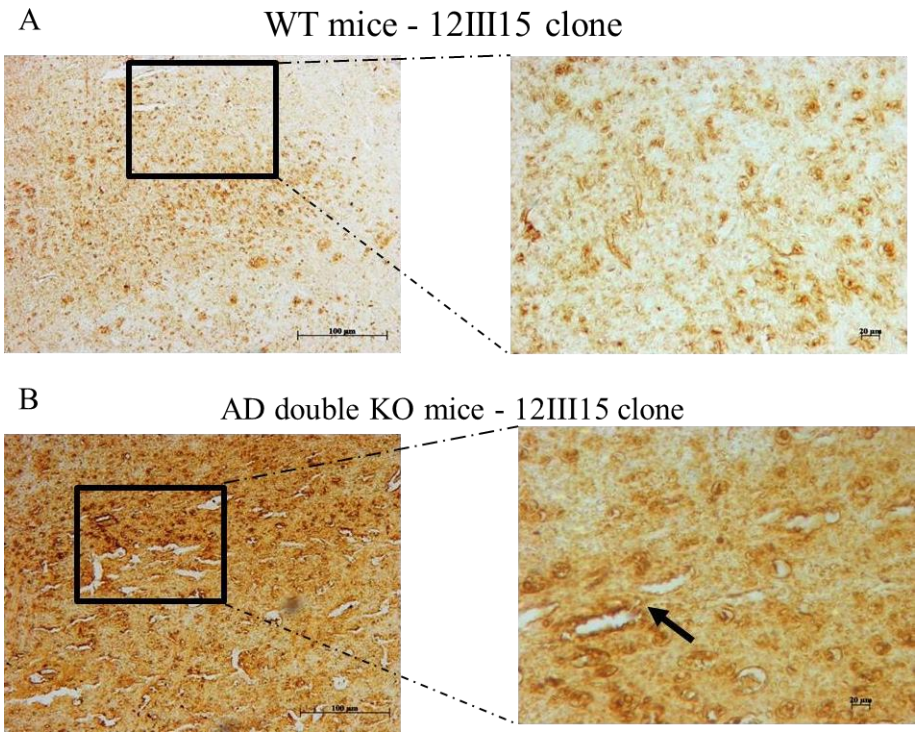

Fig. 19 *Immunohistochemical analysis of phage clone 12III15. Panel A represents the control group (WT mice, negative staining) at magnification 10X (100 µm) and 40X (20 µm). Panel B shows the positive binding staining for clone 12III15 in the cortex of AD double KO mice at 10X and 40X.*

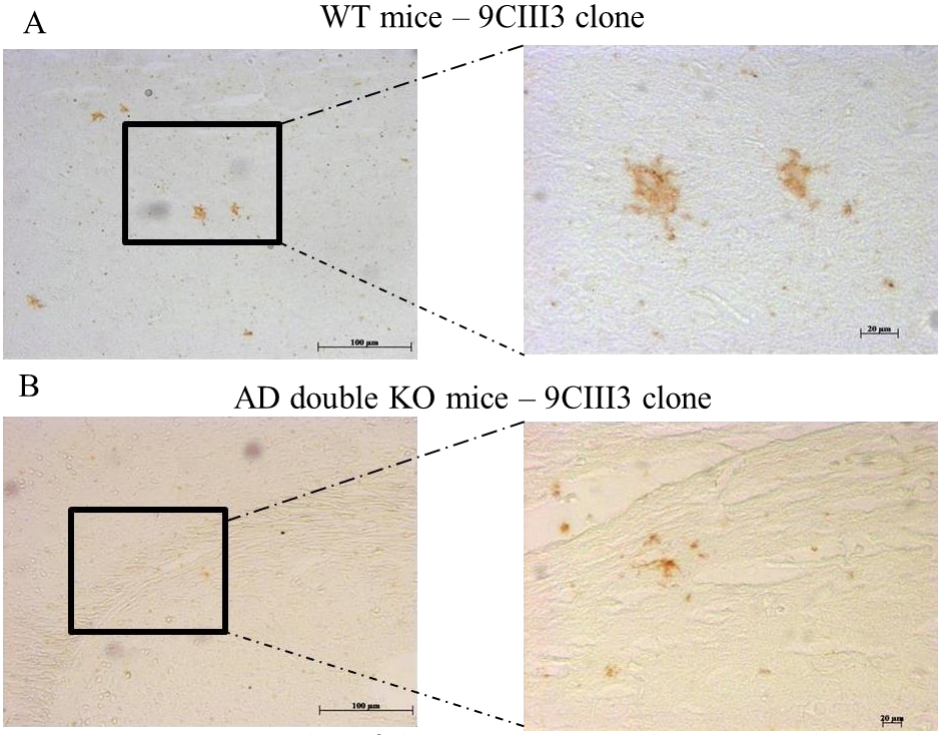

Fig. 20 *Immunohistochemical analysis of phage clone 9CIII3. Panel A represents the control group (WT mice, negative staining) at magnification 10X (100 µm) and 40X (20 µm). Panel B didn't show any binding staining for clone 9CIII3 in the brain of AD double KO mice at 10x and 40x.*

In order to evaluate the different binding capacity on Aβ plaques by the different peptides, a densitometric analysis was performed (Fig.21).

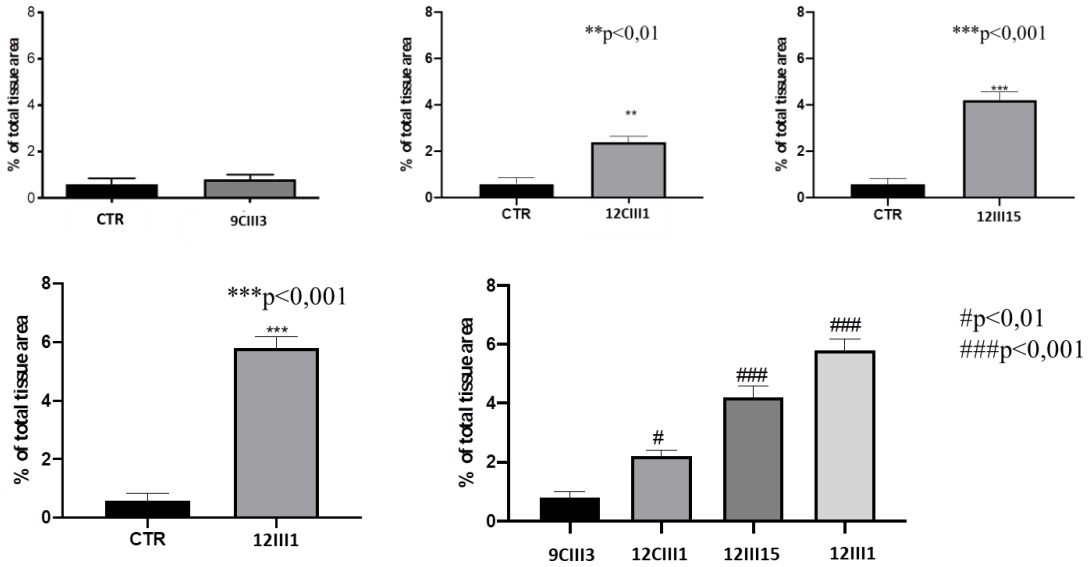

Fig. 21 *Densitometric analyses*

The percentage of the immunoreactive area was highly significative ($p < 0.001$) for 12III1 and 12III15 and significative ($p < 0.05$) for 12CIII1. 9CIII3 did not show

immunoreactivity in either control or double KO mice. The data confirm that the clones showed the peptides selected by double binding were able to bind to the amyloid plaques of AD brain sections, but they weren't on healthy control mice.

These data confirmed the specificity of binding with amyloid plaques, determined by the arrangement of the distint configuration of the functional mimotopes. Finally, these data suggest that it will be possible to use phage-functionalised metallic nanoparticles as "probe for *in vivo* imaging" to detect plaque distribution in brain areas, to follow the progression of the disease.

V. Phage diplay mediated Immuno-PCR for Alzheimer's diagnosis

Currently, the number of people who develop AD increases dramatically, so it is urgent to develop diagnostic tests suitable for people throughout their lives. Indeed, the confirmatory diagnosis of AD in the early stages could facilitate early therapeutic intervention and treatment of the disease. Compared to brain imaging, the search for blood biomarkers is particularly desirable as it is fast, non-invasive and easily accessible.

At this purpose, previously the ability 12III1 phage clone to discriminate between 29-human sera of AD subjects and 26-human sera of healthy using an ELISA-indirect assay has been demonstrated [163].

In order to design a new diagnostic system to detect antibodies against the different conformational epitopes presented in AD sera, 12III1 (as reference) and one different mimotope clone were tested in a Sandwich Enzyme-linked immunosorbent assay (ELISA) with G protein (fig. 22).

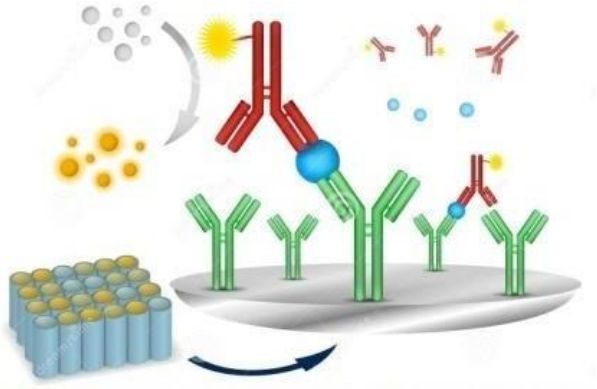

Fig. 22 *Representative graphic of the components of the ELISA assay: Protein G-functionalised plate (gray), Serum Antibodies (green), Phage Clone (blue), HRP-AntiM13 Antibody (red)*

Subsequently, in order to investigate the immune responses against amyloid conformational epitopes related to the state and stage of the disease, eight phage clones were simultaneously tested in a new combinatorial diagnostic system, based on Phage mediated Immuno PCR.

The system combined:

1. A plate coated with protein G, to orient and immobilize the serum IgGs;
2. Phages binding to IgGs-AD;
3. Release of phage DNA by phage thermal lysis at 95°C for 10';
4. Quantification of the number of phages bound by antibodies by Real Time PCR amplification.

Graphical representation of Phage mediated Immuno-PCR (Fig.23).

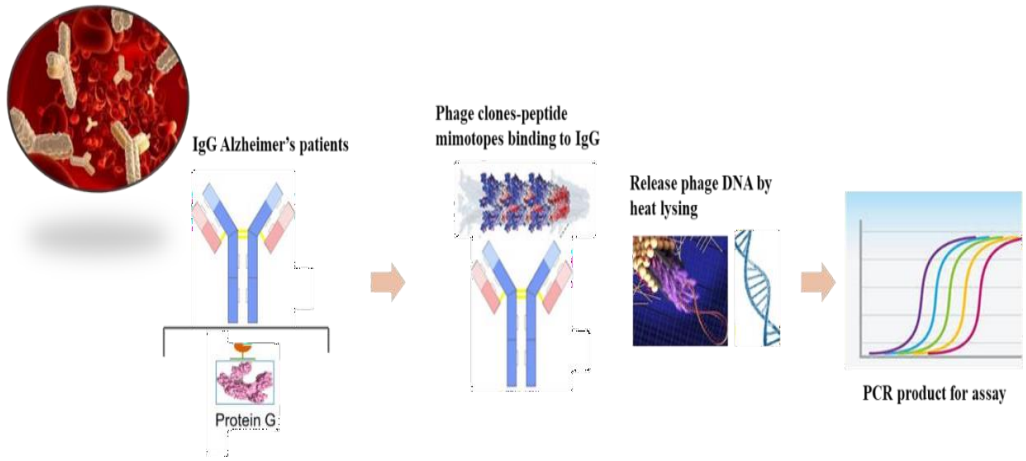

Fig. 23 *Graphical representation of Phage mediated Immuno-PCR*

E.S. V.1 Human samples

13 sera of AD patients, diagnosed according to the criteria of the National Institute of Neurological and Communicative Disorders and Stroke and the Alzheimer's Disease and Related Disorders Association, attending the Neurologic Unit of the University Hospital "Policlinico Vittorio Emanuele" in Catania, were selected. AD patients information are shown below:

Table 4. *AD-patients infomation*

Cod. Sera	Gender	Age	MMSE	TREATMENT
226	Female	77	6.8	-
218	Female	87	8	-
205	Female	79	8	-
237	Female	62	9.5	-
249	Female	76	8	-

115-15	Female	77	12	-
182	Male	78	16	-
42-15	Male	76	14.8	Rivastigmina
147-13	Male	56	16.7	Rivastigmina
120-15	Male	76	14.8	Rivastigmina
189	Male	77	20.2	-
251	Male	78	21	-

All AD patients underwent clinical and instrumental evaluations and the presence and severity of cognitive impairment was assessed through the Mini-Mental State Examination (MMSE). The MiniMental State Examination (MMSE) is a reliable index of AD-related cognitive status at a given point in time. However, its rate of decline varies with severity, and mildly impaired patients show little MMSE decline even after several years.

A sample (n-227) was added as a diagnosis of not confirmed AD.

13 sera of healthy subjects underwent a standard neurological examination in order to exclude the presence of neurological disorders and presented a mean age 65.3. The study was approved by the Ethic Committee of the Policlinico Vittorio Emanuele of Catania.

V.2 Sandwich Enzyme-linked immunosorbent assay (ELISA)

The procedure was optimized as follows:

- absorption of G protein on the polystyrene microtitre plate (Maxisorp, 96-wells, Nunc), in order to bind class G immunoglobulins (IgG) in an oriented way: 0.2 - 0.4 - 0.5 - 0.10 - 0.20 µg/ml were tested. The optimal concentration was 0.5 µg/ml in a $NaHCO_3/NaCO_3$ coating buffer.
- Number of washes in washing buffer (PBS; 0.05% Tween20): three washes with 250 µl/well allowed greater elution and elimination of non-specific bonds.
- Dilutions of serum: 1:25 - 1:50 - 1:10 - 1:1000 have been tested to have a correct immunoglobulin titer. 200 µl/well of 1:50 diluted serum in dilution buffer (PBS; 4% nonfat Milk; 0.1% Tween 20) was the best condition. The plate was incubated at 37 °C for 1 h under stirring at 100 rpm.

- Blocking buffer compositions: (PBS, 6% nonfat Milk, 0.05% Tween 20, 50% globulin free fetal bovine serum and 1% decomplemented Horse Serum, Donor Herd – Sigma; PBS containing 5% (w/v) skimmed milk; TBS (Tris Buffered Saline) containing 5% (w/v) skimmed milk (TBSM)). 300 µl/well of TBSM were added to the wells and the plate incubated at 37 °C for 2 h in static.
- Logarithmic scale dilutions of phages ($1x10^{12}$, $1x10^{11}$, $1x10^{10}$) have been tested for recognition. The procedure showed to give maximal phage specific binding for all sera used with phage concentration at 1×10^{11} TU/mL/well. Then the plate was incubated for 1 h at 37 °C under stirring at 100 rpm.

Finally, after three washes, the plate was emptied and 100 µl/well of Anti M13-pIIIV-HRP diluted 1:7500. The plate was then incubated for 1 h at 37 °C under 100 rpm stirring, and washed with 250 µl/well of washing buffer; then, 100ul/well of TMB were added and allowed to incubate for 20 minutes at room temperature. The reaction was finally stopped with 100 µl/well of H_2SO_4 0.6N and absorbance at 450nm was measured by Multiskan microplate reader.

All reagents were purchased from Sigma–Aldrich.

V.3 Phage mediated Immuno-PCR (PI-PCR)

V.3.1 DNA phage extraction

Scalar phage concentrations 10^2-10^4-10^6-10^8-10^{10}-10^{12} TU/mL, determined by NanoDrop® ND-1000 UV-Vis Spectrophotometer at 269 nm were heat treated. After treatment, the samples were quantized and amplified in PCR. The 220 bp product was visualized in 2% agarose electrophoretic gel.

V.3.2. Quantitative evaluation of phage DNA and standard curves

In order to derive the amount of phage detected in PI-PCR to discriminate AD patients sera from healthy subjects sera, a standard curve was constructed on known quantities of phages.

Then the DNA of 10^{12} up to 10^2 phages after thermal lysis was amplified in Real Time PCR.

For each sample, an amplification curve was obtained, the threshold was defined and the related CT (Cycle Threshold) inversely proportional to the amount of initial template DNA contained in the sample was calculated. Then, the intercept with the y

axis in the semi-logarithmic graph of the standard curve, which corresponded to the number of cycles necessary to detect a copy of the target DNA (theoretical limit of detection of the reaction), was obtained.

V.3.3. PI-PCR

200 µl/well of G Protein (0.5 µg/ml) in a $NaHCO_3/NaCO_3$ coating buffer were added to each well of the plate (polystyrene microtitre plate Maxisorp, 96-wells, Nunc) and incubated over night at 4 °C. The wells were washed with 250 µl/well of washing buffer (PBS; 0.05% Tween20); 200 µl/well of AD/CTR-sera diluted 1:50 were added and the plate was incubated at 37 °C for 1 h at 100 rpm. After 5 washes, 300 µl/well of blocking buffer (TBS (Tris Buffered Saline) containing 5% (w/v) skimmed milk (TBSM)) were added in each well and the plate was incubated at 37 °C for 2h in static. After three washes with 250 µl/well of washing buffer, the phage preparations 10^{11} TU/mL were added into a 96-well microtiter plate and incubated for 1 h at 37 °C under stirring 100 rpm. Finally, TBSET (TBS buffer containing 5 mM EDTA and 0.1% Tween-20) was used to remove unbound phages and 50 µl of distilled H_2O were added into the microtiter wells. The plate was then incubated in water bath (95°C for 10 min) to lyse the bound phages [184].

All the real-time PCRs were carried out with SsoAdvanced Universal SYBR Green BIORAD.

The PCR premix consisted of 4 µl of phage lysate as template, 5 µl of Taq supermix (2X), 0.2 mM primer forward (E24-5'GCTACCCTCGTTCCGATGCTGTC3') and reverse (M13 -40-5'GTTTTCCCAGTCACGAC3'). The step program for PCR was as follows: 94 °C for 5 min, followed by 30 cycles at 94 °C for 30 s; 52 °C 30 s; 72 ° C for 30 s. In addition, negative control containing no template DNA was included in each batch of PCR tests. The threshold level was determined to be above the background signals and the cycle threshold (Cts) values were set as the cycle at which the measured fluorescence intersected the cycle threshold line. Subsequent analysis was accomplished with Excel software (Microsoft).

V.3.4. Data analysis

Finally, in order to obtain the Phage Quantity ($10^{\wedge}$), the calibration line at known concentrations was interposed with the concentration of the unknown sample (i.e. the

phage DNA detected by the PI-PCR test in terms of CT). By applying the formula (x; y_known; x _known) it was possible to obtain the phage quantity retained by the antibodies and expressed in TU/mL.

Finally, the quantity of phages bound to the target was expressed as a percentage and calculated according to the formula:

$$\%\ Phage\ bound\ to\ target = \frac{TU/mL(i)}{TU/mL(i0)} \times 100$$

where TU/mL(i) is the quantity of phage calculated by means of the Ct and interpolation with the calibration line at a known concentration, indicating the quantity of antibody-binding clones after washing, and TU/mL(i_0) indicated the initial concentration of phage clones (input), determined by UV-visible spectroscopy at 269 nm and used as absolute values. The phage at 0.1 mg/mL gives a standard absorbance of 0.38. [185]. Thus, 1 unit of absorbance at 260 nm corresponded to $2.2x10^{12}$ TU/mL.

The values obtained were elaborated in an Excel graph expressed as % of phages bound to target (TU/mL). Such values give information on the recognition pattern by the different probes against each single AD and CTR serum, in order to define the status and stage of AD in the array diagnosis.

R.S. Results Section

The phage clone 12III1 showed the ability to discriminate sera from AD patients from healthy individuals (CTR) in ELISA assay [163]. Results obtained showed a mean OD_{450} value of 1.89 and 0.51 in AD and healthy sera, respectively, demonstrating the presence of serum IgG levels towards the displayed peptide significantly higher in AD patients. Subsequently, the same sera were tested in a sandwich ELISA assay and the 12III1 and 12CIII1 clones were investigated. The averages of the values obtained are shown below (Fig. 24).

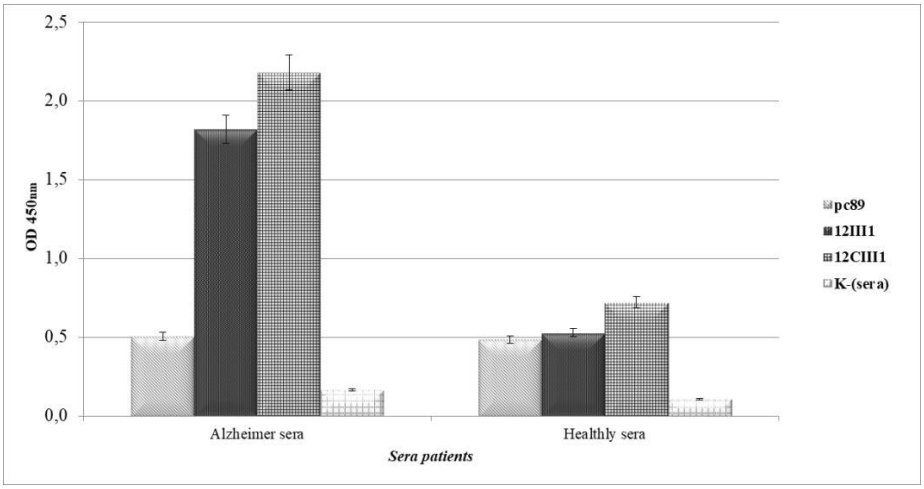

Fig. 24 *Sandwich ELISA assay of AD and Healthy sera*

The results obtained with clone 12CIII1 showed a mean OD_{450} value of 2.1 and 0.67 in AD and healthy sera, respectively (p value <0.0011). Data obtained with 12III1 were similar with what previously obtained.

The assay has been optimized in order to immobilize and orient the serum immunoglobulins present in patients. The phage were used in solution not adsorbed at the plate, in order to favor the conformational interactions of the peptides exposed on the surface with the antibodies without interference.

Therefore, the possibility of combining the response with other clones deriving from the same selection was evaluated. The diagnostic system envisaged the use of the phage as a probe for the detection of antibodies of patients with AD immobilized and quantized in an Phage mediated Immuno-PCR.

Phage mediated Immuno-PCR

DNA phage extraction

The PI-PCR provides a quantification by Real Time PCR of the antibody-binding phage DNA after thermal lysis.

In order to verify the efficiency of lysis after heat treatment, the phage clones were quantized through NanoDrop® spectrophotometer and TU/mL count in agar plates with ampicillin. The results showed that 95 °C for 10 min was sufficient to lyse the entire phage population present in the sample. In fact, no *E. coli* infecting phage particles were present in the plate; moreover, in PCR it was possible to detect the band of the specific amplification product related to the DNA of M13 phage.

Quantitative evaluation of phage DNA and standard curves

DNA of 10^{12} up to 10^2 phages was lysed and amplified in Real Time PCR, in order to draw the calibration line to be exploited to derive the known concentration of the relevant phages from the diagnostic system. Therefore, the known concentration of phages and the related cycle thresholds were processed in an equation of the line y = 2.785x+41 obtaining a value of the coefficient $R^2 = 0.985$ (Fig.25).

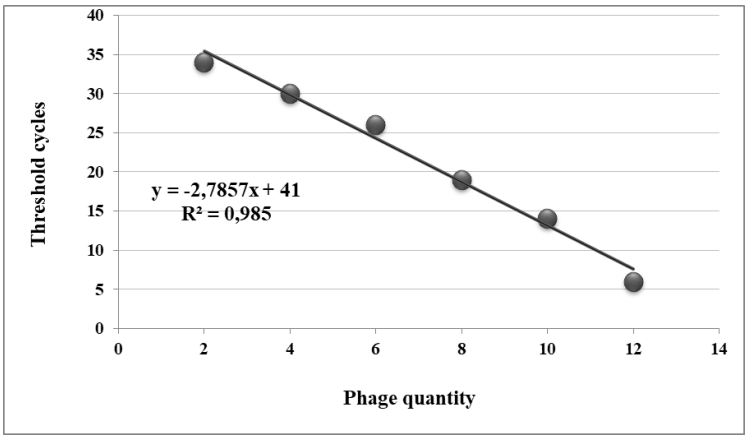

Fig. 25 *Calibration line at known concentrations of the phage quantity*

Phage mediated Immuno-PCR

These experiments were designed to detect IgG based on the state and stage of the disease. For this purpose, the serological platform and the combinatorial study of the different peptides have been expanded. 13 AD patients diagnosed by MMSE as mild (3), moderate (5) and severe (5), with an index comprised between 22 and 6.8 and 13 healthy-sera subjects (control) were recruited and the samples were tested.

6 clones with 12 aa were inserted in the platform: 12III1,12CIII1, 12CIII3,12CIII4,12III15,12IV14; two clones with 9 aa: 9CIII3 and 9IV and the pc89 as a clone without insert. The serum of the single patients was tested individually against the clones of the realized platform.

After immobilizing the antibodies to G protein, the ELISA assay was performed. The different phage clones were tested as mimotopic probes for Aβ binding antibodies and added separately within specific wells. After the lysis of the phage bound to the specific antibodies, the DNA has been quantized in Real Time PCR and used as calibration standard. The data were expressed as % TU/mL of phages linked to the antibody target and shown below:

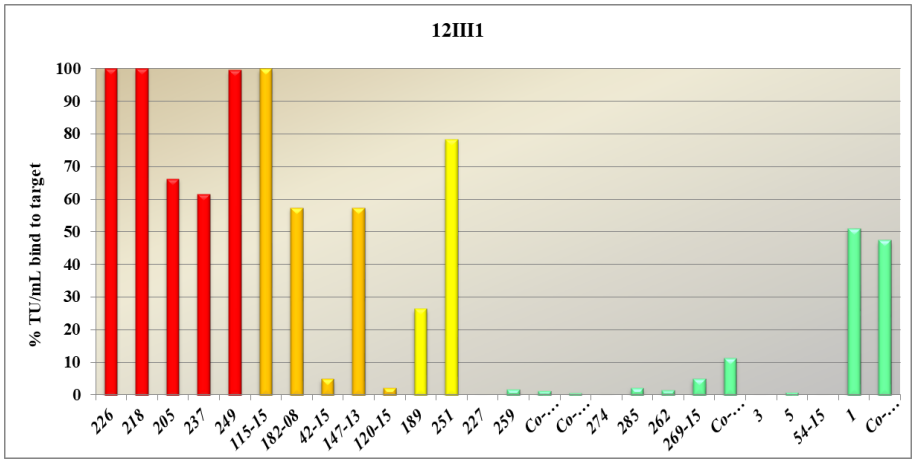

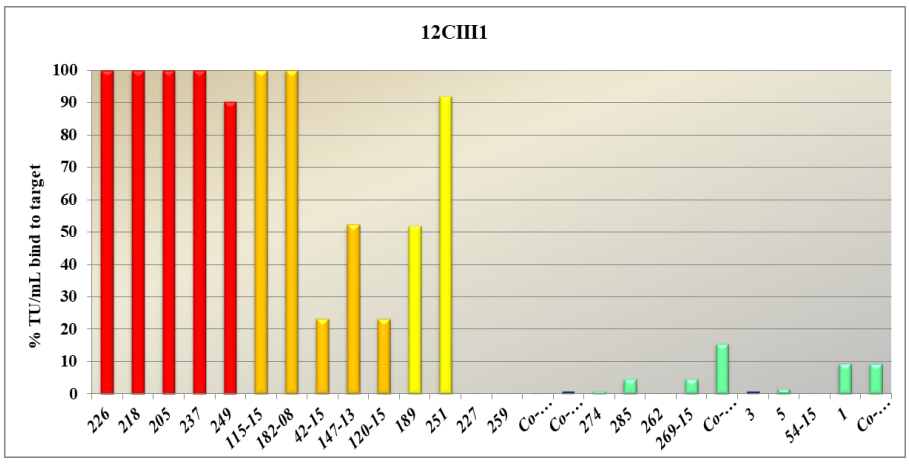

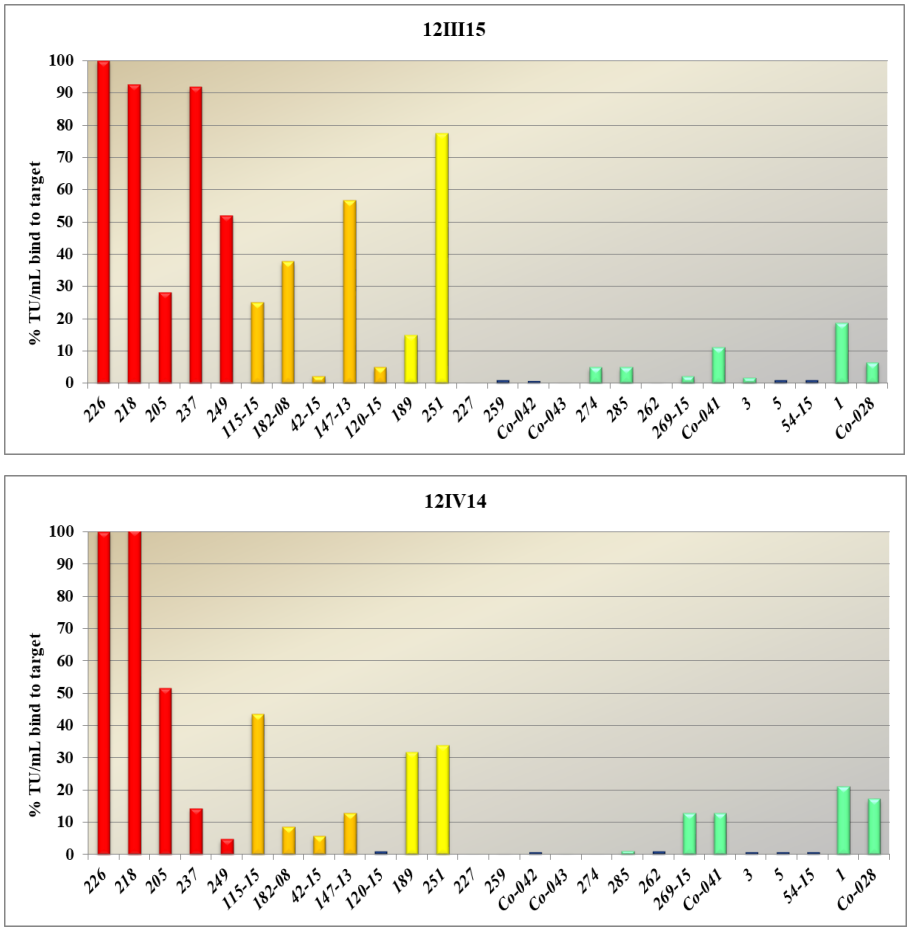

Graph. 1 *% TU/mL of phages linked to the antibody target with 12III1(A)12CIII1(B)12III15(C)12IV14(D).*
In red, severe AD; in orange, moderate AD; in yellow, mild AD; in green, healthy sera

The results indicated that antibodies against the exposed peptide by clone 12III1 were detected at high titer for all AD sera, except for two samples (182-08 120-15). In control sera, only two cases were recognized as positive, whereas the remaining of the samples were not. Clone 12CIII1 discriminated against all subjects with severe AD with high responsiveness. In addition, in healthy control sera, no positive response was detected. Thus, it is possible to attribute to clone 12CIII1 the ability to detect antibodies directed towards epitopes more represented in these subjects. Furthermore, in the two sera (42-15 and 120-15), where the detection was lower with both clones 12III1 and 12CIII1, the presence of an aggregative state of Aβ present in the specific stage of the disease of these subjects could be detected. Thus, the ability to combine data from 12III1/12CIII1 clones would allow for further information and a predictive index of disease status.

Clone 12III15 showed a trend similar to 12III1, recognizing all severe AD sera, but not two moderate sera and reported two false positives in healthy controls. However, the data obtained from 12III15 are interesting to correlate with the 12CIII1 clone. The different detection index in patients with severe AD compared to 12CIII1, could indicate the co-presence of different epitope portions recognized in these patients.

The 12IV14 compared to clone 12III1, 12CIII1 and 12III15, responded mainly with severe AD, while detected a lower value in the remaining cases (Graphics 1 A-B-C-D).

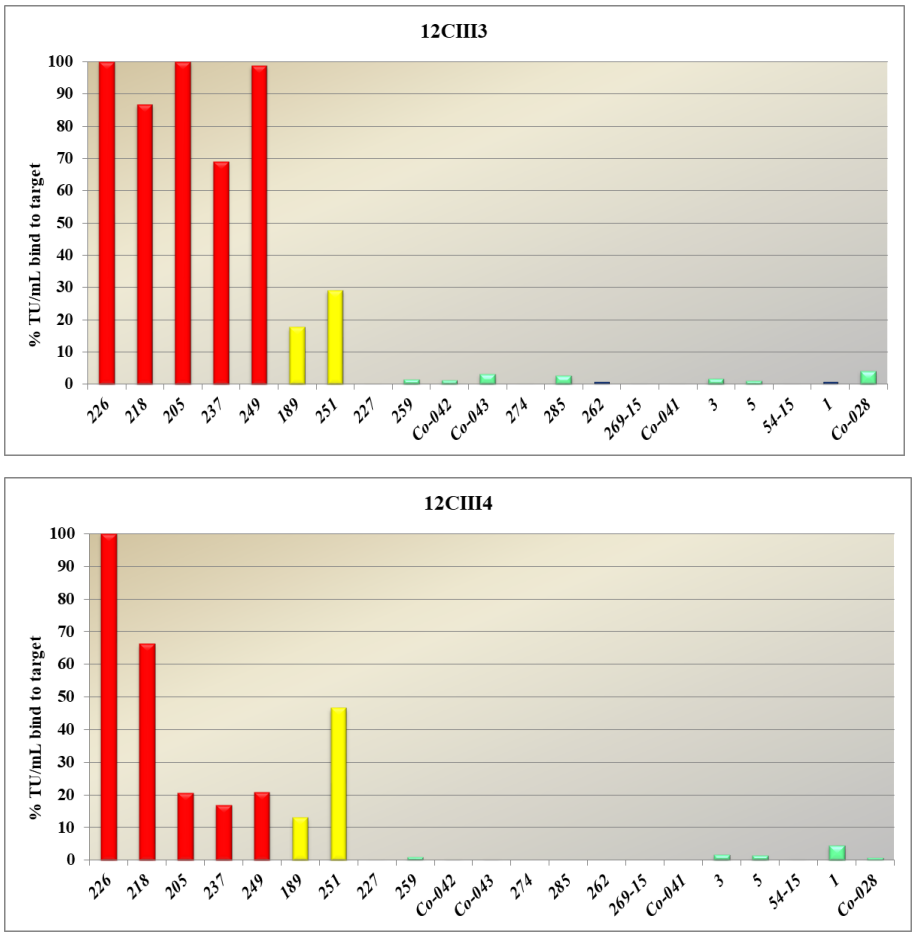

Graph. 2 *% TU/mL of phages linked to the antibody target with 12CIII3(A)12CIII4(B). In red, severe AD; in orange, moderate AD; in yellow, mild AD; in green, healthy sera*

Clone 12CIII3 showed a high reactivity in all subjects with severe AD and a lower positivity only in subjects with mild AD.

Clone 12CIII4 detected only 20% of patients with severe AD (Graph 2.A-B).

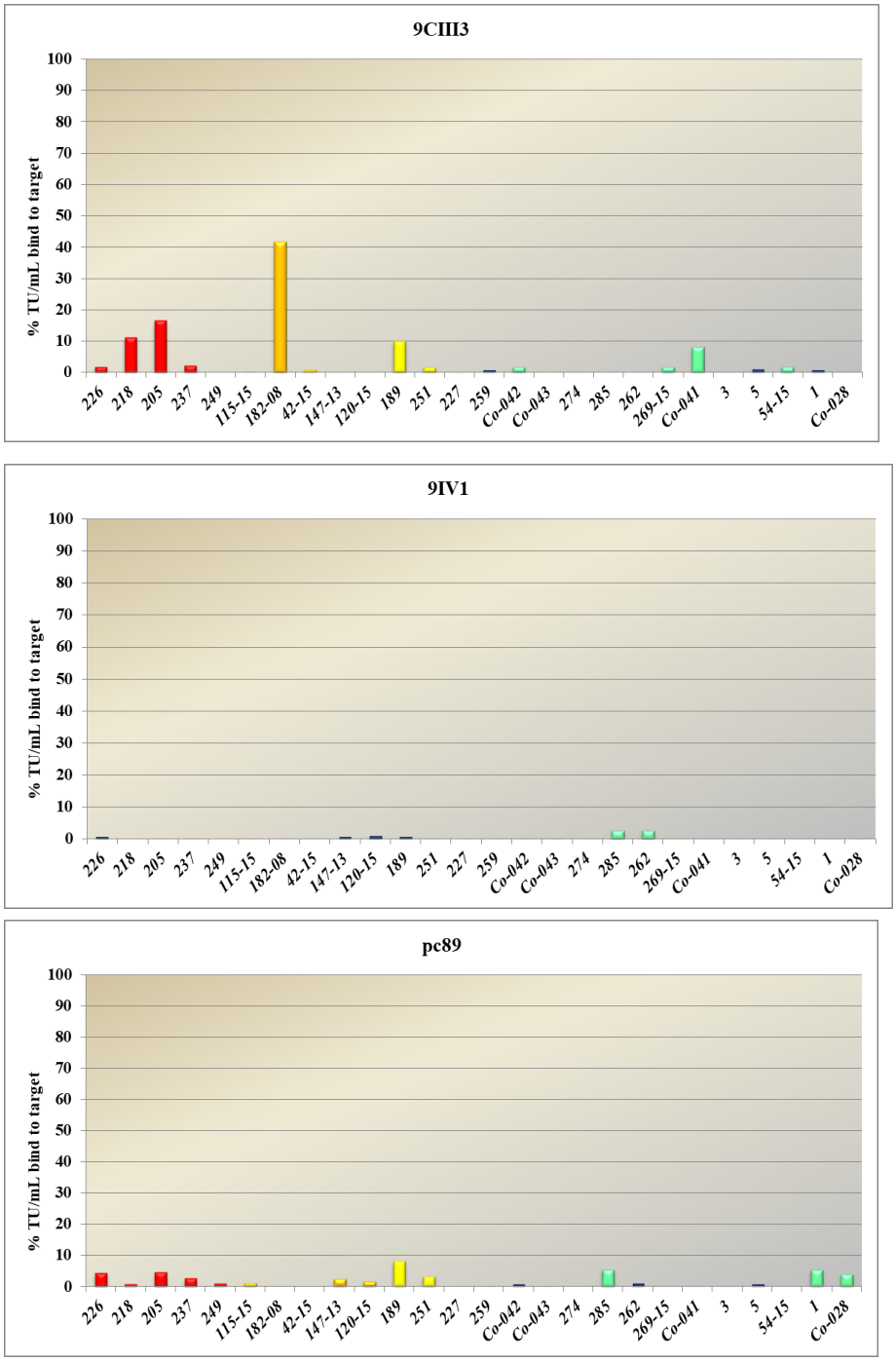

Graph. 3 *% TU/mL of phages linked to the antibody target with 9CIII3(A)9IV1(B)pC89(C)*

Clone 9CIII3 showed a mild signal in sera with severe AD, as well as in two cases with moderate and mild AD. Clone 9IV1 did not show significant positivity to all tested sera. Probably, the 9aa library exhibited a conformation that did not evoke an antibody response, confirmed the low reactivity against mAb YP and AD-IgG reported in the ELISA test.

The pc89 clone without insert confirmed the specific conformation recognition by peptide expressed in engineered phage clones selected according to the double binding (Graph 3 A-B-C).

The data suggested that the displayed peptides, although selected also by the monoclonal antibody specific for Caf1, probably mimicked several conformational epitopes recognized by circulating IgG from AD patients, confirming the presence of distinct states of the Aβ aggregates.

A combinatorial analysis of each serums against all the clones was subsequently performed, as shown by the following graphics:

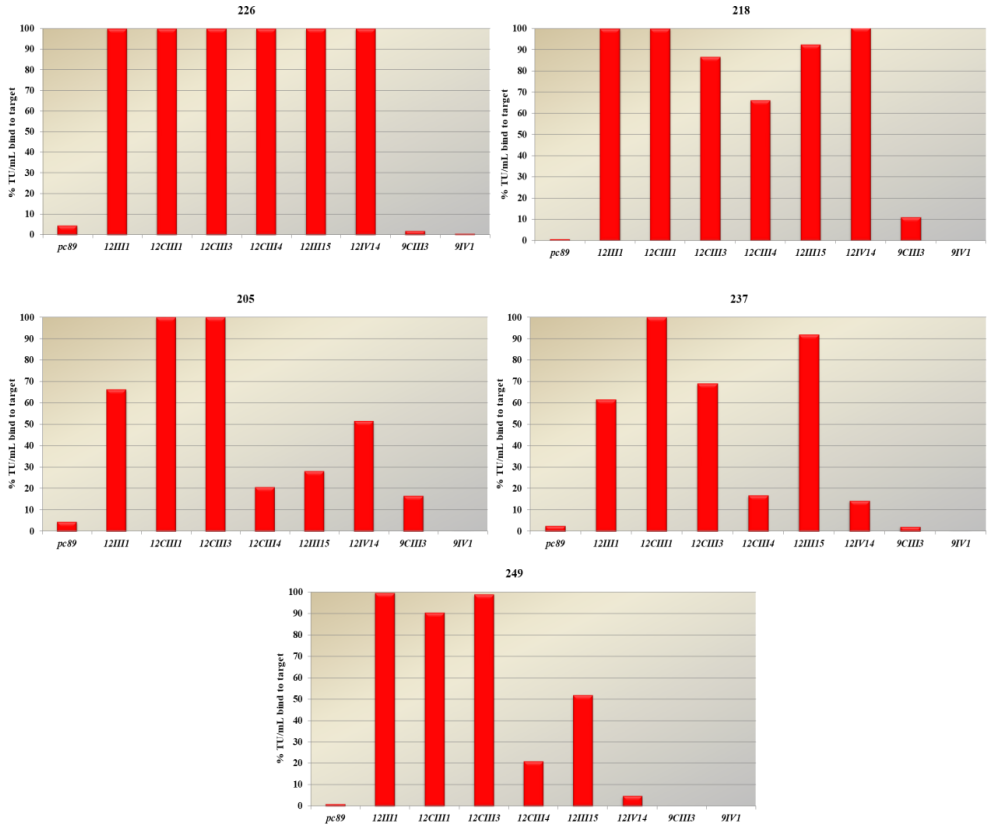

Graph. 4 . *% TU/mL of phages linked to the antibody target in severe AD*

By analyzing the sera it was possible to have an individual response, due to the different peptides tested. The different peptides, in fact, mimic the distinct conformations of Aβ, evoking different antibody responses between the various stages of the disease.

A first differentiative response was observed in subjects with severe AD. In particular, in sera 226 and 218 all clones detected high levels of antibodies, while in

sera 205, 237 and 249 a different antibody level was observed, as highlighted for clone 12CIII3 12III15 and 12IV14.

Thus, different portions of the conformational epitope exposed by the peptides detected different levels of antibodies. Consequently, elevated levels of antibodies in 226 and 218 were indicative of multiple aggregative forms of Aβ and consequently of advanced disease. While, different levels e.g. in sera 205, 237, 249 were indicative of the presence of a lower number of aggregative states (Graph. 4.). Infact it is known that during AD progression, fibril accumulation leads to the fragmentation of existing fibrils, generating several epitope portions [186].

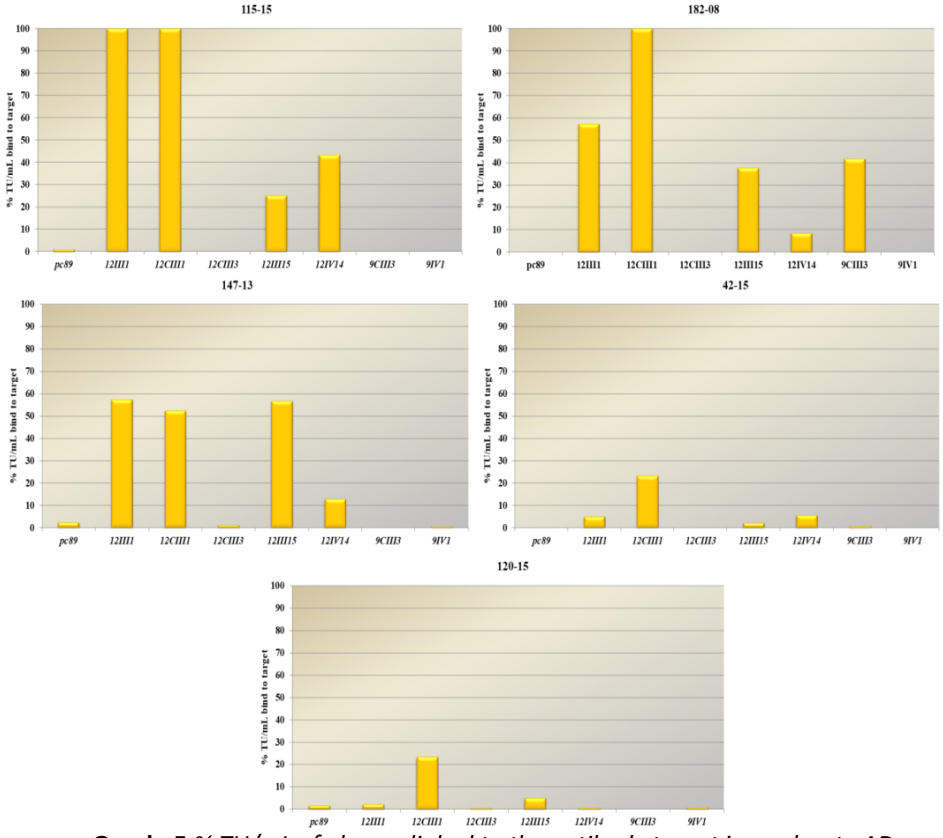

Graph. 5 *% TU/mL of phages linked to the antibody target in moderate AD*

In sera 115-15 and 182-08, clones 12III1 12CIII1 showed high antibody responses, while it was low for the remaining clones. This would allow the assignment of a more advanced state of the disease in these subjects.

In patients 147-13 42-15 and 120-15 the antibody detected was lower for all tested clones (Graph. 5).

Surprisingly, these patients were observed to have been on drug treatment since 2 years. Treatments with cholinesterase inhibitors (ChEI) such as the cholinergic drugs

donepezil, galantamine and rivastigmine are known to modify the manifestations of mild to moderate AD [187]. Furthermore, ChEI drugs act on amyloidogenic pathways by processing the Aβ precursor protein (APP) into potentially neurotoxic Aβ [188]. Based on the results, it is possible to think that in these subjects the levels of antibodies directed against Aβ aggregation were reduced, suggesting an improvement in the disease progression status.

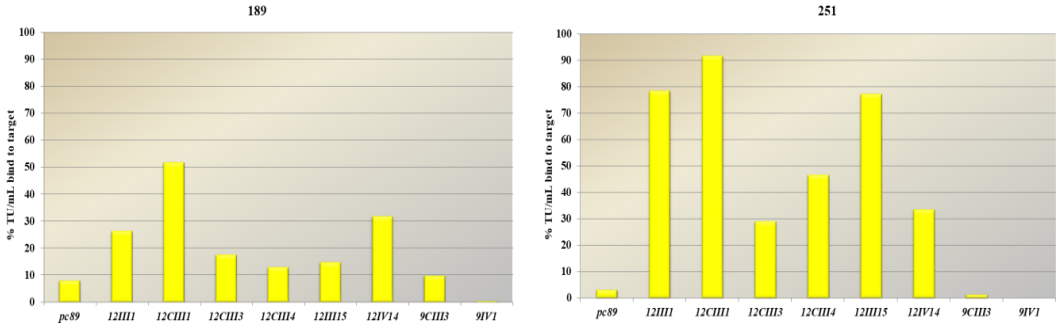

Graph. 6 *% TU/mL of phages linked to the antibody target in mild AD*

In serum 189, all clones detected low levels of reactivity confirming a mild disease state.

While, higher antibody levels in serum 251 suggested a progression of the stage disease in this subject (Graph. 6).

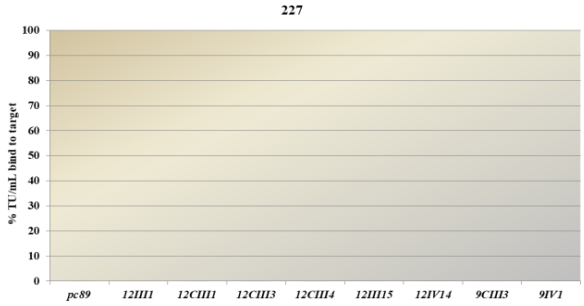

Graph. 7 *% TU/mL of phages linked to the antibody target in patient with a not confirmed AD*

In the sample n-227 (Graph.7), from a patient with a not confirmed AD, no reactivity with any of all clones was observed. This data suggested that this patient may not have AD.

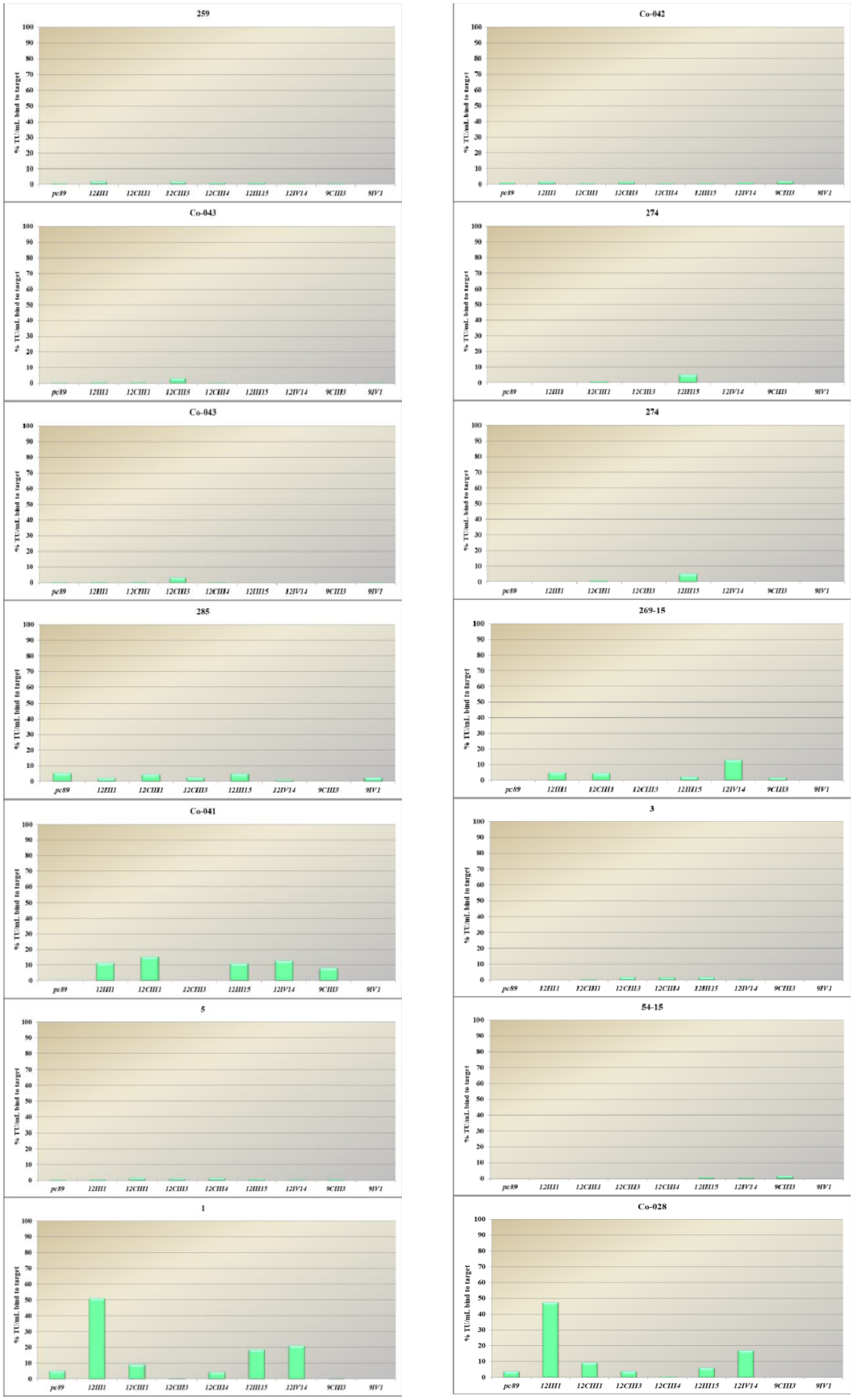

Graph. 8 *% TU/mL of phages linked to the antibody target in healthy subject sera*

For all sera from healthy subjects, no significant antibody recognition was observed, except for serum 1 and Co-028, detected by clone 12III1 and 12IV14. This observation may indicate the onset of AD in apparently healthy patients; if confirmed, these clones mat be suitable in an early screening analysis to detect the onset of AD in some subjects (Graph. 8).

The tested sera were selected to evaluate an initial response and the feasibility of the diagnostic system. The work led to fine-tuning and optimization of the array. The subsequent experiments, combinatorial analyzes with PET, RSM, and plaque development, as well as the increase in statistical analysis, will serve to obtain more information on the variation of the antibody response profile over time and for a follow-up analysis of each clinical case considered. In this study, the discriminative response of the clones selected could open new diagnostic perspectives, not only as biomarkers of state and stage of AD, but also as a predictive onset test.

VI. Micro array system in CDC Biochip

An antibody microarray is a specific form of microarray used for medical and diagnostic applications. Antibody microarrays are often used for detecting protein, biomarkers from various biofluids including serum, plasma and cell or tissue lysates. In order to realize a combinatorial micro-array system for Lab on Chip, the P-IPCR design was transferred in biochip (Fig. 26). In this technology, captured antibodies are fixed on a silicon chip, and the interaction between the antibody and its target antigen is detected by RealTime CDC-biochip technology.

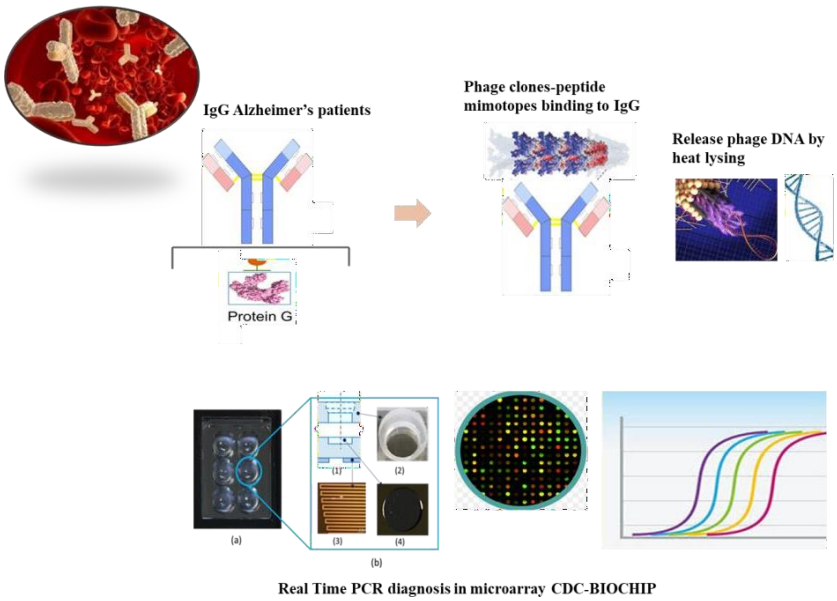

Fig. 26 *P-IPCR design realised as biochip*

E.S. VI.1 CDC-biochips fabrication

The CDC-biochip technology is proprietary design [189, 190] manufactured by silicon-plastic hybrid technology. The biochip assemblies a silicon device (a) with a plastic part (b) in a monolithic final bioreactor (Fig 27). The silicon device (1.7cmx 1.3cm) is manufactured by a standard VLSI (Very-large-scale integration) technology according to the process described in [191] and integrates temperature sensors and heaters in the bottom part (Fig. 27a) and silicon cavities (diameter of 3 mm height of 0.4 mm – volume of ~1.3 µl) in the top part (see Fig. 27 d-4). The plastic part is made in polycarbonate manufactured by molding technology. Chip contains 6 microwells obtained by 2 intersected cylinders featured by two different

diameters of 3.8 mm for the top cylinder (height of 1.0 mm – volume of ~9.6 µl) (Fig. 27c). The two parts are glued by a conductive resin (DELO MONOPOX, Sudbury, Boston, USA). The CDC-biochips are mounted on a plastic holder to be properly handled and used. They are appropriately thermally and optically driven for biochemical experiments by a specific optical reader instrument developed by ST Microelectronics containing 2 independent optical channels featured by excitation wavelengths centered at 470 and 530 nm and emission detection centered at 520 nm and 556 nm, respectively. A smart software was developed for the image analysis, it is based on a fully automatic image quantification, by a set of algorithms for image analysis process, a numerical computation and graphical output [192, 193].

VI.2 CDC-biochip functionalization

In order to create a device that could integrate the multiple functions in a single chip for an one-step process, in the preliminary phase, the surface of the wells of the cdc-biochip was functionalized [194].

VI.2.1 The chemical process consists of the following steps:

(a) cleaning and activation process, carried out by plasma O_2 treatment for 10 min at 100W (Sentech plasma Instrument) was performed to remove organic contamination and to increase the Hydroxy group (-OH) density at silicon surface of chip.

(b) vapor phase silanization was carried out under vacuum Oven with the following conditions: 4 h, 0.1 Atm, and 125 C (10 ml of GOPS reagent) was performed to create a reactive epoxy layer at Si surface. The chemical process was characterized by XPS analysis.

(c) protein anchoring: $NaHCO_3/NaCO_3$ coating buffer containing 0.5µg/ml G protein was added to each well of the silanized chip and the chip incubated overnight. 10uL of Anti-Mouse Goat HRP was added to the well. After incubation at 37 °C for 1h, 10 µL of TMB were added for visualization.

R.S. Results Section

CDC BioChips

The architecture of the CDC-biochip technology used is reported in Fig. 27. The biochips are made of a silicon-plastic hybrid technology containing integrated temperature sensors and heaters (Fig. 27a) and flexible to be configured to obtain microreactors with volumes ranging from hundred to tens of µl. In particular, the 6W-CDC chip is illustrated in Fig. 27c-d and it is featured by 6 microreactors of ~25 µl each. The CDC design has been optimized to obtain relevant advantages for biochemical reactions requiring an accurate thermal control and using optical signals for the detection. Actually, the silicon cavities on the bottom of the microchambers ensure a very efficient heat exchange between the whole volume of the reaction mix and the heat source (silicon chip) without any barrier of tube material (Fig.27(d)-(1-3;4)). Additionally, the proper design of the double cylinder structure of the polycarbonate part (Fig.27(d)-(2)) induces a relevant enhancement of the optical signals up to 4 times respect to standard equipment. These architectural and functional features have been already proved to produce an improvement of PCR amplification by one order of magnitude in sensitivity if compared to the standard RT-PCR method [182].

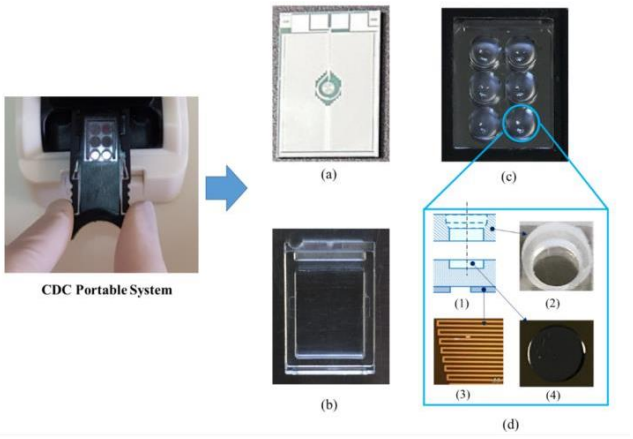

Fig. 27 *CDC-biochip Technology: (a) CDC-biochip bottom view: integrated temperature sensors and heaters; (b) SW-CDC top view: single PC chamber (420 ul); (c) 6W-CDC top view: 6 chambers (25 ul ~25 µl each); (d) 6W-CDC details: (1) section view; (2) single PC double cylinder; (3) temperature heaters; (4) silicon cavity.*

CDC-biochip functionalization

After plasma-O_2 process the diagnostic XPS peaks for Si2p (30%) and O1s (56.5%), proving the effectiveness cleaning and activation. Upon silanization, the XPS spectrum in the range of 0–1000 eV shows the peaks for Si2p (27%), O2p (51.6%), and C1s (10%). A Gaussian-Lorentz deconvolution for the C1s peak indicates two main components centered at about 285.2 eV (C-C and C-H) and a second centered at about 286.7 eV (C-O). The ratio C1s/Si2p value for silanized surface is 0.37. This is diagnostic of the presence of organic layer covering the substrate surface. The effectiveness of the chemical process was confirmed also by water contact angle (CA) measurements. In detail, a CA value of 40° ±5° for recorded for untreated silicon chip surface, while a very hydrophilic surface was obtained after plasma cleaning with CA value of 3°±2°. After silanization step, an increasing of surface hydrophobicity was observed according to the formation of epoxy layer (CA value of 40° ±5°).

Finally, absorbance values at 450 nm at +/- 2.50 confirm the binding of the antibody to the protein and therefore the correct functionalization of the silicon with reactive groups to bind the protein.

All the real-time PCRs were carried out with SsoAdvanced Universal SYBR Green BIORAD using the CDC-biochip Technology.

Subsequent investigations and experimental tests will be conducted in order to create an integrated microfluidics system for a one-step in Lab On Chip investigation for AD diagnosis.

CONCLUSION

Alzheimer's Disease (AD) is the main progressive neurodegenerative disorder characterized by specific neuropathological changes, including extracellular amyloid-containing plaques formation and intracellular neurofibrillary tangles that induce the degeneration of neuronal activity at the base of forebrain. Although the course of the disease is different for each individual patient, AD progresses in three main phases: mild, intermediate and advanced. The onset and progression of the disease correlates with polymorphic aggregation states of Aβ in the brain. Currently, definite AD diagnosis relies on confirmation of brain pathology by autopsy. Thus, the discovery of new biomarkers to define the state or stage of the disease is required in order to provide personalized therapy. Conformation dependent antibodies have been reported that specifically recognize distinct assembly states of amyloids, including prefibrillar oligomers and fibrils. In order to detect antibodies correlated with the aggregational states of the disease and consequently to obtain a profile on the state and stage of the disease of an AD patient, proteins conformationally similar to Aβ were searched using bioinformatics tools. Using an alternative biopanning "double biding" phage display, with sera IgG-AD and mAb-YPF19, it was possible to identify alternative conformational mimotopes of misfold Aβ typical of the state / stage of the disease. The 12III1 phage clone was able to interact *in vitro* with Aβ42 and prevent both aggregation and promote the disaggregation of preformed fibrils of the amyloid, improving viability in SH-SY5Y cells. In addition, other phage clones resulting from the same double binding selection showed the ability to interact with amyloid plaques in AD mouse brain sections with high significance, confirming that the selected peptides were amyloid mimotopes recognized by conformation- dependent antibodies. In order to realize a diagnostic micro-array to detect conformational antibodies present in the different stages and states of the disease, the selected phage clones were used in a new Phage mediated Immuno PCR CDC Biochip. Combinatorial analysis allowed to discriminate AD from healthy sera and to define the progression of the disease.

Future perspectives

The data would pave the way for the use of these conformationally Aβ mimotopes to assess the status and stage of AD. This could be very useful for a personalized pharmacological treatment on the patient, avoiding the progression of the disease.

Since these peptides have interacted with amyloid plaques in brain sections, they could be used as detection probes for imaging. Furthemore, their ability to disaggregate the preformed fibrils of the amyloid could lead to use them in therapeutic practices.

ACKNOWLEDGEMENTS AND COLLABORATIONS

This activity was funded by Italian Ministry of Education, University and Research (MIUR) by means of the national Program PONR&C2007–2013, under the project "Hippocrates– Development of Micro and Nano-Technologies and Advanced Systems for Human Health (PON02_00355_29641931).

This activity was carried out in collaboration with:

Salvatore Cuzzocrea, Emanuela Esposito and Michela Campolo, Department of Chemical, Biological, Pharmaceutical and Environmental Sciences, University of Messina.

Mario Zappia and Alessandra Nicoletti, Neurology Clinic, Department "G.F. Ingrassia", Section of Neurosciences, University of Catania.

Concetta Gugliandolo and Vincenzo Zammuto, Department of Chemical, Biological, Pharmaceutical and Environmental Sciences, University of Messina.

Sabrina Conoci and Salvatore Petralia, Department of Chemical, Biological, Pharmaceutical and Environmental Sciences, University of Messina and Department of Drug Sciences, University of Catania.

REFERENCES

1. Murray M. J., Murray C. F. Complications in Anesthesia (Second Edition) (2007) Pages 493-495.
2. Tanzi R. E., Bertram L. New frontiers in Alzheimer's disease genetics. *Neuron* 2001, 32, 181–184.
3. Klein W. L., Krafft, G. A., Finch C. E. Targeting small Abeta oligomers: the solution to an Alzheimer's disease conundrum? *Trends Neurosci.* 2001, 24,219–224
4. Hardy J., Selkoe D. J. The Amyloid Hypothesis of Alzheimer's Disease: Progress and Problems on the Road to Therapeutics *Science* 2002, 297, 353–356.
5. Price D. L., Sisodia S. S. Mutant genes in familial Alzheimer's disease and transgenic models. *Annu. Rev. Neurosci.* 1998, 21, 479–505.
6. Mucke L., Masliah E., Yu G. Q., Mallory M., Rockenstein E. M., Tatsuno G., Hu K., Kholodenko D., Johnson-Wood K., McConlogue L. High-level neuronal expression of abeta 1-42 in wild-type human amyloid protein precursor transgenic mice: synaptotoxicity without plaque formation *J. Neurosci.* 2000, 20, 4050–4058 .
7. Mullan M., Crawford F. The molecular genetics of Alzheimer's disease. *Mol. Neurobiol.* 1994, 9, 15–22.
8. Morgan D. Dysregulation of Na+/K+ ATPase by amyloid in APP+PS1 transgenic mice *Neurochem. Res.* 2003, 28, 1029–1034.
9. Noble, W., Olm, V., Takata, K., Casey, E., Mary, O., Meyerson, J., Davies, P. (2003). Cdk5 is a key factor in tau aggregation and tangle formation in vivo. *Neuron*, 2003, 38, 555-565., *et al. Neuron* 38, 555–565.
10. Johnson G. V., Bailey C. D. *J. Alzheimer's Dis.* 2002, 4, 375–398.
11. Sze C. I., Troncoso J. C., Kawas C., Mouton P., Price D. L., Martin L. J. Loss of the presynaptic vesicle protein synaptophysin in hippocampus correlates with cognitive decline in Alzheimer disease *J. Neuropathol. Exp. Neurol.* 1997, 56, 933–944 .
12. Scheff, S. W., Price, D. A. Alzheimer's disease-related synapse loss in the cingulate cortex. *Journal of Alzheimer's Disease*, 2001, 3(5), 495-505.
13. Masliah, E., Mallory, M., Hansen, L., Richard, D., Alford, M., Terry, R. (1994). Synaptic and neuritic alterations during the progression of Alzheimer's disease. *Neurosci. Lett.* 1994, 174, 67–72.
14. Aksenov, M. Y., Aksenova, M. V., Butterfield, D. A., Geddes, J. W., Markesbery, W. R. Protein oxidation in the brain in Alzheimer's disease. *Neuroscience* 2001103(2), 373-383.
15. Bickford, P. C., Gould, T., Briederick, L., Chadman, K., Pollock, A., Young, D., Joseph, J. Antioxidant-rich diets improve cerebellar physiology and motor learning in aged rats. Brain research, 2000, 866(1-2), 211-217.
16. Gibson G. E., Neurodegenerative diseases and oxidative stress *Free Radical Biol. Med*. 32, 1061–1070 (2002).
17. Gemma, C., Mesches, M. H., Sepesi, B., Choo, K., Holmes, D. B., Bickford, P. C. Diets enriched in foods with high antioxidant activity reverse age-induced decreases in cerebellar β-adrenergic function and increases in proinflammatory cytokines. *Journal of Neuroscience*, 2002, 22(14), 6114-6120.
18. Mrak, R. E., Griffin, W. S. T. Interleukin-1, neuroinflammation, and Alzheimer's disease. Neurobiology of aging, 2001, 22(6), 903-908.
19. Finch, C. E., Longo, V. D. The gero-inflammatory manifold. In *Neuroinflammatory Mechanisms in Alzheimer's Disease Basic and Clinical Research* 2001 (pp. 237-256). Birkhäuser, Basel.
20. Rogers J., Webster S., Lue L. F., Brachova L., Civin W. H., Emmerling M., Shivers B., Walker D., McGeer P. Inflammation and Alzheimer's disease pathogenesis *Neurobiol. Aging* 1996, 17, 681–686 .
21. Nixon R. A., Mathews P. M., Cataldo A. M. The neuronal endosomal-lysosomal system in Alzheimer's disease *J. Alzheimer's Dis*. 2001, 3, 97–107 .
22. Forman, M. S. (2003). Lee VM, Trojanowski JQ.'. Unfolding" pathways in neurodegenerative disease. *Trends Neurosci*, 26, 407-410.

23. Disterhoft, J. F., Moyer, J. R., Thompson, L. T. (). Calcium hypothesis of aging and dementia. *Ann. N. Y. Acad.Sci.* 1994, 747, 382–406.
24. Landfield, P. W., Thibault, O., Mazzanti, M. L., Porter, N. M., & Kerr, D. S.. Mechanisms of neuronal death in brain aging and Alzheimer's disease: role of endocrine-mediated calcium dyshomeostasis. *J. Neurobiol.* 1992, 23, 1247–1260.
25. Nixon, R. A., Saito, K. I., Grynspan, F., Griffin, W. R., Katayama, S., Honda, T., ... & Beermann, M. Calcium-activated neutral proteinase (calpain) system in aging and Alzheimer's disease. *Ann. N. Y. Acad. Sci.* 1994,747, 77–91.
26. Mattson, M. P., LaFerla, F. M., Chan, S. L., Leissring, M. A., Shepel, P. N., Geiger, J. D. Calcium signaling in the ER: its role in neuronal plasticity and neurodegenerative disorders. *Trends Neurosci.* 2000, 23, 222–229.
27. Thibault, O., Porter, N. M., Chen, K. C., Blalock, E. M., Kaminker, P. G., Clodfelter, G. V.Landfield, P. W. (1998). Calcium dysregulation in neuronal aging and Alzheimer's disease: history and new directions. Cell calcium, 24(5-6), 417-433.. (1998) *Cell Calcium* 24, 417–433.
28. Arendt, T. Alzheimer's disease as a loss of differentiation control in a subset of neurons that retain immature features in the adult brain. *Ann. N. Y. Acad. Sci.* 2000, 920, 249–255.
29. Bowser, R., Smith, M. A. Cell cycle proteins in Alzheimer's disease: plenty of wheels but no cycle. *J. Alzheimer's Dis.* 2002, 4, 249–254.
30. Petanceska S.S., DeRosa S., Olm V., Diaz N., Sharma A., Thomas-Bryant T., Duff K., Pappolla M., Refolo L. M. *J. Mol. Neurosci.* 2002, 19, 155–161.
31. Puglielli, L., Konopka, G., Pack-Chung, E., Ingano, L. A. M., Berezovska, O., Hyman, B. T.,Kovacs, D. M. (2001). Acyl-coenzyme A: cholesterol acyltransferase modulates the generation of the amyloid β-peptide. Nature cell biology, 3(10), 905-912.. *Nat. Cell Biol.* 2001, 3, 905–912.
32. Green, P. S., & Simpkins, J. W. (2000). Estrogens and Estrogen-Like Non-Feminizing Compounds: Their Role in the Prevention and Treatment of Alzheimer's Disease.. J. W. (2000) *Ann. N.Y. Acad. Sci*. 924, 93–98.
33. Hoffer, B. J., and Olson, L. (1997). Treatment strategies for neurodegenerative diseases based on trophic factors and cell transplantation techniques. In *Advances in Research on Neurodegeneration* (pp. 1-10). Springer, Vienna.
34. Forestier A., Douki T., De Rosa V., Beal D., Rachidi W., Combination of Aβ secretion and oxidative stress in an Alzheimer-like cell line leads to the over-expression of the nucleotide excision repair proteins DDB2 and XPC. *Int. J. Mol. Sci.,* 2015, *16*(8), 17422-17444.
35. Liu J., Liu Z., Zhang Y., Yin F. A novel antagonistic role of natural compound icariin on neurotoxicity of amyloid β peptide. *Indian J. Med. Res.,* 2015, *142*(2), 190-195.
36. Pereira, P. M. C. D. M. Doença de Alzheimer: perspetivas de tratamento (Doctoral dissertation, Universidade da Beira Interior 2013.
37. Alves L., Correia A.S., Miguel R., Alegria P., Bugalho P., Alzheimer's disease: a clinical practice-oriented review. *Front. Neurol.,* 2012 3, 63.
38. Stancu, I. C., Vasconcelos, B., Terwel, D. Dewachter, I. (2014). Models of β-amyloid induced Tau-pathology: the long and "folded" road to understand the mechanism. *Mol. Neurodegener*, 9, 1-14, 2014.
39. Holtzman, D. M., Morris, J. C., & Goate, A. M. (2011). Alzheimer's disease: the challenge of the second century. *Sci. Transl. Med.,* 2011, *3*(77), 77sr1.
40. Perl, D. P. Neuropathology of Alzheimer's disease. *Mount Sinai Journal of Medicine: A Journal of Translational and Personalized Medicine* 2010, 77(1), 32-42.
41. Hendrie H.C., Hake A., Lane K., Purnell C., Unverzagt F., Smith-Gamble V., Murrell J., Ogunniyi A., Baiyewu O., Callahan C., Saykin A., Taylor S., Hall K., Gao S. Statin use, incident dementia and Alzheimer disease in elderly african americans. *Ethn. Dis.,* 2015, 25(3), 345-354.
42. Dubois B., Felldmann H.H., Jacova C. Research criteria for the diagnosis of Alzheimer's disease: revising the NINCDS-ADRDA criteria. *The Lancet Neurology*, 2007, 6(8),734-746
43. Marksteiner J., Humpel C., Hinterhuber H. Cerebrospinal fluid biomarkers for diagnosis of Alzheimer's disease: beta-amyloid, tau, phosfotau-181 and total protein. *Drug Today*, 2007, 43(6), 423 – 431.
44. Clark L.F., Kodadek T. Advances in blood-based protein biomarkers for Alzheimer's disease *J. Alzheimers Res Ther*, 2013, 5(3),18.

45. Snyder, H. M., Carrillo, M. C., Grodstein, F., Henriksen, K., Jeromin, A., Lovestone, S., Soares, H. (2014). Developing novel blood-based biomarkers for Alzheimer's disease. *Alzheimers Dement*, 2014,10(1):109-114.
46. Sinha, S., Anderson, J. P., Barbour, R., Basi, G. S., Caccavello, R., Davis, D., Jacobson-Croak, K. (1999). Purification and cloning of amyloid precursor protein β-secretase from human brain *Nature* 1999, 402, 537–540 .
47. Vassar, R., Bennett, B. D., Babu-Khan, S., Kahn, S., Mendiaz, E. A., Denis, P., Luo, Y. (). β-Secretase cleavage of Alzheimer's amyloid precursor protein by the transmembrane aspartic protease BACE. *Science* 1999, 286, 735–741.
48. Ahmed, M., Davis, J., Aucoin, D., Sato, T., Ahuja, S., Aimoto, S., Elliott J.I., Van Nostrand W. Smith, S. O. (2010). Structural conversion of neurotoxic amyloid-β 1–42 oligomers to fibrils. *Nat. Struct. Mol. Biol.* 2010, 17(5), 561.
49. Mayeux, R., Tang, M. X., Jacobs, D. M., Manly, J., Bell, K., Merchant, C., Mehta, P. D. Plasma amyloid β-peptide 1–42 and incipient Alzheimer's disease. Annals of Neurology: *Official Journal of the American Neurological Association and the Child Neurology Society* 1999, 46(3), 412-416.
50. Castellani, R. J., Lee, H. G., Zhu, X., Perry, G., & Smith, M. A. Alzheimer disease pathology as a host response. *J. Neuropathol. Exp. Neurol*. 2008, 67, 523–31 .
51. Knopman, D. S., Parisi, J. E., Salviati, A., Floriach-Robert, M., Boeve, B. F., Ivnik, R. J., McDonald, W. C. (2003). Neuropathology of cognitively normal elderly. *Journal of Neuropathology & Experimental Neurology*, 62(11), 1087-1095..
52. Schütz, A. K., Vagt, T., Huber, M., Ovchinnikova, O. Y., Cadalbert, R., Wall, J., Meier, B. H. Atomic-resolution three-dimensional structure of amyloid β fibrils bearing the Osaka mutation... *Angew. Chem. Int. Ed. Engl.* 2015, 54(1), 331-335
53. Tycko, R. (2015). Amyloid polymorphism: structural basis and neurobiological relevance. Neuron, 86(3), 632-645.
54. Xiao, Y., Ma, B., McElheny, D., Parthasarathy, S., Long, F., Hoshi, M., & Ishii, Y. Aβ (1–42) fibril structure illuminates self-recognition and replication of amyloid in Alzheimer's disease. *Nat. Struct. Mol. Biol* 2015, 22(6), 499-505.
55. Hatami A., Albay R., Monjazeb S., Milton S., Glabe, C. Monoclonal antibodies against Aβ42 fibrils distinguish multiple aggregation state polymorphisms in vitro and in Alzheimer disease brain. *J. Biol. Chem* 2014, 289, 32131–32143.
56. Eisele YS, Obermuller U, Heilbronner G, Baumann F, Kaeser SA, Wolburg H, Walker LC, Staufenbiel M, Heikenwalder M, Jucker M. Peripherally applied Aβ-containing inoculates induce cerebral β-amyloidosis. *Science*. 2010; 330:980–982.
57. Frost B., Jacks R.L., Diamond M.I.. Propagation of tau misfolding from the outside to the inside of a cell. *J Biol Chem.* 2009; 284,12845–12852.
58. Iba M., Guo J.L., McBride J.D., Zhang B., Trojanowski J.Q., Lee V.M.Y.. Synthetic tau fibrils mediate transmission of neurofibrillary tangles in a transgenic mouse model of Alzheimer's-like tauopathy. *J Neurosci*. 2013; 33:1024–1037.
59. Kfoury N., Holmes B.B., Jiang H., Holtzman D.M., Diamond M.I.. Trans-cellular propagation of tau aggregation by fibrillar species. *J Biol Chem*. 2012; 287:19440–19451.
60. Langer F., Eisele Y.S., Fritschi S.K., Staufenbiel M., Walker L.C., Jucker M. Soluble Aβ seeds are potent inducers of cerebral β-amyloid deposition. *J Neurosci*. 2011; 31:14488–14495.
61. Luk K.C., Kehm V., Carroll J., Zhang B., O'Brien P., Trojanowski J.Q., Lee V.M.Y.. Pathological α-synuclein transmission initiates Parkinson-like neurodegeneration in nontransgenic mice. *Science*. 2012a; 338:949–953.
62. Luk K.C., Kehm V.M., Zhang B., O'Brien P., Trojanowski J.Q., Lee V.M.Y.. Intracerebral inoculation of pathological α-synuclein initiates a rapidly progressive neurodegenerative α-synucleinopathy in mice. *J Exp Med*. 2012b; 209:975–986.
63. Meyer-Luehmann M., Coomaraswamy J., Bolmont T., Kaeser S., Schaefer C., Kilger E., Neuenschwander A., Abramowski D., Frey P., Jaton A.L. et al. Exogenous induction of cerebral β-amyloidogenesis is governed by agent and host. *Science*. 2006; 313:1781–1784.
64. Sanders D.W., Kaufman S.K., DeVos S.L., Sharma A.M., Mirbaha H., Li A.M., Barker S.J., Foley A.C., Thorpe J.R., Serpell L.C. et al. Distinct tau prion strains propagate in cells and mice and define different tauopathies. *Neuron*. 2014; 82:1271–1288.

65. Stohr J., Condello C., Watts J.C., Bloch L., Oehler A., Nick M., DeArmond S.J., Giles K., DeGrado W.F., Prusiner S.B. Distinct synthetic Aβ prion strains producing different amyloid deposits in bigenic mice. *Proc Natl Acad Sci U S A*. 2014; 111:10329–10334.
66. Stohr J., Watts J.C., Mensinger Z.L., Oehler A., Grillo S.K., DeArmond S.J., Prusiner S.B., Giles K. Purified and synthetic Alzheimer's amyloid-β (Aβ) prions. *Proc Natl Acad Sci U S A*. 2012; 109:11025–11030.
67. Volpicelli-Daley L.A., Luk K.C., Patel T.P., Tanik S.A., Riddle D.M., Stieber A., Meaney D.F., Trojanowski J.Q., Lee V.M.Y.. Exogenous α-synuclein fibrils induce Lewy body pathology leading to synaptic dysfunction and neuron death. *Neuron*. 2011; 72:57–71.
68. Watts J.C., Condello C., Stohr J., Oehler A., Lee J., DeArmond S.J., Lannfelt L., Ingelsson M., Giles K., Prusiner S.B. Serial propagation of distinct strains of Aβ prions from Alzheimer's disease patients. *Proc Natl Acad Sci U S A*. 2014; 111:10323–10328.
69. Bousset L., Pieri L., Ruiz-Arlandis G., Gath J., Jensen P.H., Habenstein B., Madiona K., Olieric V., Bockmann A., Meier B.H., Melki R. Structural and functional characterization of two α-synuclein strains. *Nat Commun*. 2013; 4
70. Frederick K.K., Debelouchina G.T., Kayatekin C., Dorminy T., Jacavone A.C., Griffin R.G., Lindquist S. Distinct prion strains are defined by amyloid core structure and chaperone binding site dynamics. *Chem Biol*. 2014; 21:295–305.
71. Gath J., Bousset L., Habenstein B., Melki R., Bockmann A., Meier B.H. Unlike twins: An NMR comparison of two α-synuclein polymorphs featuring different toxicity. *PLoS One*. 2014, 9(3), e90659.
72. Paravastu A.K., Leapman R.D., Yau W.M., Tycko R. Molecular structural basis for polymorphism in Alzheimer's β-amyloid fibrils. *Proc Natl Acad Sci U S A*. 2008; 105:18349–18354.
73. Petkova A.T., Leapman R.D., Guo Z.H., Yau W.M., Mattson M.P., Tycko R. Self-propagating, molecular-level polymorphism in Alzheimer's β-amyloid fibrils. *Science*. 2005: 307:262–265.
74. Xue W.F., Hellewell A.L., Gosal W.S., Homans S.W., Hewitt E.W., Radford S.E. Fibril fragmentation enhances amyloid cytotoxicity. *J Biol Chem*. 2009; 284:34272–34282.
75. Lesne S., Koh M.T., Kotilinek L., Kayed R., Glabe C.G., Yang A., Gallagher M., Ashe K.H. A specific amyloid-β protein assembly in the brain impairs memory. *Nature*. 2006; 440:352–357.
76. Lesne S.E., Sherman M.A., Grant M., Kuskowski M., Schneider J.A., Bennett D.A., Ashe K.H. Brain amyloid-β oligomers in ageing and Alzheimer's disease. *Brain*. 2013; 136:1383–1398.
77. Shankar G.M., Li S.M., Mehta T.H., Garcia-Munoz A., Shepardson N.E., Smith I., Brett F.M., Farrell M.A., Rowan M.J., Lemere C.A. et al. Amyloid-β protein dimers isolated directly from Alzheimer's brains impair synaptic plasticity and memory. *Nat Med*. 2008; 14:837–842.
78. Walsh D.M., Klyubin I., Fadeeva J.V., Cullen W.K., Anwyl R., Wolfe M.S., Rowan M.J., Selkoe D.J. Naturally secreted oligomers of amyloid-β protein potently inhibit hippocampal long-term potentiation in vivo. *Nature*. 2002; 416:535–539.
79. Kayed R., Head E., Thompson J.L., McIntire T.M., Milton S.C., Cotman C.W., Glabe C.G. Common structure of soluble amyloid oligomers implies common mechanism of pathogenesis. *Science*. 2003; 300:486–489.
80. Noguchi A., Matsumura S., Dezawa M., Tada M., Yanazawa M., Ito A., Akioka M., Kikuchi S., Sato M., Ideno S. et al. Isolation and characterization of patient-derived, toxic, high mass amyloid β-protein (Aβ) assembly from Alzheimer disease brains. *J Biol Chem*. 2009; 284:32895–32905.
81. Paravastu A.K., Leapman R.D., Yau W.M., Tycko R. Molecular structural basis for polymorphism in Alzheimer's β-amyloid fibrils. *Proc Natl Acad Sci U S A*. 2008; 105:18349–18354.
82. Petkova A.T., Yau W.M., Tycko R. Experimental constraints on quaternary structure in Alzheimer's β-amyloid fibrils. *Biochemistry*. 2006; 45:498–512.
83. Spies P.E., Slats D., Sjogren J.M.C., Kremer B.P.H., Verhey F.R.J., Rikkert M., Verbeek M.M. The cerebrospinal fluid amyloid-β(42/40) ratio in the differentiation of Alzheimer's disease from non-Alzheimer's dementia. *Curr Alzheimer Res*. 2010; 7:470–476.

84. Gravina S.A., Ho L.B., Eckman C.B., Long K.E., Otvos L., Younkin L.H., Suzuki N., Younkin S.G. Amyloid-β protein (Aβ) in Alzheimers-disease brain: Biochemical and immunocytochemical analysis with antibodies specific for forms ending at Aβ40 or Aβ42(43). *J Biol Chem*. 1995; 270:7013–7016.
85. Antzutkin O.N., Leapman R.D., Balbach J.J., Tycko R. Supramolecular structural constraints on Alzheimer's β-amyloid fibrils from electron microscopy and solid state nuclear magnetic resonance. *Biochemistry*. 2002; 41:15436–15450.
86. Luhrs T., Ritter C., Adrian M., Riek-Loher D., Bohrmann B., Doeli H., Schubert D., Riek R. 3D structure of Alzheimer's amyloid-β (1–42) fibrils. *Proc Natl Acad Sci U S A*. 2005; 102:17342–17347.
87. Olofsson A., Lindhagen-Persson M., Sauer-Eriksson A.E., Ohman A. Amide solvent protection analysis demonstrates that amyloid-β(1–40) and amyloid-β(1–42) form different fibrillar structures under identical conditions. *Biochem J*. 2007; 404:63–70.
88. Sato T., Kienlen-Campard P., Ahmed M., Liu W., Li H.L., Elliott J.I., Aimoto S., Constantinescu S.N., Octave J.N., Smith S.O. Inhibitors of amyloid toxicity based on β-sheet packing of Aβ40 and Aβ42. *Biochemistry*. 2006; 45:5503–5516.
89. Torok M., Milton S., Kayed R., Wu P., McIntire T., Glabe C.G., Langen R. Structural and dynamic features of Alzheimer's Aβ peptide in amyloid fibrils studied by site-directed spin labeling. *J Biol Chem*. 2002; 277:40810–40815.
90. Selkoe D., Mandelkow E., Holtzman D. Deciphering Alzheimer disease. *Cold Spring Harb Perspect Med*, 2012,2(1):a011460
91. Koyama A., Okereke O.I., Yang T. et al. Plasma amyloid- beta as a predictor of dementia and cognitive decline: a systematic review and meta-analysis *J. Arch Neurol*, 2012,69 (7):824-831.
92. Toledo J.B., Vanderstichele H., Figurski M. et al. Factors affecting Abeta plasma levels and their utility as biomarkers in ADNI. *Acta Neuropathol*, 2011,122(4):401-413
93. Du Y., Dodel R., Hampel H. et al. Reduced levels of amyloid beta-peptide antibody in Alzheimer disease. *Neurology*, 2001,57(5):801-805.
94. Weksler M.E., Relkin N., Turkenich R. et al. Patients with Alzheimer disease have lower levels of serum anti-amyloid peptide antibodies than healthy elderly individuals. *Exp Gerontol*, 2002,37(7):943-948.
95. Song M.S., Mook-Jung I., Lee H.J. et al. Serum anti-amyloid-beta antibodies and Alzheimer's disease in elderly Korean patients. *J Int Med Res*, 2007,35(3):301-306.
96. Brettschneider S., Morgenthaler N.G., Teipel S.J. et al. Decreased serum amyloid beta(1-42) autoantibody levels in Alzheimer's disease, determined by a newly developed immuno-precipitation assay with radiolabeled amyloid beta(1-42) peptide. *Biol Psychiatry*, 2005,57(7):813-816.
97. Moir R.D., Tseitlin K.A., Soscia S. et al. Autoantibodies to redox-modified oligomeric Abeta are attenuated in the plasma of Alzheimer's disease patients. *J Biol Chem*, 2005,280(17):17458-17463.
98. Hyman B.T., Smith C., Buldyrev I. et al. Autoantibodies to amyloid-beta and Alzheimer's disease. *Ann Neurol*, 2001,49(6):808-810.
99. Baril L., Nicolas L., Croisile B. et al. Immune response to Abeta-peptides in peripheral blood from patients with Alzheimer's disease and control subjects. *Neurosci Lett*, 2004,355(3):226-230
100. Klaver A.C., Coffey M.P., Smith L.M. et al. ELISA measurement of specific non-antigen-bound antibodies to Abeta1- 42 monomer and soluble oligomers in sera from Alzheimer 9s disease, mild cognitively impaired, and noncognitively impaired subjects. *J Neuroinflammation*, 2011,8:93.
101. Gustaw, K. A., Garrett, M. R., Lee, H. G., Castellani, R. J., Zagorski, M. G., Prakasam, A., Friedland, R. P. Antigen-antibody dissociation in Alzheimer disease: a novel approach to diagnosis. *J Neurochem*, 2008,106(3):1350-1356.
102. Mruthinti, S., Buccafusco, J. J., Hill, W. D., Waller, J. L., Jackson, T. W., Zamrini, E. Y., Schade, R. F. Autoimmunity in Alzheimer's disease: increased levels of circulating IgGs binding Aβ and RAGE peptides. *Neurobiol Aging*, 2004,25(8):1023-1032.
103. Gruden, M. A., Davidova, T. B., Mališauskas, M., Sewell, R. D., Voskresenskaya, N. I., Wilhelm, K., Morozova-Roche, L. A. Differential neuroimmune markers to the onset of

Alzheimer's disease neurodegeneration and dementia: autoantibodies to Abeta(25-35) oligomers, S100b and neurotransmitters. *J Neuroimmunol*, 2007,186(1-2):181-192.

104. Gustaw-Rothenberg, K. A., Siedlak, S. L., Bonda, D. J., Lerner, A., Tabaton, M., Perry, G., & Smith, M. A. Dissociated amyloid-beta antibody levels as a serum biomarker for the progression of Alzheimer's disease: a population-based study. *Exp Gerontol*, 2010,45(1):47-52.
105. Li, Q., Gordon, M., Cao, C., Ugen, K. E., Morgan, D. Improvement of a low pH antigen-antibody dissociation procedure for ELISA Autoantibodies in Alzheimer's Disease measurement of circulating anti-Abeta antibodies. *BMC Neuroscience*, 2007,8:22.
106. Maftei, M., Thurm, F., Schnack, C., Tumani, H., Otto, M., Elbert, T., Von Arnim, C. A. Increased levels of antigen-bound beta-amyloid autoantibodies in serum and cerebrospinal fluid of Alzheimer's disease patients. *PLoS One*, 2013,8(7):e68996.
107. Qu, B. X., Gong, Y., Moore, C., Fu, M., German, D. C., Chang, L. Y., Diaz-Arrastia, R. Beta-amyloid auto-antibodies are reduced in Alzheimer's disease. *J Neuroimmunol*, 2014,274(1-2):168-173.
108. Wu J.W., Breydo L., Isas J.M., Lee J., Kuznetsov Y.G., Langen R., Glabe C. Fibrillar oligomers nucleate the oligomerization of monomeric amyloid-β but do not seed fibril formation. *J Biol Chem*. 2010; 285:6071–6079.
109. Lasagna-Reeves C.A., Glabe C.G., Kayed R. Amyloid-β annular protofibrils evade fibrillar fate in Alzheimer disease brain. *J Biol Chem*. 2011; 286:22122–22130.
110. Tomic J.L., Pensalfini A., Head E., Glabe C.G. Soluble fibrillar oligomer levels are elevated in Alzheimer's disease brain and correlate with cognitive dysfunction. *Neurobiol Dis*. 2009; 35:352–358.
111. Asa Hatami, Ricardo Albay, III,Sanaz Monjazeb,Saskia Milton, and Charles Glabe Monoclonal Antibodies against Aβ42 Fibrils Distinguish Multiple Aggregation State Polymorphisms *in Vitro* and in Alzheimer Disease Brain. *J Biol Chem*. 2014 Nov 14; 289(46): 32131–32143
112. Kayed R., Head E., Sarsoza F., Saing T., Cotman C.W., Necula M., Margol L., Wu J., Leonid Breydo L., Thompson J.L., Rasool S., Gurlo T., Butler P., Glabe C.G. Fibril specific, conformation dependent antibodies recognize a generic epitope common to amyloid fibrils and fibrillar oligomers that is absent in prefibrillar oligomers. *Molecular Neurodegeneration*, 2007, 2(1), 18.
113. Kayed R., Canto I., Breydo L., Rasool S., Lukacsovich T., Wu J., Albay R., Pensalfini A., Yeung S., Head E., Marsh J.L., Glabe C. Conformation dependent monoclonal antibodies distinguish different replicating strains or conformers of prefibrillar Aβ oligomers Mol Neurodegener. 2010; 5: 57.
114. Hatami A., Albay R., Monjazeb S., Milton S., Glabe C. Monoclonal antibodies against Aβ42 fibrils distinguish multiple aggregation state polymorphisms in vitro and in Alzheimer disease brain. *J. Biol. Chem.* 2014, 289, 32131–32143. .
115. Lu, J. X., Qiang, W., Yau, W. M., Schwieters, C. D., Meredith, S. C., Tycko, R. Molecular structure of β-amyloid fibrils in Alzheimer's disease brain tissue. *Cell* 2013,154(6), 1257-1268.
116. Pensalfini, A., Albay III, R., Rasool, S., Wu, J. W., Hatami, A., Arai, H., Kawas, C. H. Intracellular amyloid and the neuronal origin of Alzheimer neuritic plaques *Neurobiol. Dis.* 2014, 71: 53-6.
117. Kayed, R., Head, E., Thompson, J. L., McIntire, T. M., Milton, S. C., Cotman, C. W., Glabe, C. G. Common structure of soluble amyloid oligomers implies common mechanism of pathogenesis. Science, 2003, 300(5618), 486-489.
118. Kayed, R., Head, E., Sarsoza, F., Saing, T., Cotman, C. W., Necula, M., Rasool, S. Fibril specific, conformation dependent antibodies recognize a generic epitope common to amyloid fibrils and fibrillar oligomers that is absent in prefibrillar oligomers. *Mol. Neurodegener.* 2007, **2**, 18.
119. Kayed, R., Pensalfini, A., Margol, L., Sokolov, Y., Sarsoza, F., Head, E., Glabe, C. . Annular protofibrils are a structurally and functionally distinct type of amyloid oligomer. *J. Biological Chemistry*, 2009, 284(7), 4230-4237.
120. Kayed, R., Canto, I., Breydo, L., Rasool, S., Lukacsovich, T., Wu, J., Marsh, J. L. Conformation dependent monoclonal antibodies distinguish different replicating strains or conformers of prefibrillar Aβ oligomers. *Mol. Neurodegener.*2010, **5**, 57.

121. Bazan J., Całkosinski I., Gamian A. Phage display—A powerful technique for immunotherapy. *Hum. Vaccines Immunother*. 2012,8, 1817–1828.
122. O'Callaghan R., Bradley R., Paranchych W. The effect of M13 phage infection upon the F pili of *E. coli*. *Virology* 1973, 54, 220–229.
123. Van Wezenbeek P.M., Hulsebos T.J., Schoenmakers J.G. Nucleotide sequence of the filamentousbacteriophage M1.3 DNA genome: Comparison with phage fd.Gene. 1980,11, 129–148.
124. Berkowitz S.A., Day L.A. Mass, length, composition and structure of the filamentous bacterial virus fd. *J. Mol. Biol.*1976,102, 531–547
125. Jacobson A. Role of F Pili in the Penetration of Bacteriophage *fl.J. Virol.*1972,10, 835–843.
126. Riechmann L., Holliger P. The C-terminal domain of TolA is the coreceptor for filamentous phage infectionof *E. coli*. *Cell* 1997, 90, 351–360
127. Click E.M., Webster R.E. Filamentous phage infection: Required interactions with the TolA protein. *J. Bacteriol*. 1997, 179: 6464–6471.
128. Weigel C. Bacteriophage replication modules. *FEMS Microbiol. Rev*. 2006, 30, 321–381
129. Asano S., Higashitani A., Horiuchi K. Filamentous phage replication initiator protein gpII forms a covalent complex with the 5′end of the nick it introduced. *Nucleic Acids Res*. 1999, 27, 1882–1889.
130. Clackson T., Lowman H. Phage Display: A Practical Approach. *Oxford University Press: Oxford*, UK, 2004
131. Rakonjac J. Filamentous phage are released from the bacterial membrane by a two-step mechanism involvinga short C-terminal fragment of pIII. *J. Mol. Biol*. 1999, 289, 1253–1265.
132. Bakhshinejad B., Zade H.M., Shekarabi H.S., Neman S. Phage display biopanning and isolation of target-unrelated peptides: in search of nonspecific binders hidden in a combinatorial library. *Amino Acids* 2016, 48 (12): 2699-2716
133. Geysen H.M., Rodda S.J., Mason T.J. A priori delineation of a peptide which mimics a discontinuous antigenic determinant. *Mol Immunol* 1986, 23(7),709-15.
134. Fack F., Hügle-Dörr B., Song D., Queitsch I., Petersen G., Bautz E.K. Epitope mapping by phage display: random versus gene-fragment libraries. *J Immunol Methods* 1997, 206(1-2):43-52.
135. Caberoy N.B., Zhou Y., Jiang X., Alvarado G., Li W. Efficient identification of tubby-binding proteins by an improved system of T7 phage display. *J Mol Recognit* 2010, 23(1):74-83.
136. Bratkovic T. Progress in phage display: evolution of the technique and its application. *Cell Mol Life Sci* 2010, 67(5):749-67.
137. Chen C.L., Rosi N.L. Peptide-based methods for the preparation of nanostructured inorganic materials. *Angew Chem Int Ed Engl* 2010, 49(11):1924-42.
138. Lee J.W., Song J., Hwang M.P., Lee K.H. Nanoscale bacteriophage biosensors beyond phage display. *Int J Nanomedicine* 2013, 8:3917-25.
139. Cochran R., Cochran F. Phage display and molecular imaging: expanding fields of vision in living subjects. *Biotechnol Genet Eng Rev* 2010, 27:57-94.
140. Aghebati-Maleki L., Bakhshinejad B., Baradaran B., Motallebnezhad M., Aghebati-Maleki A., Nickho H., Yousefi M., Majidi J. Phage display as a promising approach for vaccine development. *J Biomed Sci* 2016, 23(1):66.
141. Sioud M. Phage Display Libraries: From Binders to Targeted Drug Delivery and Human Therapeutics. *Mol Biotechnol* 2019, 61(4):286-303.
142. Murphy M.P. and LeVine H. Alzheimer's Disease and the β-Amyloid Peptide. J Alzheimers Dis. 2010 Jan; 19(1): 311. doi: 10.3233/JAD-2010-1221.
143. Wu J., Li L.. Autoantibodies in Alzheimer's disease: potential biomarkers, pathogenic roles, and therapeutic implications. *The Journal of Biomedical Research*, 2016, 30(000):000-000 Review Article
144. Nagele E., Han M., Demarshall C., Belinka B., Nagele, R. Diagnosis of Alzheimer's disease based on disease-specific autoantibody profiles in human sera. *PLoS One*. 2011, 6(8), e23112.
145. Lista S., Dubois B., Hampel H. Paths to Alzheimer's disease prevention: from modifiable risk factors to biomarker enrichment strategies. *J. Nutr. Health Aging*. 2015, 19(2), 154-163.

146. Schneider P., Hampel H., Buerger K. Biological marker candidates of Alzheimer's disease in blood, plasma, and serum. *CNS Neurosci. Ther.* 2009, 15(4), 358-374.
147. Klaver A.C., Coffey M.P., Smith L.M., Bennett D.A., Finke J.M., Dang L., Loeffler D.A. ELISA measurement of specific non-antigen-bound antibodies to Aβ1-42 monomer and soluble oligomers in sera from Alzheimer's disease, mild cognitively impaired, and noncognitively impaired subjects. *J. Neuroinflammation.* 2011, 8, 93.
148. Jianping L., Zhibing Y., Wei Q., Zhikai C., Jie X., Jinbiao L.. Low avidity and level of serum anti-Aβ antibodies in Alzheimer disease. *Alzheimer Dis. Assoc. Disord.* 2006, 20(3), 127-132.
149. Jellinger K.A. Criteria for the neuropathological diagnosis of dementing disorders: routes out of the swamp? *ActaNeuropathol*. 2009, 117(2), 101-110.
150. Gustaw-Rothenberg K.A., Siedlak S.L., Bonda D.J., Lerner A., Tabaton M., Perry, G., Smith M.A. Dissociated amyloid-beta antibody levels as a serum biomarker for the progression of Alzheimer's disease: a population-based study. *Exp. Gerontol*. 2010, 45(1), 47-52.
151. Maftei M., Thurm F., Leirer V.M., Von Arnim C.A., Elbert T., Przybylski M., Kolassa I.T., Manea M. Antigen-bound and free β-amyloid autoantibodies in serum of healthy adults. *PLoS One*. 2012,7(9), e44516.
152. Du Y., Wei X., Dodel R., Sommer N., Hampel H., Gao F., Ma Z., Zhao L., Oertel W.H., Farlow M.. Human anti-beta-amyloid antibodies block beta-amyloid fibril formation and prevent beta-amyloid-induced neurotoxicity. *Brain*. 2003, 126(9), 1935-1939.
153. Kayed R., Canto I., Breydo L., Rasool S., Lukacsovich T., Wu J., Albay R., Pensalfini A., Yeung S., Head E., Marsh J.L., Glabe C. Conformation dependent monoclonal antibodies distinguish different replicating strains or conformers of prefibrillar Aβ oligomers *Molecular Neurodegeneration.* 2010, 5, 57.
154. Wetzel R., Shivaprasad S., Williams A.D. Plasticity of amyloid fibrils. *Biochemistry*. 2007, 46(1),1-10.
155. Lu J.X., Qiang W., Yau W.M., Schwieters C.D., Meredith S.C., Tycko R. Molecular structure of β-amyloid fibrils in Alzheimer's disease brain tissue. *Cell*. 2013,12, 154(6), 1257-1268.
156. Kayed R., Pensalfini A., Margol L., Sokolov Y., Sarsoza F., Head E., Hall J., Glabe C. Annular protofibrils are a structurally and functionally distinct type of amyloid oligomer. *J. Biol. Chem*. 2009, 284(7), 4230-4237.
157. Yang A. J., Knauer M., Burdick D. A., Glabe C. Intracellular Aβ1–42 aggregates stimulate the accumulation of stable, insoluble amyloidogenic fragments of the amyloid precursor protein in transfected cells. *J. Biol. Chem*. 1995, 270, 14786–14792
158. Kayed R., Head E., Thompson J. L., McIntire T. M., Milton S. C., Cotman C. W., Glabe C. G. Common structure of soluble amyloid oligomers implies common mechanism of pathogenesis. *Science* 2003, 300, 486–489
159. Lambert M. P., Viola K. L., Chromy B. A., Chang L., Morgan T. E., Yu J., Venton D. L., Krafft G. A., Finch C. E., Klein W. L. Vaccination with soluble Aβ oligomers generates toxicity-neutralizing antibodies. *J. Neurochem.* 2001, 79, 595–605
160. Kayed R., Head E., Sarsoza F., Saing T., Cotman C. W., Necula M., Margol L., Wu J., Breydo L., Thompson J. L., Rasool S., Gurlo T., Butler P., Glabe C. G. Fibril specific, conformation dependent antibodies recognize a generic epitope common to amyloid fibrils and fibrillar oligomers that is absent in prefibrillar oligomers. *Mol. Neurodegener*. 2007, 2, 18.
161. Hrncic R., Wall J., Wolfenbarger D.A., Murphy C.L., Schell M., Weiss D.T., Solomon A. Antibody-mediated resolution of light chain-associated amyloid deposits. *Am J Pathol*. 2000; 157:1239–1246.
162. O'Nuallain B., Wetzel R. Conformational Abs recognizing a generic amyloid fibril epitope. *Proc Natl Acad Sci U S A*. 2002; 99,1485–1490.
163. De Plano LM, Carnazza S, Franco D, Rizzo MG, Conoci S, Petralia S, Nicoletti A, Zappia M, Campolo M, Esposito E, Cuzzocrea S., and Guglielmino SPP. Innovative IgG Biomarkers based on Phage Display Microbial Amyloid Mimotope for State/Stage Diagnosis in Alzheimer's Disease. *ACS Chem Neurosc* 2020. doi: 10.1021/acschemneuro.9b00549
164. Petkova A.T., Leapman R.D., Guo Z., Yau W.M., Mattson M.P., Tycko R. Selfpropagating, molecular-level polymorphism in Alzheimer's beta-amyloid fibrils. *Science* 2005, 307(5707), 262-265.

165. Paravastu A.K., Leapman R.D., Yau W.M., Tycko R.. Molecular structural basis for polymorphism in Alzheimer's beta-amyloid fibrils. *Proc. Natl. Acad. Sci*. 2009, USA. 105(47), 18349-1835
166. Kheterpal I., Chen M., Cook K.D., Wetzel R.. Structural differences in Abeta amyloid protofibrils and fibrils mapped by hydrogen exchange--mass spectrometry with on-line proteolytic fragmentation. *J. Mol. Biol.* 2006, 361(4), 785-795.
167. Whittemore N.A., Mishra R., Kheterpal I., Williams A.D., Wetzel R., Serpersu E.H.. Hydrogen-deuterium (H/D) exchange mapping of Abeta 1-40 amyloid fibril secondary structure using nuclear magnetic resonance spectroscopy. *Biochemistry*. 2005, 44(11), 4434-4441.
168. Lührs T., Ritter C., Adrian M., Riek-Loher D., Bohrmann B., Döbeli H., Schubert D., Riek R3D structure of Alzheimer's amyloid-beta(1-42) fibrils. *Proc. Natl. Acad. Sci*. 2005, USA, 102(48),17342-17347.
169. Gremer L., Schölzel D., Schenk C., Reinartz E., Labahn J., Ravelli R.B.G., Tusche M., Lopez-Iglesias C., Hoyer W, Heise H., Willbold D., Schröder G.F. Fibril structure of amyloid-β(1-42) by cryo-electron microscopy. *Science*. 2017, 358(6359), 116-119.
170. Ali R., Naqvi R.A., Kumar S., Bhat A.A., Rao D.N. Multiple antigen peptide containing B and T cell epitopes of F1 antigen of Yersinia pestis showed enhanced Th1 immune response in murine model. *Scand. J. Immunol*. 2013, 77(5), 361-371.
171. Sabhnani L., Rao D.N. Identification of immunodominant epitope of F1 antigen of Yersinia pestis. *FEMS Immunol. Med. Microbiol*.2000, 27(2), 155-162.
172. Frenkel D., Balass M., Solomon B. N-terminal EFRH sequence of Alzheimer's betaamyloid peptide represents the epitope of its anti-aggregating antibodies. *J. Neuroimmunol*. 1998, 88(1- 2), 85-90.
173. Frenkel D., Katz O., Solomon B. Immunization against Alzheimer's beta-amyloid plaques via EFRH phage administration. *Proc. Natl. Acad. Sci*. USA. 2000, 97(21), 11455-11459.
174. Przybylski M., Stefanescu R., Bacher M., Manea M., Moise A., Perdivara I., Marquardt M., Dodel R.C. Molecular approaches for immunotherapy and diagnosis of Alzheimer's disease based on epitope-specific anti- beta-amyloid antibodies. *J. Peptide Sci*. 2006,12, 99.
175. Dodel R., Bacher M., Przybylski M., Stefanescu R., Manea M. Diagnosis of Alzheimer's disease and other neurodementing disorders. Patent International Application No.: PCT/IB2008/000456, Pub. No.: WO/2008/084402
176. McLaurin J., Cecal R., Kierstead M.E., Tian X., Phinney A.L., Manea M., French J.E., Lambermon M.H., Darabie A.A., Brown M.E., Janus C., Chishti M.A., Horne P., Westaway D., Fraser P.E., Mount H.T., Przybylski M., St George-Hyslop P. Therapeutically effective antibodies against amyloid-beta peptide target amyloid-beta residues 4-10 and inhibit cytotoxicity and fibrillogenesis. *Nat. Med*. 2002, 8(11), 1263-1269.
177. Stefanescu R., Iacob R.E., Damoc E.N., Marquardt A., Amstalden E., Manea M., Perdivara I., Maftei M., Paraschiv G., Przybylski M. Mass spectrometric approaches for elucidation of antigen antibody recognition structures in molecular immunology. *Eur. J. Mass Spectrom*. (Chichester). 2007, 13(1), 69-75.
178. Hung L.W., Ciccotosto G.D., Giannakis E., Tew D.J., Perez K., Masters C.L., Cappai R., Wade J.D., Barnham K.J.. Amyloid- Peptide (A) Neurotoxicity is modulated by the rate of peptide aggregation: adimers and trimers correlate with neurotoxicity. *J. Neurosci*. 2008, 28(46):11950-11958.
179. Sarkar D., Chakraborty I., Condorelli M., Ghosh B., Mass T., Weingarth M., Mandal A.K., La Rosa C., Subramanian V., Bhunia A. Self-Assembly and neurotoxicity of β-Amyloid (21–40) peptide fragment: the regulatory role of GxxxG motifs. *ChemMedChem* (2020), 15, 293–301.
180. Frenkel D., Katz O., Solomo B. Immunization against Alzheimer'sb-amyloid plaquesvia EFRH phage administration. *Proceedings of the National Academy of Sciences*, 97(21), 11455-11459.
181. Munter L.M., Voigt P., Harmeier A., Kaden D., Gottschalk K., Weise C., Pipkorn R., Schaefer M., Langosch D., Multhaup G. GxxxG motifs within the amyloid precursorprotein transmembrane sequence are critical forthe etiology of Ab42. *EMBO J*. 2007; 26(6):1702-1712
182. Messing J. Phage M13 for the treatment of Alzheimer and Parkinson disease. *Gene*. 2016, 583, 85-89.

183. Krishnan R., Tsubery H., Proschitsky M.Y., Asp E., Lulu M., Gilead S., Gartner M., Waltho J.P., Davis P.J., Hounslow A.M., Kirschner D.A., Inouye H., Myszka D.G., Wright J., Solomon B., Fisher R.A. A bacteriophage capsid protein provides a general amyloid interaction motif (GAIM) that binds and remodels misfolded protein assemblies. *J. Mol. Biol*., 2014,426(13), 2500- 2519.
184. Guo Y., Zhou Y., Zhangv X., Zhang Z., Qiao Y., Bi L., Wen J., Liang M., Zhang J.. Phage display mediated immuno-PCR,. *Nucleic acids research*, 2006, 34(8), e62-e62.
185. Kai Li, Yi Chen, Siqi Li, Huong Giang Nguyen, Zhongwei Niu, Shaojin You, Charlene M. Mello, Xiaobing Lu, and Qian Wang. Chemical Modification of M13 Bacteriophage and Its Application in Cancer Cell Imaging. *Bioconjugate Chem*. 2010, 21, 7, 1369–137.
186. Jucker, M., & Walker, L.C.. Self-propagation of pathogenic protein aggregates in neurodegenerative diseases. *Nature*, 2013, 501(7465), 45-51.
187. Hansen R.A., Gartlehner G., Webb A., Morgan L., Moore C.G., Jonas D.E.. Efficacy and safety of donepezil, galantamine, and rivastigmine for the treatment of Alzheimer's disease: A systematic review and meta-analysis. *Clin Interv Aging*. 2008, Jun; 3(2): 211–225
188. Ray, B., Maloney, B., Sambamurti, K., kumar Karnati, H., Nelson, P. T., Greig, N. H., Lahiri, D. K. Rivastigmine modifies the α-secretase pathway and potentially early Alzheimer's disease. *Translational psychiatry*, 2020,10(1), 1-17.
189. Conoci, S., Castagna, M. E., Lazzara, A., & Giuffrida, R. (2016). *U.S. Patent Application No*. 14/989,711, 2015, US2016244807.
190. Battaglia, S., Petralia, S., Vicario, N., Cirillo, D., & Conoci, S.. An innovative silicon-chip for sensitive real time PCR improvement in pathogen detection. *Analyst*, 2019, 144(7), 2353-2358.
191. Guarnaccia, M., Iemmolo, R., Petralia, S., Conoci, S., & Cavallaro, S. Miniaturized real-time PCR on a Q3 system for rapid KRAS genotyping. *Sensors*, 2017, 17(4), 831, ISSN 1424-8220.
192. Bianchessi M., Cossi A., Patent US9016936B
193. Spata, M. O., Castagna, M. E., Conoci, S. Image data analysis in qPCR: A method for smart analysis of DNA amplification. *Sensing and bio-sensing research* 2015, 6, 79-84.6, 79-84
194. Sciuto E.L., Bongiorno C., Scandurra A., Petralia S., Cosentino T., Conoci S., Sinatra F., Libertino S. Functionalization of Bulk SiO_2 Surface with Biomolecules for Sensing Applications: Structural and Functional Characterizations. *Chemosensors* 2018, 6, 59.